LMSC/F247098

(2)

~~FINAL~~ TECHNICAL REPORT
Annual

AFOSR-TR- 92 0731

# Comprehensive Mappings of Electron Precipitation and its Effects on the Atmosphere



START DATE: July 1988

CONTRACT NUMBER: F49620-88-C-0072
Air Force Office of Scientific Research

PRINCIPAL INVESTIGATOR: Dr. W.L. Imhof

CO-INVESTIGATORS:
Dr. H.D. Voss
Mr. J. Mobilia
Dr. R.R. Vondrak
Mr. E.E. Gaines
Dr. D.W. Datlowe

Lockheed Palo Alto Research Laboratory
Space Sciences Laboratory
Dept. 91-20, B/255
3251 Hanover Street
Palo Alto, California 94304



June 1992

Annual
~~FINAL~~ TECHNICAL REPORT

# Comprehensive Mappings of Electron Precipitation and its Effects on the Atmosphere

START DATE: July 1988

CONTRACT NUMBER: F49620-88-C-0072
Air Force Office of Scientific Research

PRINCIPAL INVESTIGATOR: Dr. W.L. Imhof

CO-INVESTIGATORS: Dr. H.D. Voss
Mr. J. Mobilia
Dr. R.R. Vondrak
Mr. E.E. Gaines
Dr. D.W. Datlowe

Lockheed Palo Alto Research Laboratory
Space Sciences Laboratory
Dept. 91-20, B/255
3251 Hanover Street
Palo Alto, California 94304

June 1992

UNCLASSIFIED
SECURITY CLASSIFICATION OF THIS PAGE

# REPORT DOCUMENTATION PAGE

Form Approved OMB No. 0704-0188

| | |
|---|---|
| 1a. REPORT SECURITY CLASSIFICATION<br>Unclassified | 1b. RESTRICTIVE MARKINGS |
| 2a. SECURITY CLASSIFICATION AUTHORITY | 3. DISTRIBUTION/AVAILABILITY OF REPORT<br>Approved for public release; distribution unlimited. |
| 2b. DECLASSIFICATION/DOWNGRADING SCHEDULE | |
| 4. PERFORMING ORGANIZATION REPORT NUMBER(S)<br>LMSC/F247098 | 5. MONITORING ORGANIZATION REPORT NUMBER(S) |
| 6a. NAME OF PERFORMING ORGANIZATION<br>Lockheed Palo Alto Research Lab. | 6b. OFFICE SYMBOL (If applicable) |
| 6c. ADDRESS (City, State, and ZIP Code)<br>Orgn. 91-20, Bldg. 255<br>3251 Hanover Street<br>Palo Alto CA 94304-1191 | 7a. NAME OF MONITORING ORGANIZATION<br>Air Force Office of Scientific Research |
| | 7b. ADDRESS (City, State, and ZIP Code)<br>Bldg. 410<br>Bolling AFB<br>Washington, D.C., 20332-6448 |
| 8a. NAME OF FUNDING/SPONSORING ORGANIZATION Air Force Office Scientific Research | 8b. OFFICE SYMBOL (If applicable)<br>NL |
| | 9. PROCUREMENT INSTRUMENT IDENTIFICATION NUMBER<br>F49620-88-C-0072 |
| 8c. ADDRESS (City, State, and ZIP Code)<br>Bldg. 410<br>Bolling AFB<br>Washington, D.C. 20332-6448 | 10. SOURCE OF FUNDING NUMBERS<br>PROGRAM ELEMENT NO. 61102F; PROJECT NO. 2310; TASK NO. A2; WORK UNIT ACCESSION NO. |
| 11. TITLE (Include Security Classification)<br>Comprehensive Mappings of Electron Precipitation and its Effects on the Atmosphere (U) | |
| 12. PERSONAL AUTHOR(S)<br>W.L. Imhof, H.D. Voss, J. Mobilia, R.R. Vondrak, E.E. Gaines, D. W. Darlowe | |
| 13a. TYPE OF REPORT<br>~~Final~~ Technical Report | 13b. TIME COVERED<br>FROM 7/88 TO 6/92 |
| 14. DATE OF REPORT (Year, Month, Day)<br>92/06/30 | 15. PAGE COUNT<br>52 inc. this page |
| 16. SUPPLEMENTARY NOTATION | |

| 17. COSATI CODES | | |
|---|---|---|
| FIELD | GROUP | SUB-GROUP |
| 20 | 09 | |
| 04 | 01 | |

18. SUBJECT TERMS (Continue on reverse if necessary and identify by block number)
X-ray mappings, relativistic electrons, electron precipitation, effects on the atmosphere.

19. ABSTRACT

Precipitation of energetic electrons is an important energy input to the earth's upper atmosphere and can alter the chemistry and dynamics of that region. The precipitation can be studied on a global basis using a satellite X-ray imager to make maps of the X-rays produced when the electrons stop in the atmosphere. We have used 4-40 keV X-ray data from the S81-1 SEEP satellite instrument to classify the patterns of precipitation at high latitudes; the three principal types are strong auroral arcs an the night side, extended dawnside arcs, and isolated pitches inside the polar cap. We also studied the characteristics of high energy (relativistic) electron precipitation with data from instruments that directly detect the electrons. This very penetrating radiation is important because the electrons deposit their energy down to altitudes as low as ~ 55 km. This study found that the precipitation was confined to narrow latitude bands, often at the outer boundary of the belt of trapped electrons, and that it occurs more often at midnight local time than at noontime.

| | |
|---|---|
| 20. DISTRIBUTION/AVAILABILITY OF ABSTRACT<br>☒ UNCLASSIFIED/UNLIMITED ☐ SAME AS RPT. ☐ DTIC USERS | 21. ABSTRACT SECURITY CLASSIFICATION<br>unclassified |
| 22a. NAME OF RESPONSIBLE INDIVIDUAL<br>~~Wrb. Imhof~~ James G. Stobie | 22b. TELEPHONE (Include Area Code)<br>408-742-5021 |
| | 22c. OFFICE SYMBOL<br>NL |

DD Form 1473, JUN 86 Previous editions are obsolete. SECURITY CLASSIFICATION OF THIS PAGE

# Table of Contents

Final Technical Report

Contract Number: F49620-88-C-0072

# Comprehensive Mappings of Electron Precipitation and its Effects on the Atmosphere

## Summary of Activities Pursued

*I. Process bremsstrahlung X-ray data from the SEEP program, or other appropriate satellites, to obtain the X-ray intensities and energy spectra as a function of time and position.*

The first step was to organize the available SEEP x-ray data into categories to establish which types of events have been observed. The x-ray images had previously been recorded on color prints; under this contract the X-ray features in these images were classified into the following groups:

1. Strong auroral arcs near midnight local time
2. Dawnside arcs, prominent because the satellite travelled along the arc for thousands of kilometers
3. Isolated patches of X-ray emission well inside the polar cap.

Figure 1 shows typical examples of the various auroral forms. The statistics for these events from the XRIS data, acquired in June 1982, were as follows:

| | |
|---|---|
| Midnight arcs | 50 |
| Dawnside arcs | 35 |
| Isolated patches | 38 |

Most of the midnight arcs were at high magnetic L-value, L>6.0, and were associated with narrow electron precipitation regions observed by electron detectors also on board the SEEP payload. They may be associated with auroral current systems and inverted-V type regions. Some of the midnight arcs, and all of the dawnside arcs, were located at L-values less than 6.0, and were associated

with extended particle precipitation regions. Loss of trapped electrons from the radiation belts may have been a primary source of these electrons.

Since we are interested in global energy deposition and possible atmospheric effects, the next step was to calculate the total electron flux and energy deposition in the observed features. The database of X-ray spectral fits was accessed to calculate the integral energy deposition along 1 centimeter perpendicular to the satellite path for each of the 50 midnight arc events. We found that the typical value for the energy deposition was $10^8$ ergs/cm s, and the typical electron flux was $10^{16}$ electrons/cm s. The frequency of occurrence of these parameters is presented in Figure 2.

The most intense electron precipitation event observed by XRIS occurred on 12 June 1982, as shown in Figure 3. In our classification scheme this was an isolated patch of emission, although it may be argued that the region was a westward travelling surge frozen in time by the X-ray imager. The maximum ionization rate was $2 \times 10^6$ electrons/cm$^3$ s, making it an order of magnitude more intense than the typical event from SEEP. However, we know from analysis of the X-ray spectrum that the mean energy of the precipitating electrons was 4.5 keV, so that the altitude of maximum energy deposition was 105 km, somewhat higher than the typical event observed by SEEP (Datlowe et al 1988).

The most recent developments in this phase of the investigation are study of 26 auroral arcs which were mapped in X-rays and also measured in detail by particle detectors as the satellite passed through the precipitation region. The electron data were acquired by a silicon solid state detector called LE2, which counted electrons above a threshold energy of 16 keV. Examples of the combined XRIS and LE2 data are shown in Figure 4. All of the arcs used in this study were at high geomagnetic latitudes and were on the poleward boundary of the midnight auroral zone. The high time resolution electron readouts provided detailed profiles of the electron precipitation along the track of the satellite with ~2 km resolution, while the X-ray data provided maps of the precipitation up to 320 km on either side of the satellite but with ~40 km spatial resolution. The synergy of the electron and X-ray data allows us to estimate the widths of the arcs precisely without deconvolving the 40 km X-ray imager resolution. The result is a distribution of the widths of these arcs, as follows:

| ARC WIDTH, Km | Events |
|---|---|
| <20 | 8 |
| 20-40 | 10 |
| 40-100 | 8 |

It is clear from the table that two thirds of the X-ray arcs are narrower than the resolution of the x-ray spectrometer, and that much higher spatial resolution will be very valuable in understanding the physics of auroral arcs. This work has been submitted for publication in Journal of Geophysical Research, although its origins were reported in the 29 November 1989 annual technical report.

*II . Perform selective analyses of data acquired from a variety of sensors in satellite payloads during times of unusual events, particularly for coordinated measurements with other satellite payloads.*

The precipitation of relativistic electrons into the atmosphere during enhancement events was a major focus of this investigation. This penetrating radiation can have significant effects on atmospheric chemistry down to altitudes as low as 55km. Three articles on this topic were published in the Journal of Geophysical Research under partial support from this contract. A brief summary of these papers is given here, and reprints are included as an appendix.

Data from the S81-1 spacecraft were used to study relativistic electrons precipitating in the bounce loss cone. These are electrons which will precipitate into the atmosphere within a fraction of a second. The events were generally narrow spikes less than 100 km in latitude width at L-values from four to six. The events occurred more often at midnight than at noon. The results were published in J. Geophys. Res. 96, 5619-5629, 1990.

For the first time simultaneous measurements of trapped relativistic electron enhancements at synchronous altitude, L=6.6, were compared with precipitating electrons in the bounce loss cone at low altitudes. The investigation showed that the daily variations in the precipitation flux for L>5 correlated well with the daily variations in the total flux at high altitude, both with respect to sudden enhancements as well as flux depletions. The results of this investigation are summarized in Geophys. Res. Lett. 18, 397-400, 1990.

The correlation between relativistic electron fluxes at high altitude and the precipitation observed at low altitude was extended by data from the SCATHA satellite. The SCATHA satellite observed high altitude relativistic electron data not just at the synchronous altitude of 6.6 but throughout the range from L=5.3 to L=8.7. The P78-1 satellite provided the simultaneous low-altitude observations of precipitating > 1 MeV electrons. The coordinated data permitted for the first time a comparison to be made as a function of L shell between the precipitating and the high-altitude trapped electron fluxes during relativistic

electron enhancement events, some of which included electrons with energies extending to at least 5 MeV. The low- and high-altitude fluxes of electrons > 1 MeV were found to track each other during the period studied (April to June 1979), both with respect to time and L-shell variations. The average precipitating electron fluxes measured at low altitudes in the drift-loss cone were lower than those at high altitude by a factor of about $3x10^2$. The results of this investigation are summarized in an article published in the J. Geophys. Res. (97, 6397-6403, 1992).

*III. Obtain intensity and energy spectral information on precipitating electrons and obtain the energy deposition profiles in the atmosphere.*

Direct *in situ* electron measurements and maps of X-ray production are two techniques for obtaining the intensities and spectra of precipitating electrons. Direct measurements can provide considerable detail about fine spatial variations, about spectral shapes, and about pitch angle distributions, but only along the path of the satellite. X-ray maps provide less detail about the electrons but can reach to distances hundreds of km from the satellite. X-ray images can be used to classify features (arcs, isolated regions, etc.) and define their orientation relative to the path of the satellite. In this investigation we have used both techniques, sometimes simultaneously, to obtain the spectral shapes and energy deposition rates of precipitating electrons.

From direct electron measurements we found that near local midnight the precipitation of electrons in the tens of kilovolt range is typically confined to narrow latitude regions. The locations are often near the vicinity of the outer boundary of the trapped radiation belt, which is often referred to as the trapping boundary. Frequently they occupy one or more narrow L shell regions within the outer radiation belt. This spatial distribution contrasts with the more widespread extent that often occurs in low energy electron precipitation.

From direct measurement of the energetic electron precipitation fluxes, it was found that the precipitation may be much more intense at latitudes below the trapping boundary and may extend over a much broader L shell range than the precipitation that often occurs within one degree of the background boundary. Whereas precipitation at the trapping boundary was observed on 69% of the satellite passes across that region, precipitating fluxes at more than one degree lower latitude were higher on about 38% of the passes. Although strong precipitation events at invariant latitudes as low as about 60° occurred less often than the weaker ones near the trapping boundary, their intensity was frequently great enough and they extended over such a wide longitude interval as to lead to a greater input to the atmosphere. These results are summarized in J. Geophys. Res. 95 3829-3839, 1990.

Strong precipitation was frequently limited to the immediate vicinity of the trapping boundary and the precipitation was often great enough that it could be mapped in x-rays with the detectors on the P78-1 satellite. Previous investigations have addressed precipitation near the trapping boundary at midnight based solely on direct measurements of the electrons. Under this contract, from analysis of existing x-ray imaging data it has been found that such precipitation frequently may extend uniformly in an arc pattern over a longitude interval of 60°. From the x-ray measurements, temporal periodicities in the flux of electrons precipitating near the background boundary were generally not observed on a time scale of about ten seconds to five minutes. These findings are consistent with electron precipitation at this location being caused by characteristics of the magnetic field which are not strongly dependent upon longitude.

The precipitation into the atmosphere of electrons near the edge of the bounce loss cone was considered. Many previous studies have been made of electrons at high latitudes during strong precipitation events such that the pitch angle distributions at low satellite altitudes are isotropic. When isotropy occurs some of the electrons are in the bounce loss cone and the precipitation rates into the atmosphere can be obtained directly from simple measurements on a satellite. Often, however, only locally trapped electrons are observed and yet they may eventually precipitate into the atmosphere if they are mirroring at values of B such that upon drift to more easterly longitudes they will mirror at altitudes below 100 km. Such electrons are considered to be in the drift loss cone. In this case derivation of both the rates and the longitude regions of precipitation into the atmosphere are subject to the uncertainties of the magnetic field model.

In principle, the combination of the fluxes in the bounce loss cone and the drift loss cone can provide the total loss rates into the atmosphere, but measurements of electrons in the bounce loss cone generally do not include those electrons near the edge of the loss cone where much of the precipitation may occur. The latter population may be relatively large because the representation includes those electrons that may have undergone very small scatterings near the equator. In this regard, fine resolution measurements of such electrons were studied at L=2.5 (Imhof et al., 1986). At this L shell the authors found that the loss rates were primarily due to electrons near the edge of the loss cone; the loss rates from electrons well within the bounce loss cone made only a small contribution.

The total loss rates into the atmosphere were calculated based on the detailed pitch-angle distributions and energy spectra of electrons measured at 600 -km altitude with the PRM 004 spectrometer. Since the geometric factor of this spectrometer was relatively small ( ~ 0.001 $cm^2$ sr) it was generally necessary to combine data from several spins and from more than one satellite pass through each region of interest to obtain adequate statistical accuracies. Pitch-angle distributions are shown in Figure 5 for 3 longitude intervals in the southern hemisphere. Each of these distributions is taken from 5 to 8 satellite passes. These examples contain more fluxes, slightly within the bounce loss cone than is often the case. The observed pitch-angle distributions from several passes were combined with the absolute intensities and energy spectra extrapolated to 50 keV to calculate the total loss rates of electrons into the atmosphere (Walt et al., 1968). These loss rates at L=4.5, 5.0 and 5.5 are plotted in Figure 6 as a function of longitude for electrons precipitating in the southern hemisphere. Significant variations in the precipitating fluxes appear from one satellite pass to another and these are reflected in the flux deviations from one longitude to another. It is planned to submit the results of this investigation to the Journal of Geophysical Research for publication.

## Publications

W.L. Imhof, H.D. Voss, J. Mobilia, D.W. Datlowe, and E.E. Gaines, The precipitation of relativistic electrons near the trapping boundary, J. Geophys. Res., 96, 5619, 1991.

W.L. Imhof, H.D. Voss, J. Mobilia, D.W. Datlowe, J.P. McGlennon and D.N. Baker, Relativistic electron enhancements; simultaneous measurements from synchronous and low altitude satellites, Geophys. Res. Lett., 18, 397, 1991.

W.L. Imhof, J. Mobilia, D.W. Datlowe, H.D. Voss, and E.E. Gaines, Longitude and temporal variations of energetic electron precipitation near the trapping boundary, J. Geophys. Res., 95, 3829, 1990.

W.L. Imhof and R.W. Nightingale, Relativistic electron enhancements observed over a range of L shells trapped at high altitudes and precipitating at low altitudes into the atmosphere, J. Geophys. Res., 97, 6397, 1992.

D. W. Datlowe, W. L. Imhof and H. D. Voss, Kilometer scale structures in auroral x-ray arcs detected by combining satellite x-ray images with in situ energetic electron flux profiles, J. Geophys. Res. submitted for publication, 1992.

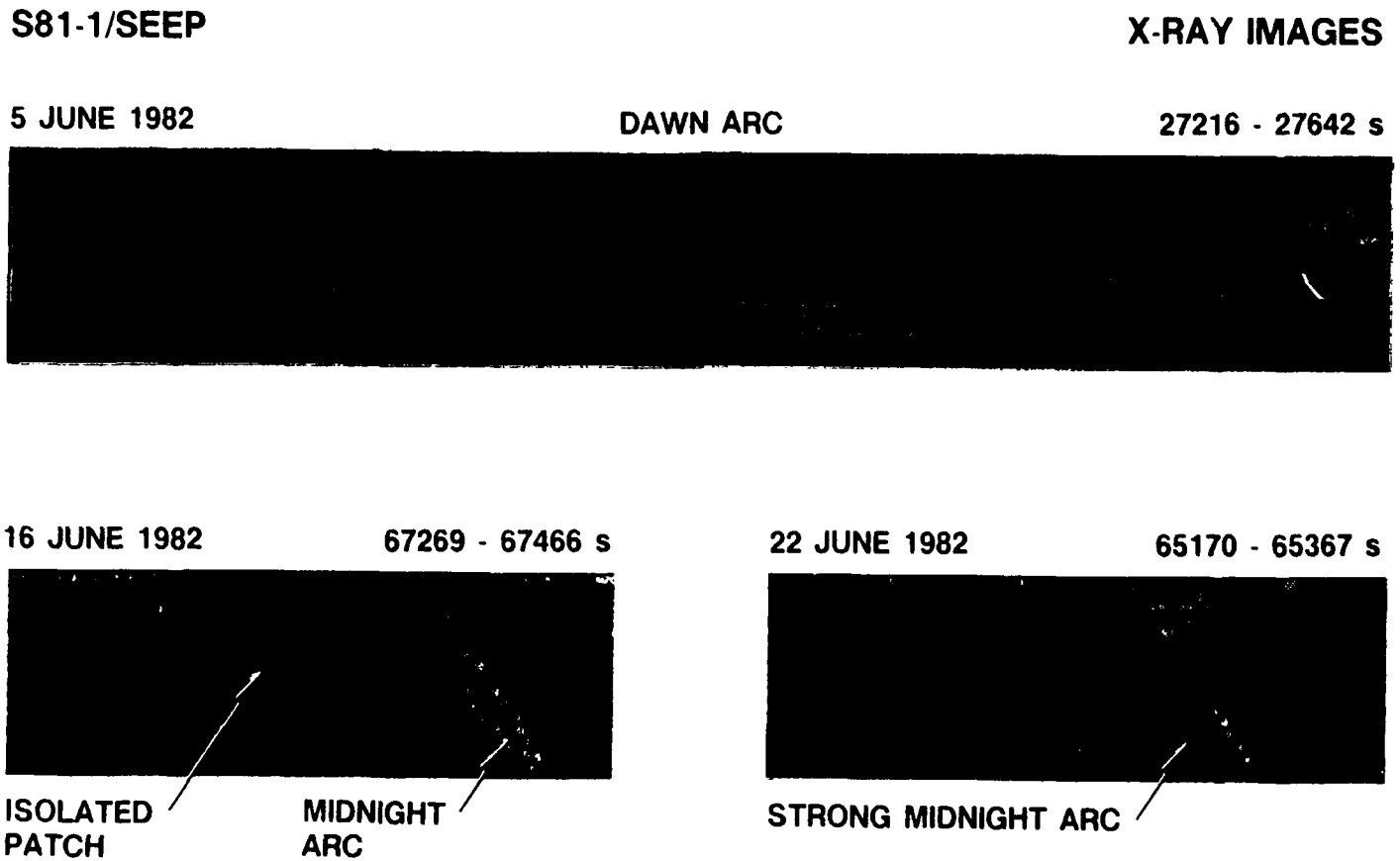


Figure 1: Images in 4 to 24 keV x-rays obtained with the SEEP payload on the S81-1 satellite. In the upper section is a dawn arc. In the lower right section is a strong midnight arc. In the lower left section is an isolated patch and a midnight arc.

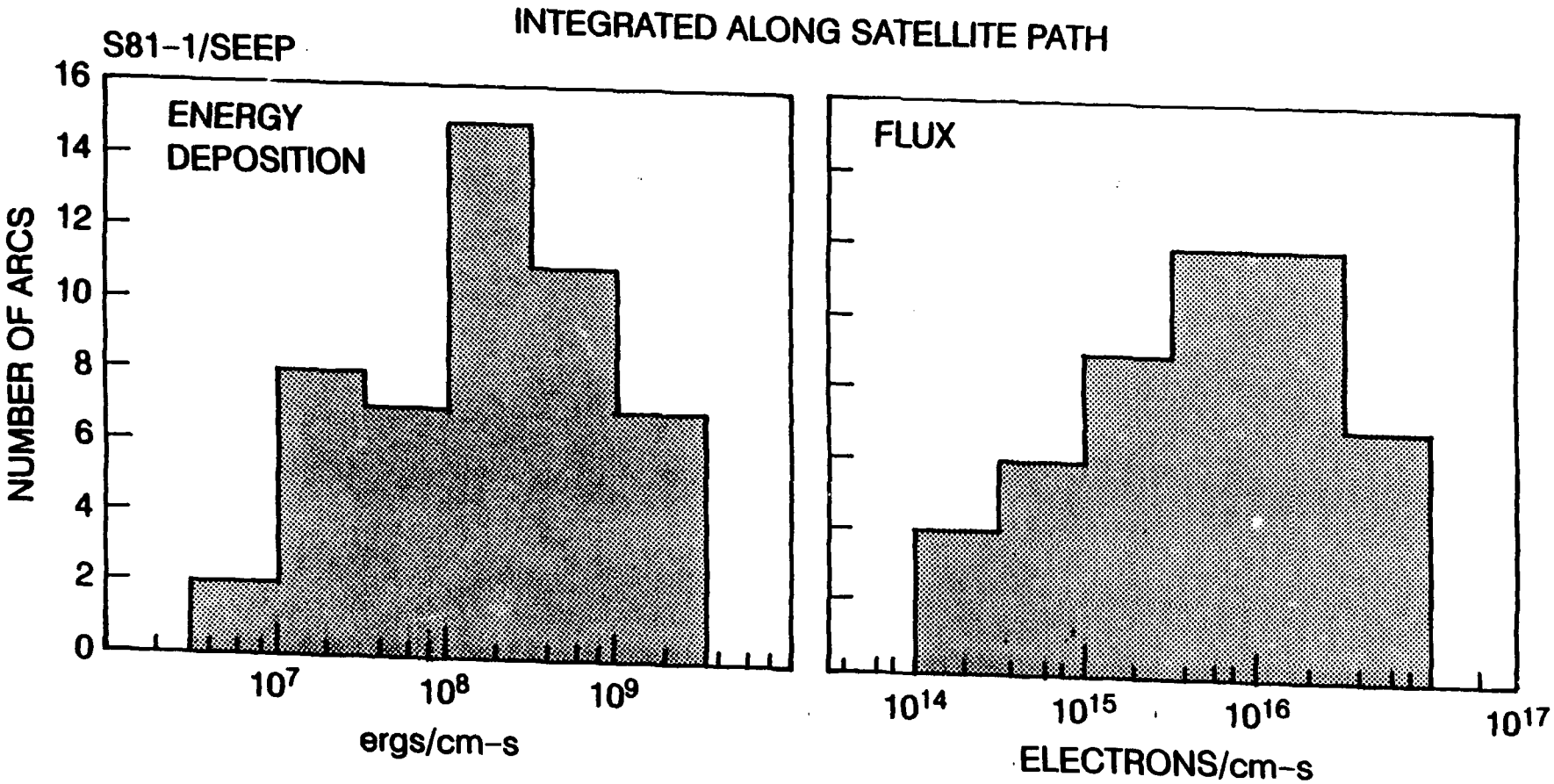


Figure 2 Distributions of the energy deposition and electron flux associated with the midnight arcs.

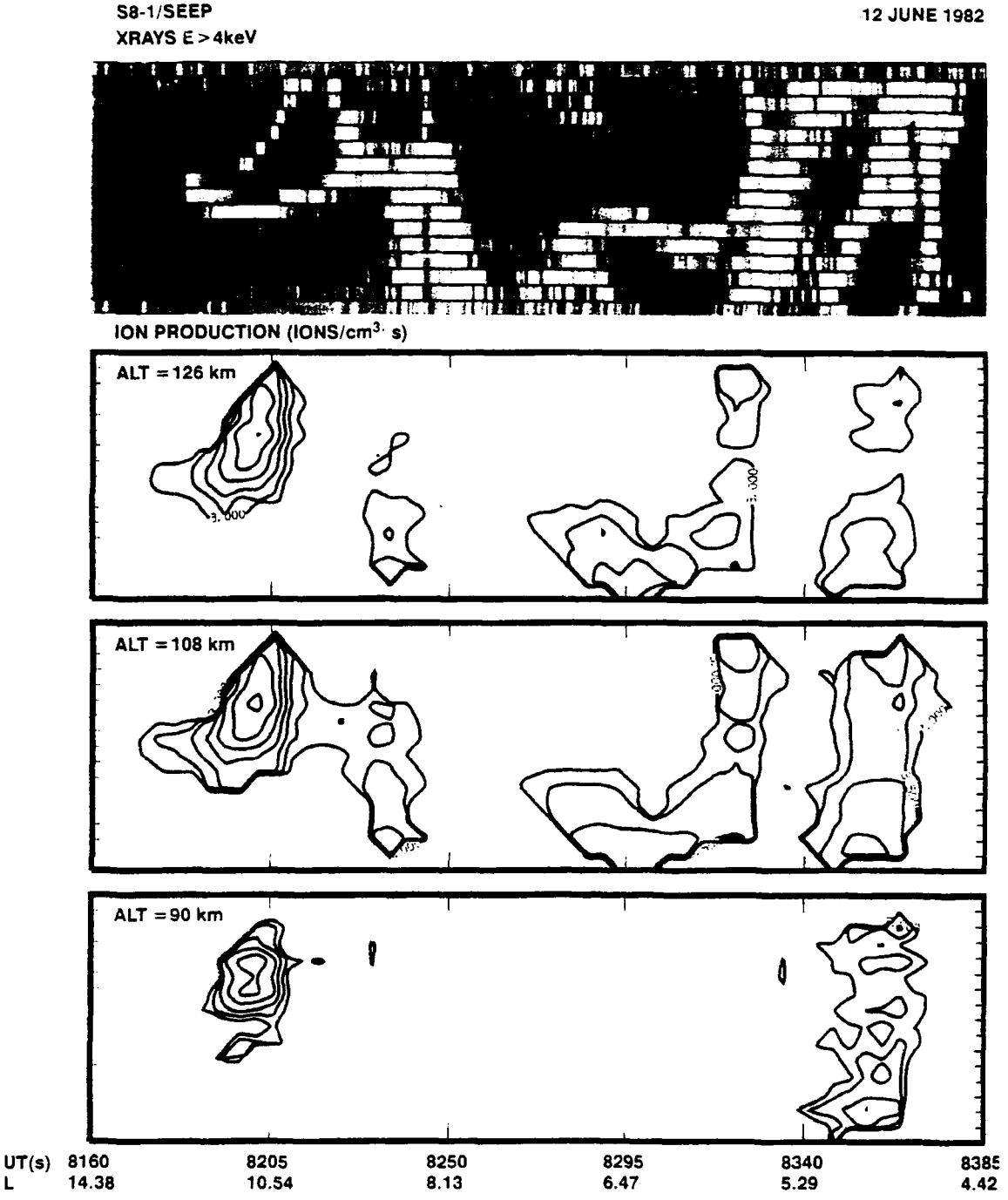


Figure (3) Image of the bremsstrahlung x-rays associated with a precipitation event on June 12, 1982 and contour maps of the ion production rate at selected altitudes of 126 km, 108 km, and 90 km. The minimum contour level is $10^3$ pairs/$cm^2$s and there are two contour levels per decade. The maximum ionization is 2 x $10^6$ ion pairs/$cm^2$s at 108 km observed at 8201s.

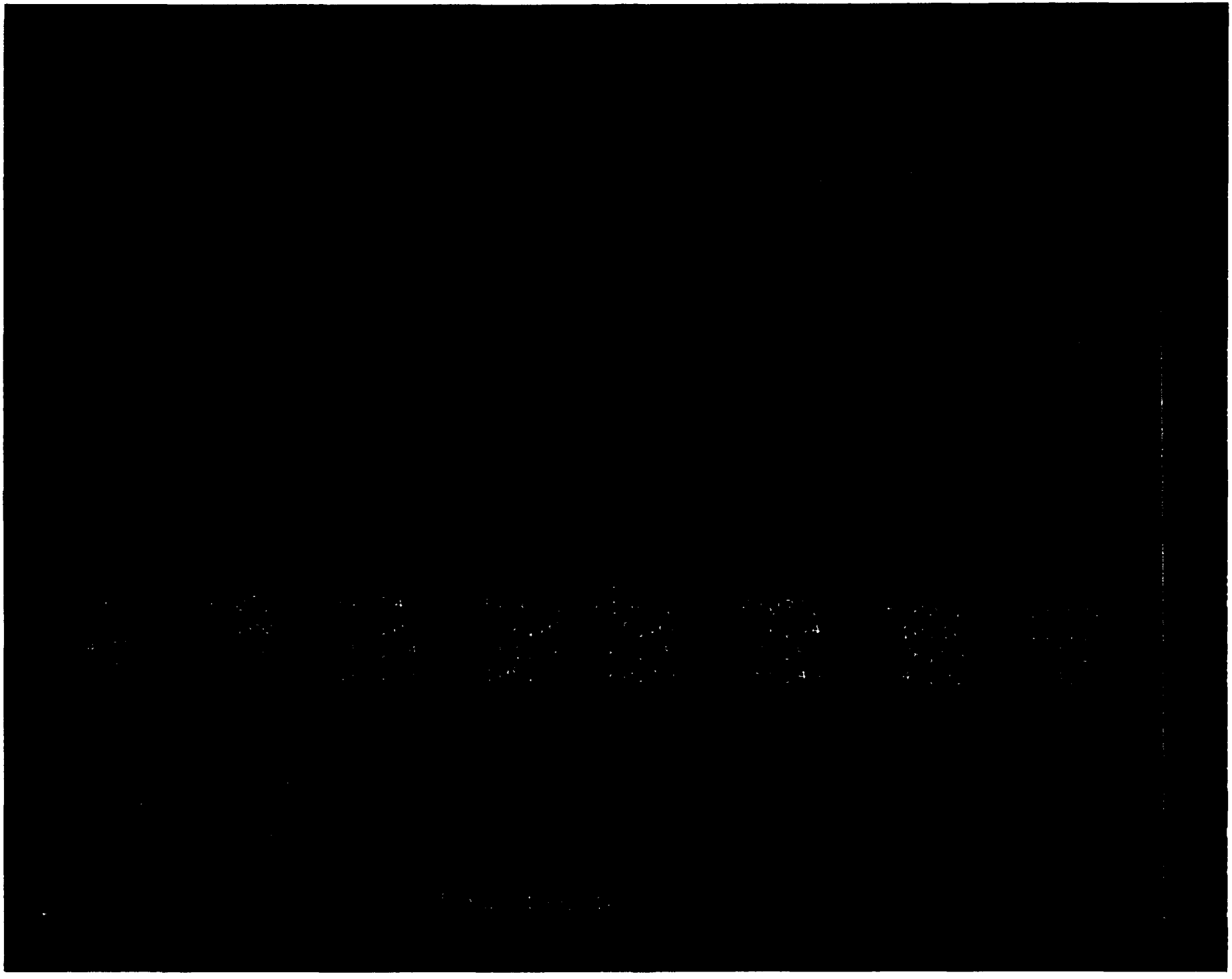

Figure 4 Examples of XRIS and LE2 data

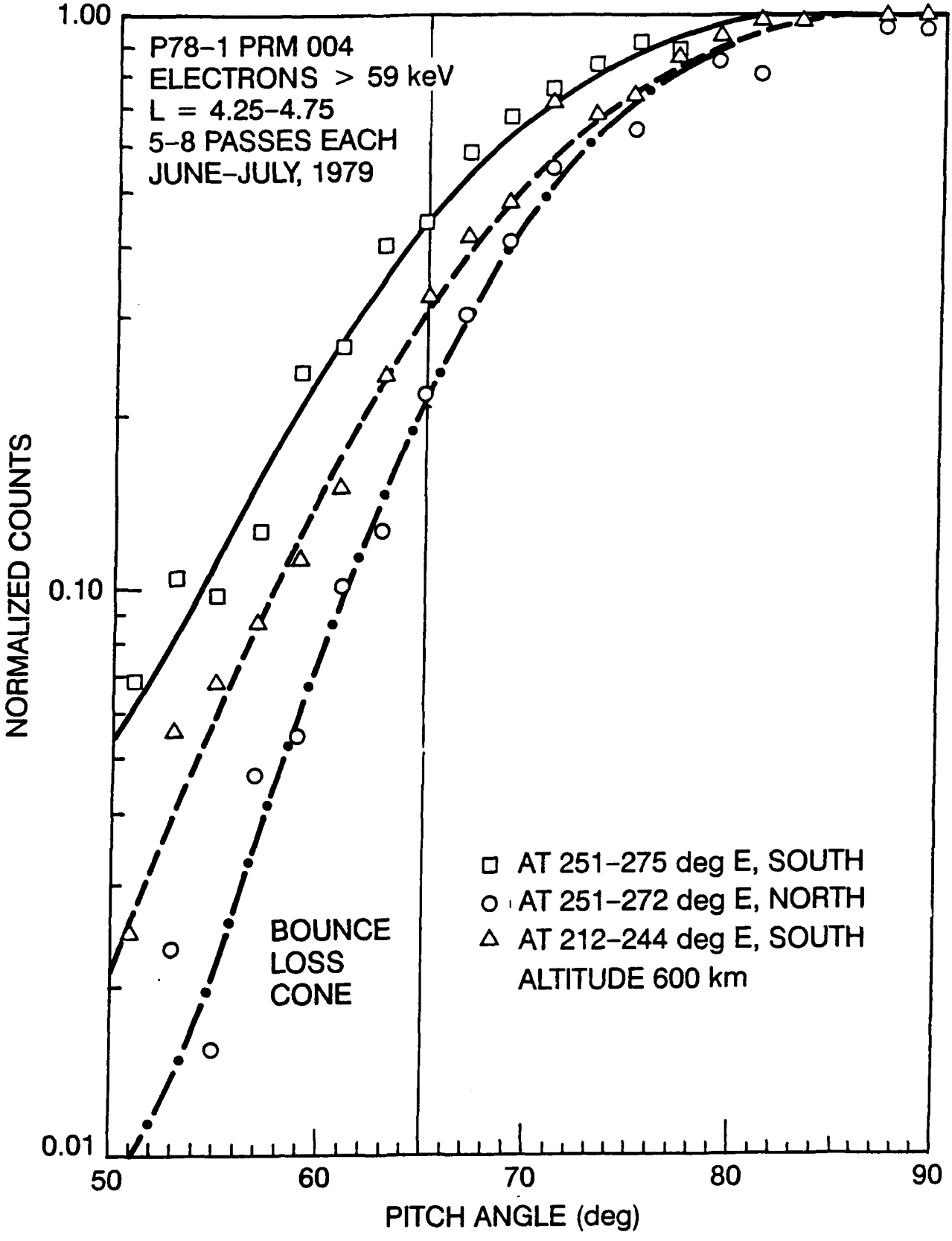


Figure 5 Pitch angle distributions for 3 longitude intervals in the southern hemisphere.

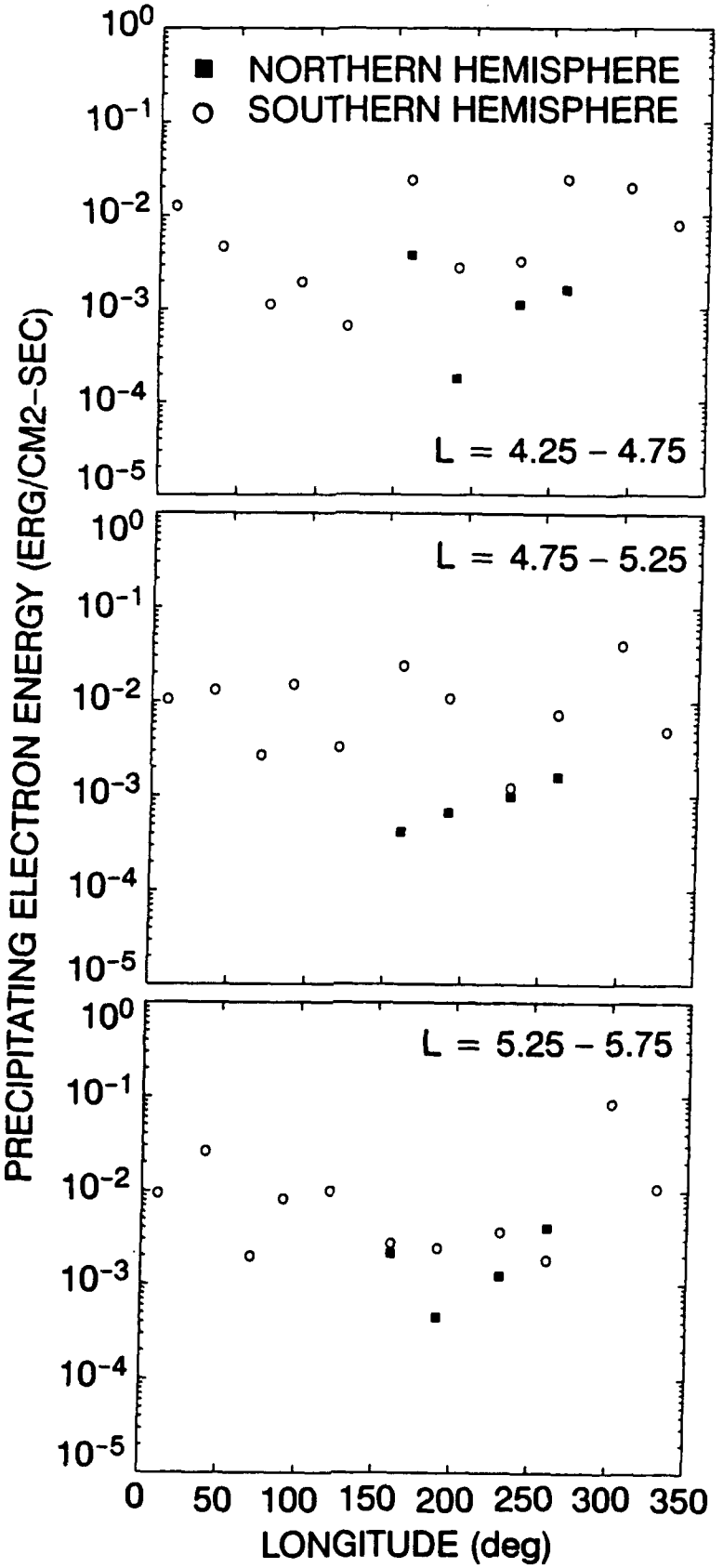


Figure 6 Loss rates as a function of longitude for electrons precipitating in the southern hemisphere.

# APPENDIX A

# THE PRECIPITATION OF RELATIVISTIC ELECTRONS NEAR THE TRAPPING BOUNDARY

JOURNAL OF GEOPHYSICAL RESEARCH, VOL. 96, NO. A4, PAGES 5619–5629, APRIL 1, 1991

# The Precipitation of Relativistic Electrons Near the Trapping Boundary

W. L. IMHOF, H. D. VOSS, J. MOBILIA, D. W. DATLOWE, AND E. E. GAINES

*Lockheed Palo Alto Research Laboratory, Palo Alto, California*

Highly relativistic electrons are known to be present at synchronous satellite altitude in time-varying and sometimes large intensities; it is therefore important to consider the fluxes and locations of relativistic electrons precipitating into the atmosphere. Here we present measurements from the low-altitude three-axis-stabilized satellite S81-1 of trapped and precipitating electrons from 6 keV to above 1 MeV. Significant fluxes of precipitating relativistic electrons above 1 MeV within the bounce loss cone are much more often observed near midnight than noon and generally in narrow spikes <100 km in width typically at $L$ values between 4 and 6 near the radiation belt boundary. The tendency for many of the relativistic spikes to be near the trapping boundary is consistent with the general pattern at lower energies confirmed by the measurements presented here of intensity and threshold energy for isotropy versus $L$ shell. A trend was observed for the higher-energy precipitating electron fluxes to peak at somewhat lower $L$ values. The precipitation of >1-MeV electrons has been measured to occur at intensities and in locations that are widely variable within a few minutes superposed on longer-term variations. On one of the days of strongest precipitation the total nighttime input to the atmosphere during 12 hours from >1-MeV electrons within the bounce loss cone near the trapping boundary was $\sim 10^{19}$ ergs, which was an order of magnitude less than the loss rates estimated by Baker et al. from high-altitude measurements, suggesting that precipitation in the drift loss cone may be significant.

## INTRODUCTION

The population of relativistic electrons at high altitudes, such as those regions traversed by synchronous satellites, is known to experience major enhancements and depletions [e.g., *Baker et al.*, 1987]. The electron flux at synchronous altitude diminishes rapidly in association with an enhancement of geomagnetic activity and then increases [*Nagai*, 1988]. An important question subsequently arises: How many of these relativistic electrons are ultimately precipitated into the Earth's atmosphere, and where does such precipitation occur? This matter is important to consider from the standpoint of understanding both the electron transport processes and the associated effects in the atmosphere of relativistic electron precipitation. Here we investigate the precipitation of relativistic electrons.

*Vampola* [1971, 1977] investigated the precipitation of relativistic electrons using some examples from the S3-3 satellite data. High-energy ($E > 1.5$ MeV) electrons were found to be scattered more readily than lower-energy ($E \approx 300$ keV) electrons. *Thorne and Andreoli* [1980] made a study of relativistic electron precipitation (REP) events using S3-3 satellite data. The electron energies were in the range of a few hundred keV. It was found that many of the events occurred near the outer limit of electron trapping, but neither time profiles of the precipitation rates nor comparisons with synchronous altitude measurements were provided.

Over a wide range of energies the loss of electrons from the radiation belts is enhanced near the outer edge [e.g., *Fritz*, 1968, 1970]. For the first time the precipitation near the midnight trapping boundary was shown often to display an energy and $L$ shell-dependent flux enhancement and an energy selectivity which varies strongly with $L$ value [*Imhof et al.*, 1977, 1979; *Imhof*, 1988]. The onset of isotropy (i.e., where the trapped and precipitating fluxes are equal) at low altitude typically occurs at a sharply defined energy threshold which decreases rapidly with increasing $L$ value. Highly relativistic electrons might therefore be expected to experience enhancements in the low $L$ shell portion of the trapping boundary.

The energy selective phenomenon observed by Imhof et al. has been interpreted in terms of the loss of adiabatic motion when the radius of field line curvature is less than an order of magnitude greater than the gyroradius of the electrons. The mechanism inherently has a threshold energy that is dependent upon the characteristics of the magnetic field line, and hence an $L$ dependent threshold for isotropy is perhaps to be expected. For various magnetic field models, theoretical calculations have been made of the expectations [*Popielawska et al.*, 1985; *Büchner and Zelenyi*, 1989], and they are consistent with some of the observations. On the other hand, for wave-particle interactions a strongly $L$ dependent threshold could result from changes with $L$ in the frequency distribution of the waves or in the plasma density. So the $L$ dependence of the threshold energy may by itself not provide a unique identification of the mechanism.

The energy selective outer boundary has been observed previously from two different satellites, but both of the earlier studies were performed from a spinning vehicle, and accordingly the precipitating fluxes were measured only within a limited duty cycle. With such a sampling, key portions of and even entire precipitation events could be missed. Several advantages are achieved when the measurements are performed from a three-axis-stabilized satellite. The advantages include the following: (1) All precipitation spikes of sufficient intensity are measured, with none being lost because of duty cycle effects. (2) Accurate measurements are obtained of the $L$ shell width of the transition region for energy selectivity. (3) Any deviations from a monotonic pattern in the threshold energy for isotropy versus $L$ value can be more readily observed.

Here we present relativistic electron precipitation data acquired with the SEEP (Stimulated Emission of Energetic Particles) experiment on the S81-1 spacecraft. Intensities



Paper number 90JA02343.
0148-0227/91/90JA-02343$05.00

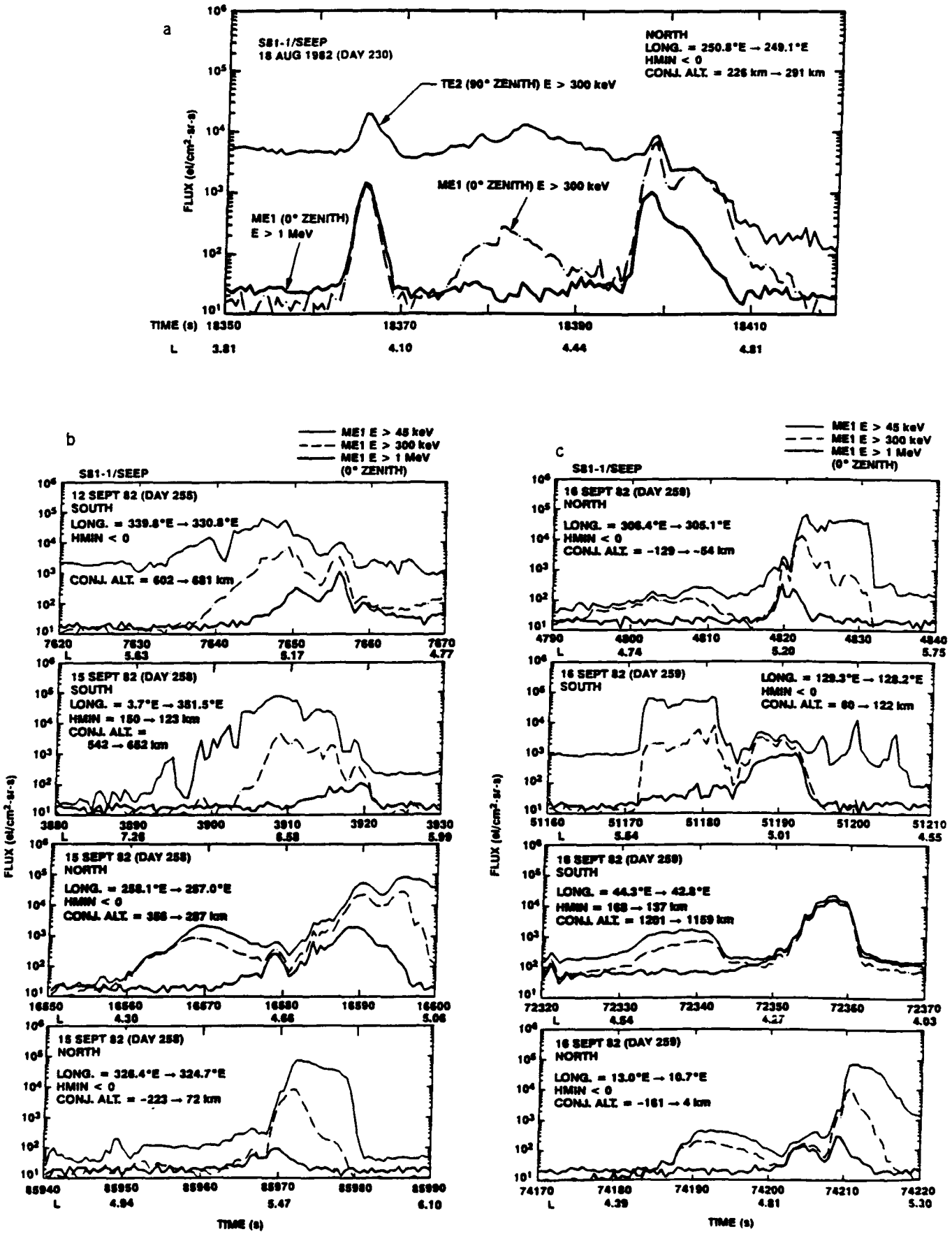


Fig. 1. Examples of flux enhancements observed on selected satellite passes. Backgrounds have not been subtracted.

and spatial distributions of precipitating electrons above 1 MeV are considered. For lower-energy electrons we investigate the threshold energy for isotropy and its dependence on $L$ shell near the trapping boundary.

## DESCRIPTION OF INSTRUMENTATION

The Stimulated Emission of Energetic Particles (SEEP) experiment on the three-axis-stabilized S81-1 spacecraft contained an array of cooled silicon solid-state detectors to measure electrons and ions [*Voss et al.*, 1982]. The data were acquired over the period from May 28, 1982, until December 5, 1982. The S81-1 satellite was in a Sun synchronous 1030 and 2230 local time polar orbit (inclination of 96.3°) at 170–280 km altitude, traveling southward during the daytime. The electron spectrometers were oriented at various angles to the local vertical. Here data are used from three of the spectrometers. The spectrometer TE2 at 90° zenith angle (approximately 90° pitch angle for the data presented) had an acceptance angle of ±20° and a geometric factor of 0.17 cm$^2$ sr. The pulse height analyzer for the data presented had a range of 6–930 keV with energy steps of 3.62 keV. The TE2 spectrometer had a very thin window on the Si detector so that >3-keV electrons and >30-keV protons could enter. The instruments ME1 and ME2 at zenith angles of 0° (approximately 30° pitch angle for most of the data presented and therefore in the bounce loss cone) and 180°, respectively, had acceptance angles of ±30°, geometric factors of 2.47 cm$^2$ sr, threshold energies of 45 keV, and energy resolutions of about 20 keV. The pulse height analyzer covered the range 45 keV to approximately 980 keV. The silicon detectors in ME1 and ME2 were surrounded except for the entrance aperture side by plastic scintillator anticoincidence shields with an internal energy threshold of about 100 keV. The ME1 and ME2 detectors had relatively thick windows; ~7 μm of Kapton double coated with ~0.1 μm of aluminum for a total thickness of ~1.1 mg/cm$^2$. The penetration threshold energy for electrons was ~22 keV and for protons was ~500 keV. Total integral counting rates above several thresholds in each of the spectrometers were recorded during successive 0.064-s intervals, and the pulse height address of the first count in each successive 0.004-s interval was recorded for TE2 and ME1.

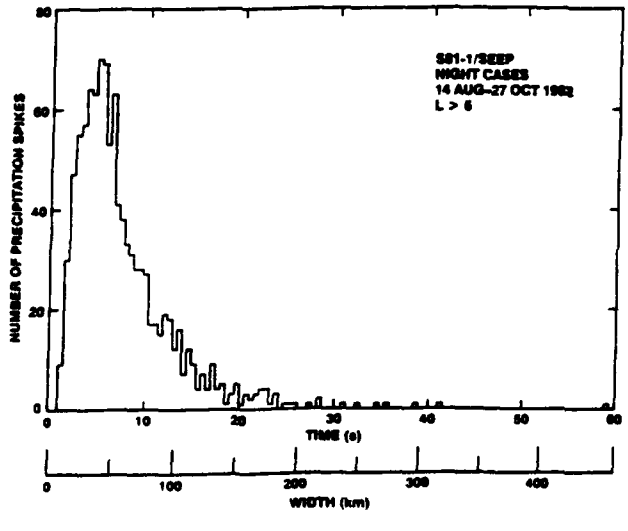


Fig. 2. Distribution in observed temporal/spatial width of the nighttime precipitation spikes.

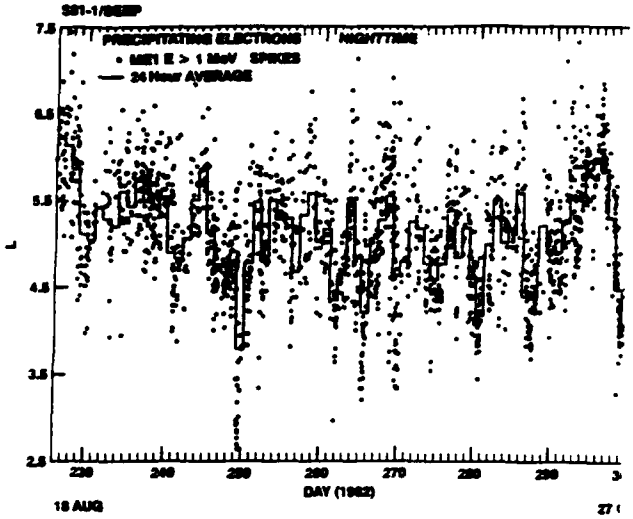


Fig. 3. $L$ value for each nighttime spike of precipitating electrons >1 MeV versus day number for days 226–300, August 1982, to October 27, 1982.

For ME2 the sampling interval is twice as long (0.008 s). During data analysis, energy spectra can be accumulated over an arbitrary time period. In the ME1 and ME2 spectrometers counts were also recorded in each corresponding anticoincidence counter, both singles and in coincidence with the silicon detector; for electrons the threshold energy was ~1 MeV. The geometric factor for the singles response was 3.09 cm$^2$ sr with an acceptance angle of ±30°. Electrons above ~15 MeV could be detected with a nearly omnidirectional response, but based on the relative responses observed in ME1 and ME2 the latter contribution is ignored for the data studied here.

In the data analysis, $L$ values were calculated using the Goddard Space Flight Center (GSFC 12/66) geomagnetic field model [*Cain et al.*, 1967] for the epoch 1980.

## LOCATIONS OF PRECIPITATING ELECTRONS ABOVE 1 MEV

On midnight passes of the S81-1 satellite at high latitudes narrow spikes of precipitating electrons above 1 MeV and well within the bounce loss cone were often observed. An example of a satellite pass with such flux enhancements is illustrated in Figure 1*a*, which shows the fluxes of mirroring (TE2) and precipitating (ME1) electrons above 300 keV. Due to the low altitude of the satellite, at certain locations locally mirroring electrons are precipitating because they are in the bounce loss cone (when the altitude of the conjugate point is below sea level), or in many places they are in the drift loss cone (when the minimum altitude upon longitude drift around the Earth, $h_{min}$, is <0 km). The case in Figure 1*a* is unusual in that within the same satellite pass, significant fluxes of electrons above 1 MeV are precipitating in narrow spikes both near the trapping boundary and at somewhat lower latitudes. If present, the precipitation observed with the ME1 detector is generally at only one location, although the widths and shapes may differ considerably, as illustrated in Figures 1*b* and 1*c*. In the latter figures are shown the fluxes of precipitating electrons above 45 keV, 300 keV, and 1 MeV. Throughout this paper the fluxes above 1 MeV are based on the total counting rate in the anticoincidence shield. The rate of coincidences between the silicon senso

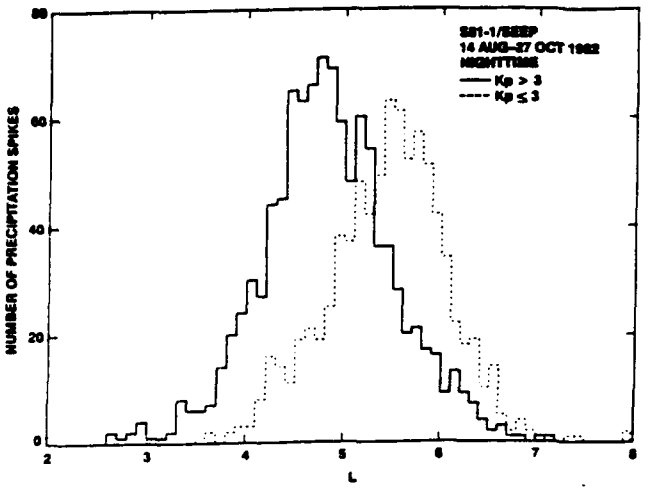


Fig. 4. Distribution in $L$ value for each nighttime spike of >1-MeV precipitating electrons, separately for $Kp \leq 3$ and for $Kp > 3$ for days 226–300, August 14, 1982, to October 27, 1982.

and the antiscintillator shield was typically about 80% of antisingles rate for the data presented here. Backgrou due to cosmic rays have not been subtracted.

A survey for relativistic electron spikes well within bounce loss cone was conducted. To be qualified as a pc in this survey, it was required that the anticoincide counting rate in the ME1 spectrometer, which was view upward, increase above background by at least a factor c and that the increase be significantly above that in antichannel of the ME2 detector, which had an acceptar angle in the downward direction. A variety of narrow spik occurred, but most commonly the enhanced fluxes abov MeV were observed for less than 10 s (77 km) and w generally between $L$ of 4 and 6. The distribution in transit ti (or equivalent spatial width) of the nighttime spikes is showr Figure 2. Here the full widths are taken to be at one-fi maximum. The equivalent spatial widths in kilometers a shown for a satellite velocity of 7.7 km/s. The transit ti intervals shown in the figure should not have been influenc by the selection criteria used in the original survey except tl

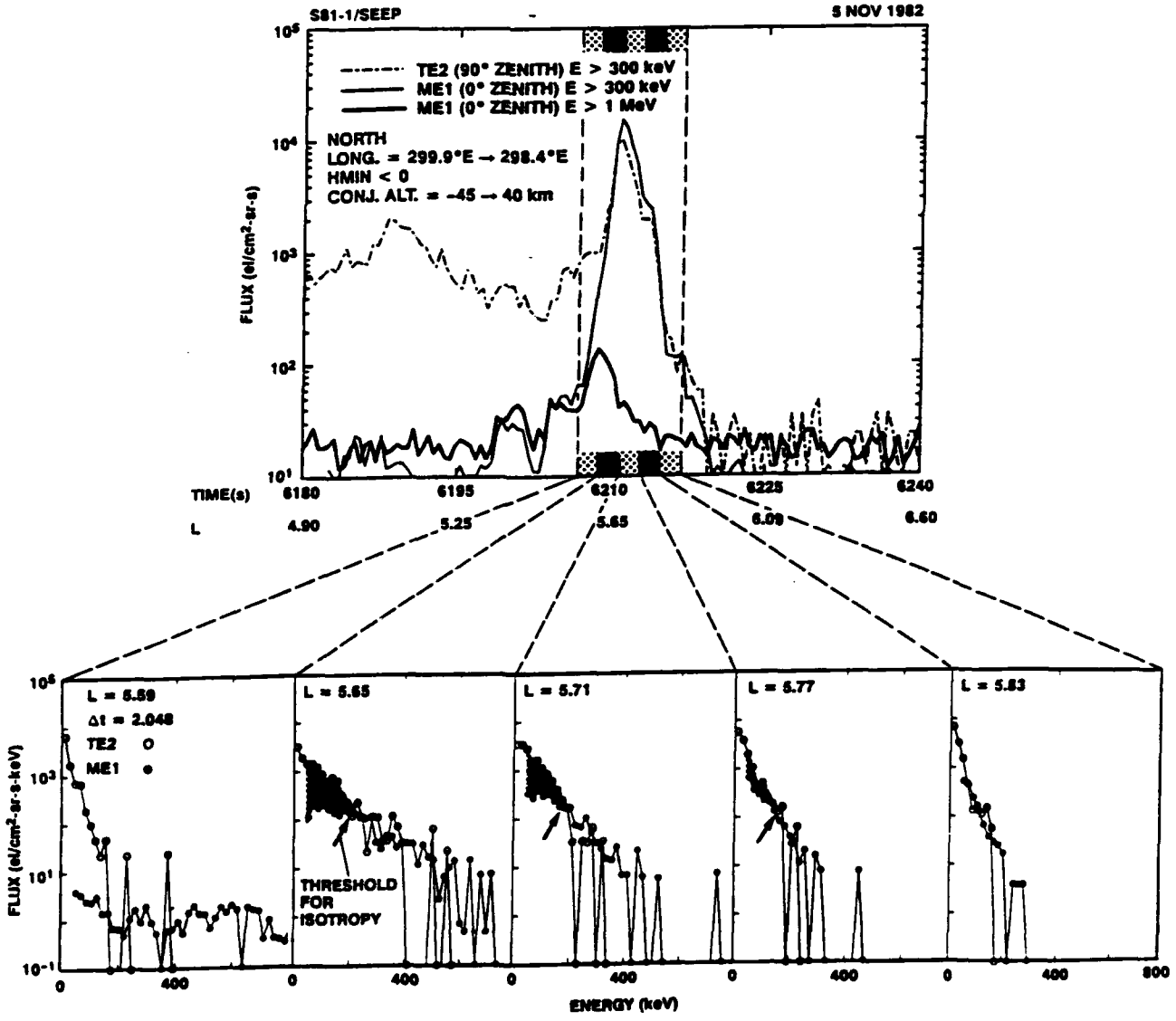


Fig. 5. Integral fluxes above various threshold energies at 0° and 90° zenith angle versus time (upper section). At selected times are shown differential energy spectra for accumulation time periods of 2.048 s each for detectors ME1 (0°) with a vertical field of view and TE2 (90°) with a horizontal field of view (lower section).

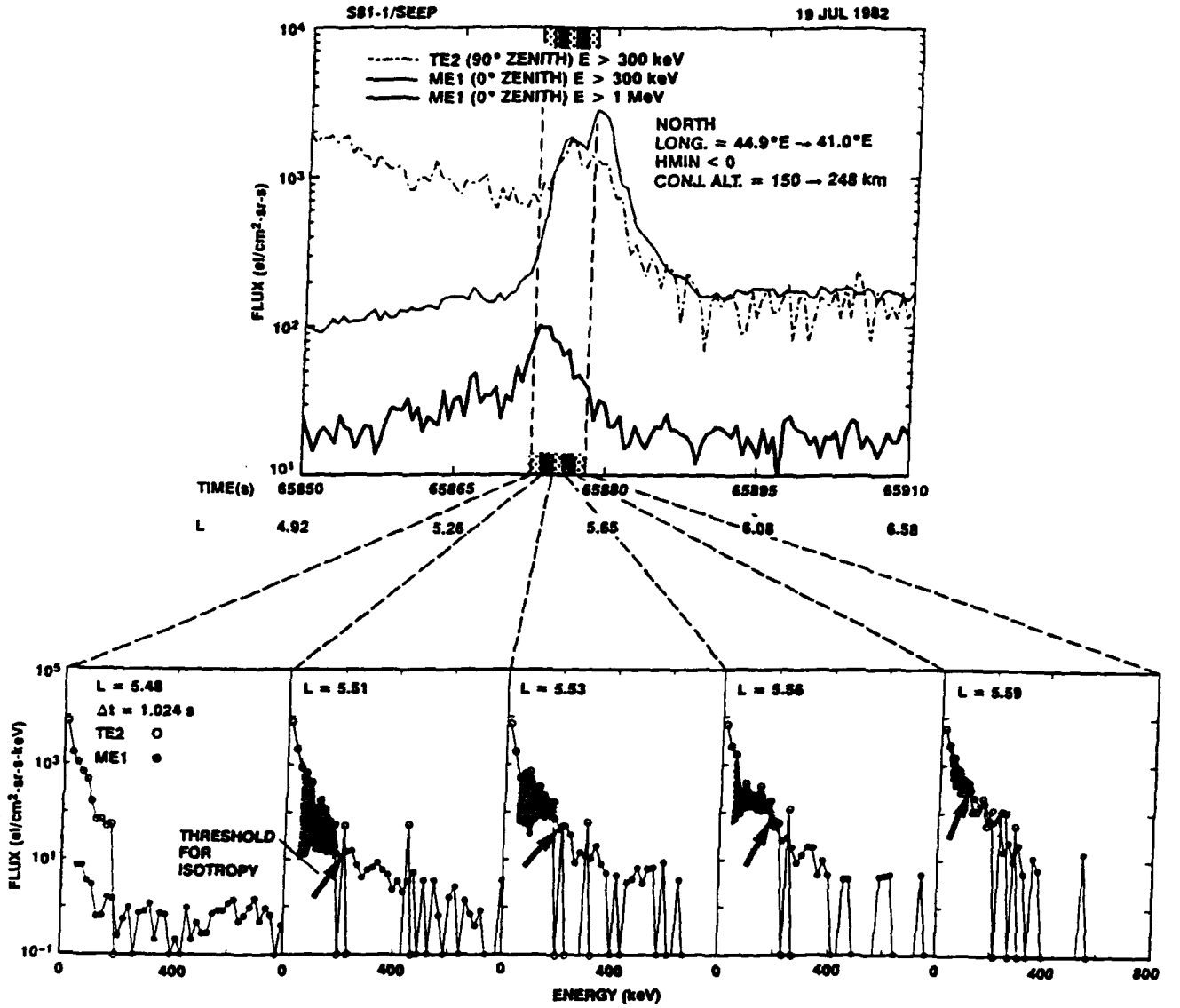


Fig. 6. Integral fluxes above various threshold energies at 0° and 90° zenith angle versus time (upper section). At selected times are shown differential energy spectra for accumulation time periods of 1.024 s each for detectors ME1 (0°) and TE2 (90°) (lower section).

spikes narrower than ~1 s were not included in the survey. The data indicate that relativistic electron precipitation in the bounce loss cone tends to occur over very localized regions. Seldom does the enhanced precipitation extend over a broad latitude interval on any given satellite pass. The average width is about 40 km, and 90% of the spikes have a width <100 km. This finding has important implications both for total energy input into the atmosphere and for efforts to understand the responsible precipitation mechanisms. Of course, some or many of the spikes may have been arclike in extent perpendicular to the satellite path.

Some of the questions which naturally arise are, What is the $L$ value at which the relativistic precipitation spikes occur, and how does the $L$ shell of this location change with geomagnetic activity? To study the problem in greater detail, a representative period, from August 14, 1982, to October 27, 1982, was selected. For this time period the location of the observed precipitation is plotted in Figure 3 for each spike. Twenty-four-hour averages are also shown in the figure. Very low latitude spikes were found on day 249 (September 6, 1982), with several precipitating flux enhancements occurring at calculated $L$ values between 2.5 and 3.0. The overall distributions in $L$ value are shown in Figure 4, separately for $Kp \leq 3$ and $Kp > 3$. It is clear from the figure that at times of higher $Kp$ the relativistic electron precipitation spikes tend to occur at lower $L$ values. Nearly all of the spikes below an $L$ value of 4.5 occur during geomagnetically active times.

## Isotropy Near the Trapping Boundary

Since the spikes of precipitating electrons above 1 MeV generally occur in the outer portions of the radiation belt, it seems appropriate to investigate the consistency of these patterns with those of lower-energy electrons at such positions. Near the midnight trapping boundary the occurrence of $L$ dependent peaks in the flux of precipitating electrons that vary with energy and energy selective thresholds for isotropy has previously been reported [*Imhof et al.*, 1977, 1979; *Imhof*, 1988], but the measurements were all from

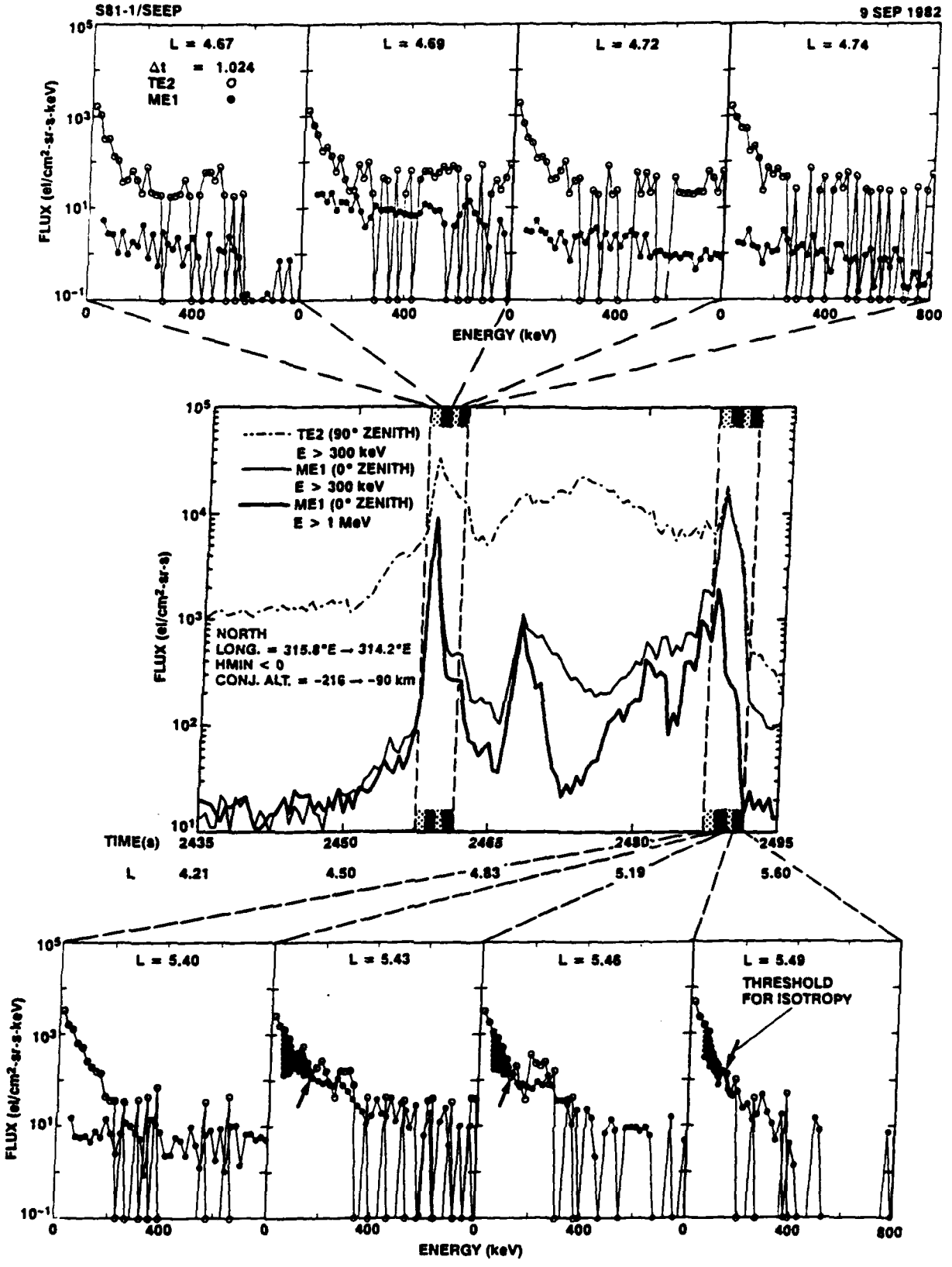


Fig. 7. Integral fluxes above various threshold energies at 0° and 90° zenith angle versus time (middle section). At selected times are shown differential energy spectra for accumulation time periods of 1.024 s each for detectors ME1 (0°) and TE2 (90°) (top and bottom section).

spinning satellites, and accordingly the precipitating electrons were recorded during only a small fraction of the observing time. Now we consider nighttime data from the S81-1 satellite in which the precipitating and trapped electrons were each observed continuously with 0.064-s time resolution. *Integral fluxes above 300 keV threshold energy* at 0° (ME1) and at 90° (TE2) zenith angle are plotted as a function of time in the upper section of Figure 5. Also plotted

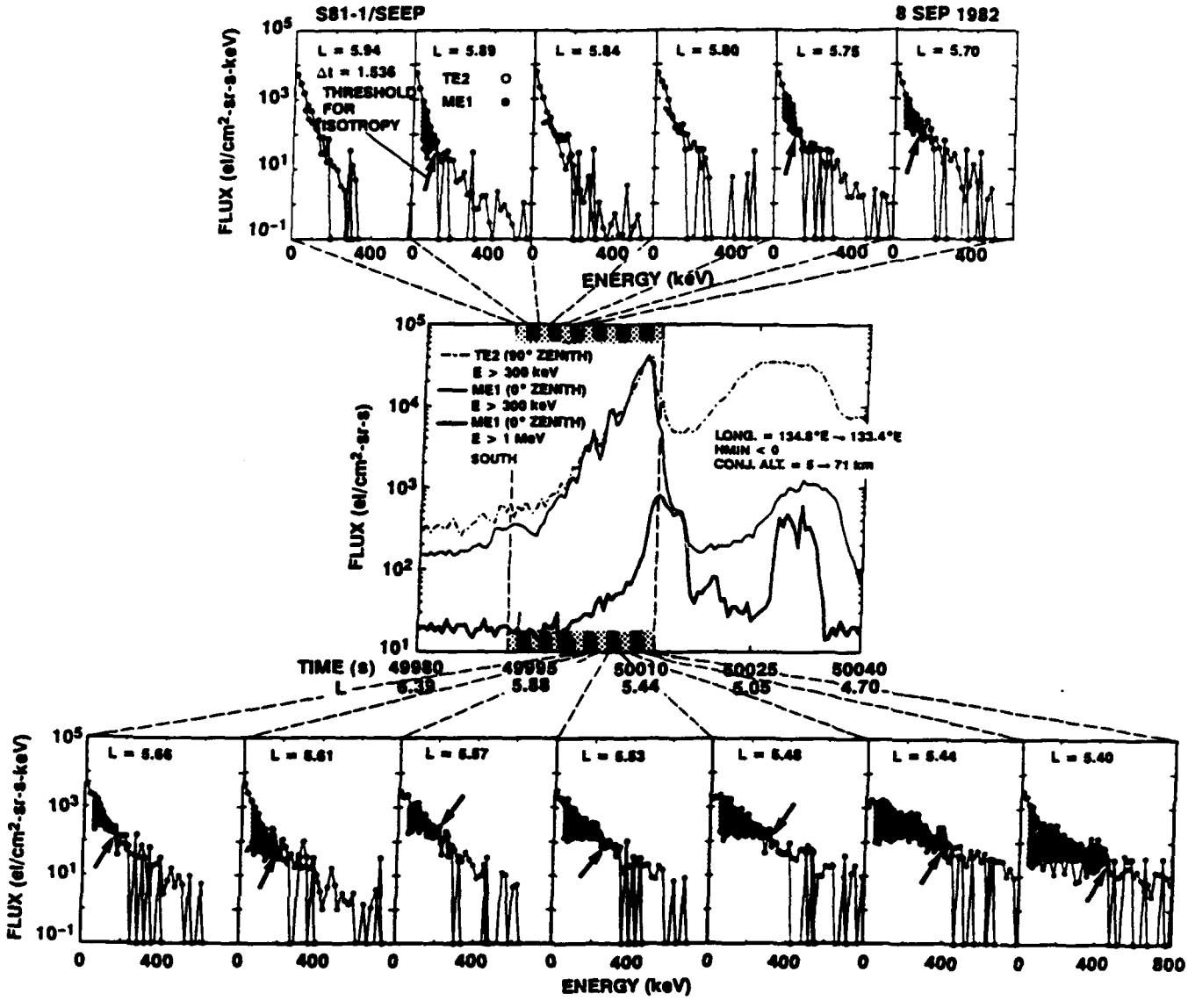


Fig. 8. Integral fluxes above various threshold energies at 0° and 90° zenith angle versus time (*middle section*). At selected times are shown differential energy spectra for accumulation time periods of 1.536 s each for detectors ME1 (0°) and TE2 (90°).

are the integral fluxes above 1 MeV of precipitating electrons as measured with the ME1 anticoincidence detector. Backgrounds, which are small compared to the counting rates in many of the spikes, have not been subtracted. The typical flux enhancement at the trapping boundary is evident. The figure illustrates the trend for the higher-energy electrons to precipitate over a more confined region at somewhat lower $L$ shells.

Differential spectra with fine energy resolution were obtained by recording individual addresses at a maximum rate of 250 per second. Differential energy spectra for detectors ME1 and TE2 are shown in the lower sections of Figure 5 at selected times during the crossing of the trapping boundary for accumulation time periods of 2.048 s each. At certain locations the appearance of a threshold energy for isotropy is evident. At energies below this threshold a crosshatch pattern is placed between the trapped and precipitating fluxes. Consistent with previous publications the threshold energy tends to decrease with increasing $L$ value. A similar pattern for another nighttime crossing of the satellite is shown in Figure 6 for spectral accumulation time periods of 1.024 s each.

Figure 7 shows an example of a nighttime satellite pass when several pronounced precipitation spikes occurred within the outer radiation belt in addition to a spike at the trapping boundary. Selected energy spectra are shown for accumulation time periods of 1.024 s each. A threshold energy for isotropy appeared in the spectra near the trapping boundary, and the energy tended to decrease with increasing $L$ value, but no such spectra appeared in the spike near 2460 s at lower $L$ values. The spectra at the lower $L$ shells were harder than those near the trapping boundary.

More complex cases than the data just shown were observed. Figure 8 contains a nighttime example in which energy selective isotropy did not display a monotonic behavior at all $L$ values. The spectral accumulation time periods were 1.536 s each. Pronounced threshold energies for isotropy occurred poleward of the trapping boundary. One might speculate that at such positions the magnetic field line geometry may be similar to that at the trapping boundary.

The changes in spectral shape of the trapped and precipitating electrons during narrow and pronounced variations in

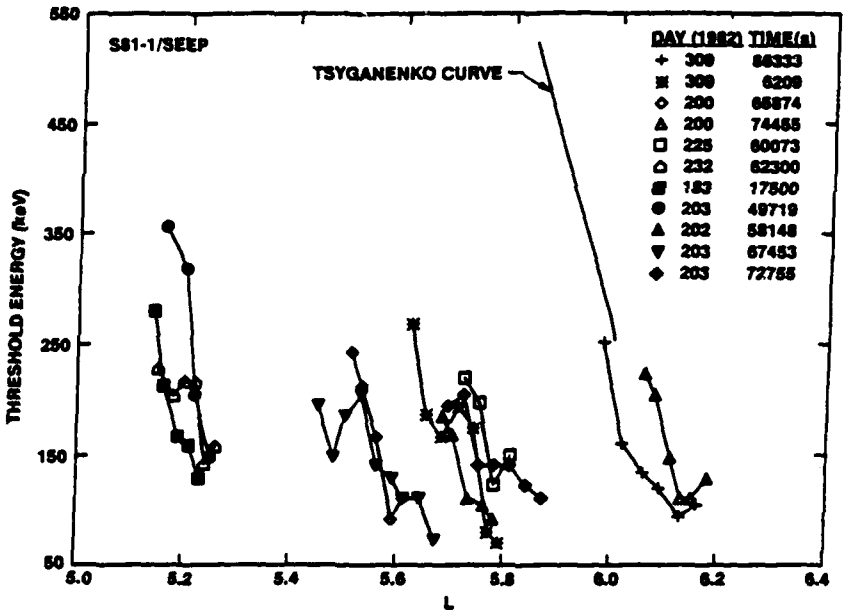


Fig. 9. Observed threshold energy for isotropy versus $L$ for 1.024-s intervals on passes near the midnight trapping boundary.

flux can be obtained with much finer time resolution by using the observed counting rates above 45, 100, and 300 keV rather than the differential spectra which have limited statistical accuracy due to the low sampling rate. From such analyses it can be shown that changes in spectral shape for the ME1 detector sometimes occur in close coincidence with the strong decreases in precipitating flux.

In Figure 9 the observed threshold energy for isotropy is plotted as a function of $L$ at positions near the midnight trapping boundary for 11 passes. The figure shows the highest energy at which the flux in the loss cone is less than the flux of locally mirroring electrons, as a function of $L$ value for each pass. Whereas the energy spectra just shown were for accumulation time periods of 1.024–2.048 s, all of the threshold energies plotted in Figure 9 were taken from spectral accumulations of 1.024 s each. Also shown are theoretical calculations using the Tsyganenko strong storm model as published in the work by *Popielawska et al.* [1985]. The slopes of the measurements are consistent with the theory. However, the data were acquired during geomagnetically quiet periods, whereas the calculations of Tsyganenko were for storm time conditions. On these passes the observed values of the threshold energy for isotropy versus $L$ are in good agreement with the calculations, assuming loss of adiabatic motion for small radii of field line curvature. However, the observed $L$ shell patterns of threshold energy for isotropy at nighttime are sometimes quite different. Such examples might indicate the importance of other mechanisms or the occurrence of variations in the magnetic field geometry.

## Electrons Above 1 MeV

We have surveyed the nighttime data on many satellite passes across the trapping boundary and searched for times when the counting rate in the ME1 anticoincidence detector was enhanced and significantly greater than in the ME2 anticoincidence counter. The peak fluxes were tabulated, as were the fluxes integrated over the time duration of each spike. The peak precipitation fluxes at $L > 5$ from August 14 through October 27, 1982, are plotted in the top section of Figure 10 as a function of time. A background of 60 counts/s was subtracted from the peak counting rate in each spike. In converting from counting rate to flux we have used a geometric factor of 3.09 $cm^2$ sr which is rigorously applicable only to isotropic fluxes. Based on other measurements of electron precipitation near the trapping boundary [e.g., *Imhof*, 1988] we have concluded that many of the electron spikes considered here are isotropic. Also shown are 24-hour averages of the average peak flux recorded on each pass, including zero flux for passes when no spikes were observed. On some days the average precipitating fluxes were below the threshold level of about 20 electrons (>1 MeV)/$cm^2$ sr s for reporting a spike since few or no precipitation spikes were observed on certain passes.

Although there is considerable variation from one pass to the next in the fluxes of precipitating electrons above 1 MeV, some overall trends are apparent. The longer-term increases of the order of days shown in Figure 10 tended to occur at the times of relativistic enhancements observed at synchronous altitude [*Baker et al.*, 1986]. Bars near the top of the figure show the time periods of these events. For comparison the *Kp* and *Dst* values are plotted in the lower two sections of Figure 10. Large variations appear in the observed flux from one satellite pass to the next.

We have investigated how much of the scatter in data points may be associated with variations in geomagnetic field geometry. The dependence of the flux upon the longitude of observation is plotted in Figure 11, separately for the northern and southern hemispheres. Figure 12 shows the variation of flux with the conjugate point altitude and with the minimum drift altitude, $h_{min}$. The precipitating fluxes show no obvious dependence upon the altitude of the conjugate point, and upon $h_{min}$. From the low-altitude S81-1 satellite, positive values of $h_{min}$ were encountered primarily in the southern hemisphere, but the range of positive $h_{min}$ values corresponds to only a small portion of the southern hemisphere longitudes plotted in Figure 11.

To see how the flux varies with geomagnetic activity, the distributions in peak flux at nighttime of the spikes of

precipitating electrons above 1 MeV are presented in Figure 13 separately for $Kp \leq 3$ and for $Kp > 3$ for the period of August 14 through October 27. This display illustrates the large variations in flux that occur and the lack of a strong dependence on $Kp$.

We can also check the day/night dependence of these events. All of the observations presented so far were acquired during satellite nighttime. A comparison with daytime observations is shown in Figure 14, which gives the frequency of occurrence versus the flux. The data come from a representative sample of the S81-1 data, using all of the precipitation events which were observed between September 6, 1982, and October 2, 1982. Satellite data coverage was nearly complete, both day and night, during this time interval. It is clear from the figure that ~80% of the cases occurred on the nightside of the Earth.

## SUMMARY AND DISCUSSION

In the vicinity of the midnight trapping boundary of the radiation belt, highly relativistic electrons frequently precipitate in the bounce loss cone in narrow spikes, often at high intensity. From a low-altitude satellite the spikes typically have an observing time duration shorter than 10 s or a width of less than 100 km. At nighttime the precipitation of electrons above 1 MeV in energy has been measured to occur at widely variable intensities and locations. Most of the nighttime precipitation spikes of such electrons occur at

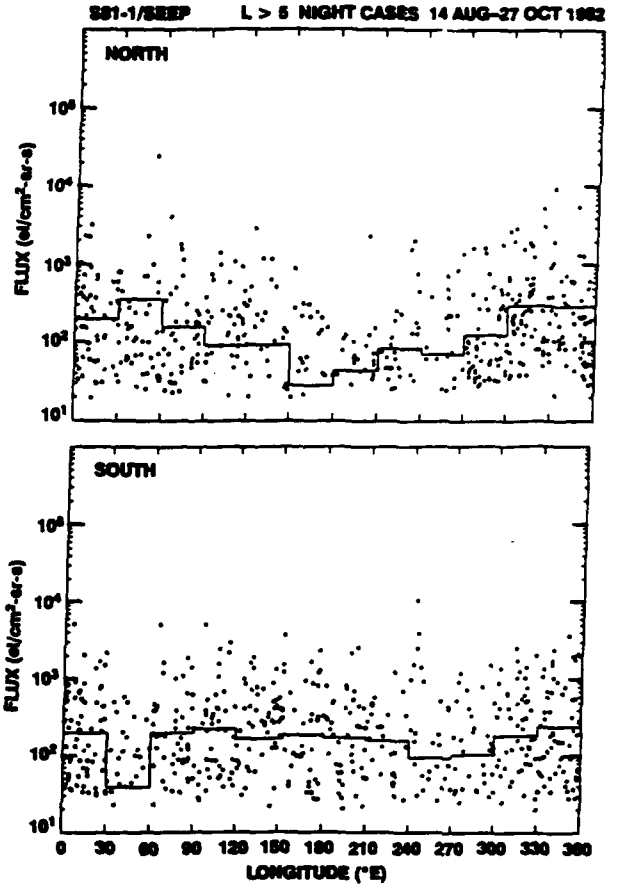


Fig. 11. Fluxes of nighttime precipitating electrons above 1 MeV plotted as a function of longitude, separately in the northern and southern hemispheres.

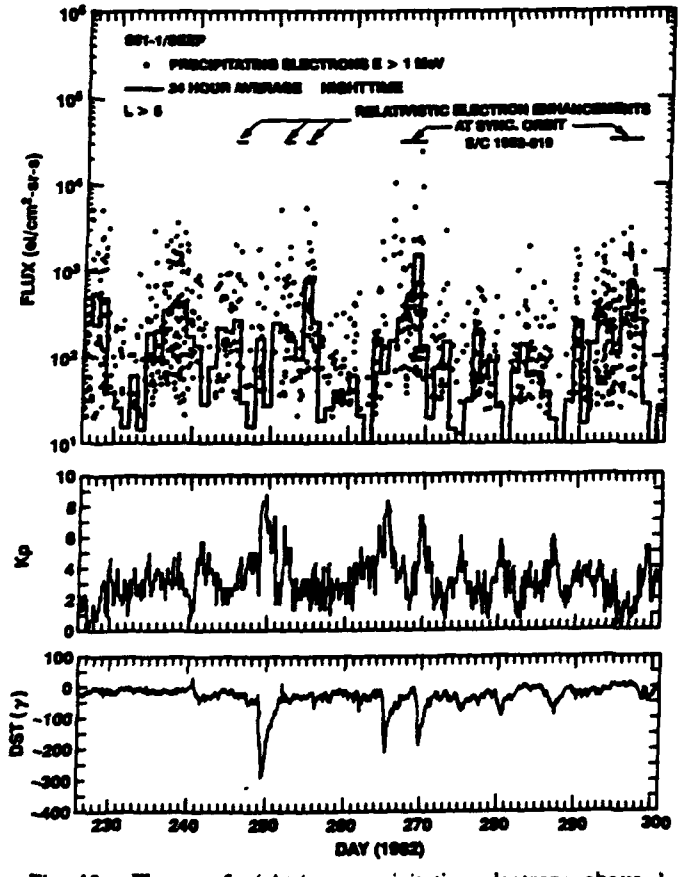


Fig. 10. Fluxes of nighttime precipitating electrons above 1 MeV plotted as a function of time (top section). The bars represent time periods of relativistic electron enhancements at synchronous altitude. The 3-hour $Kp$ index and the $Dst$ index are plotted versus time in the lower sections.

$L$ values between 4 and 6. Precipitating electrons of this energy in the bounce loss cone were also observed in the daytime, but significant precipitation occurred less often. The preferred nighttime occurrence within a narrow latitude band is consistent with the findings of *Vampola* [1971] and of *Thorne and Andreoli* [1980]. Many of the highly relativistic electron spikes presented here are near the trapping boundary, usually at the low $L$ shell portion of the boundary consistent with the general pattern at lower energies of intensity and threshold energy versus $L$ shell. Stimulated by the need to understand in detail the positions of precipitation of relativistic electrons as well as the mechanism(s) responsible for an energy threshold for isotropy we have used the SEEP data to study electron precipitation near the trapping boundary.

We have found that near the outer edge of the nighttime radiation belt the $L$ shell dependence of the energy threshold for isotropy is often consistent with loss of adiabatic motion when the radius of field line curvature is less than an order of magnitude greater than the gyroradius of the electrons. The mechanism was found by *Büchner and Zelenyi* [1989] to be more effective for very small equatorial pitch angles. It would then affect primarily electrons mirroring at low altitudes and not necessarily require that at the trapping boundary there be a collapse of the magnetic field line at high altitudes. Near the trapping boundary the observed $L$ shell patterns of threshold energy for isotropy are sometimes quite different, indicating the importance of other mechanisms or the occurrence of variations in the magnetic field geometry. These results confirm earlier studies using spinning satellites.

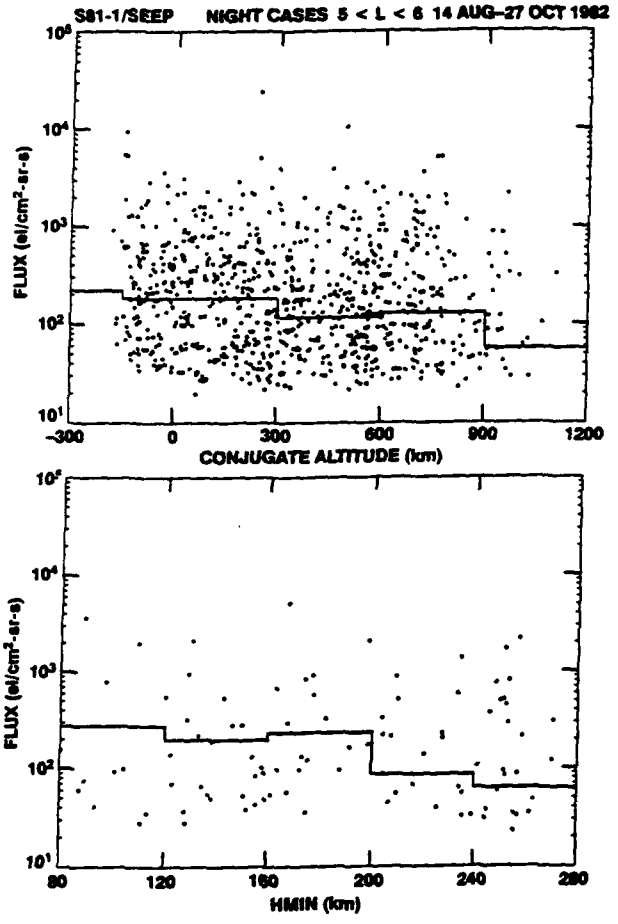


Fig. 12. Fluxes of nighttime precipitating electrons above 1 MeV plotted as a function of the conjugate altitude (upper section) and the minimum drift altitude, $h_{min}$ (lower section).

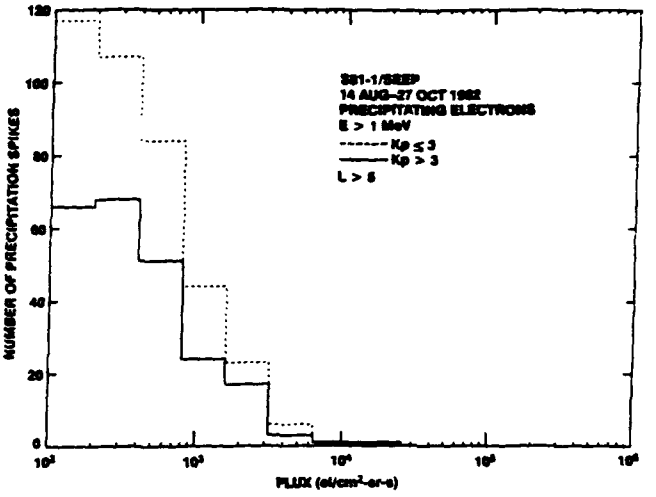


Fig. 13. Distribution in the peak flux of the spikes of precipitating electrons above 1 MeV separately for $Kp \leq 3$ and for $Kp > 3$ where $L > 5$. For the lower geomagnetic activity range there were a total of 382 spikes whereas 231 spikes occurred when $Kp$ was above 3.

Consideration should be given to the possible importance of wave-particle interactions. *Vampola* [1977] and *Koons et al.* [1972] demonstrated that a number of outer zone electron boundary phenomena can be explained on the basis of a rapid pitch angle scattering by electrostatic wave interaction. Although wave-particle interactions are clearly very important, a threshold energy for isotropy is present on most satellite passes across the boundary, and to attribute this always to waves would require the nearly continuous presence of waves at this position with a characteristic pattern for the $L$ dependence of a cutoff in frequency.

From a superposed epoch analysis of the fluxes at synchronous altitude, *Nagai* [1988] found there is a rapid decrease in the flux of electrons above 2 MeV in association with an enhancement of geomagnetic activity followed by an increase in the flux which peaks approximately 4–5 days after the enhancement of geomagnetic activity. The 24-hour averages presented in Figure 10 of this paper show time profiles for precipitating electrons above 1 MeV that are not inconsistent with those reported by *Nagai* [1988]. However, at the peak of geomagnetic activity the fluxes of >1-MeV precipitating electrons were generally located at lower $L$ values than that of a synchronous satellite and were often below $L = 5$. In a future survey, comparisons will be made between low-altitude data and available measurements at synchronous altitude.

The satellite S81-1 typically passed through the interval $L = 4$ to $L = 6$ in about 100 s. In the first 12-hour period on day 252 (September 9) the average total counts acquired at nighttime in the spikes of directly precipitating electrons above 1 MeV during a pass through all $L$ values was $10^5$, compared to $\sim 5 \times 10^3$ when there were no spikes. Most of the latter counts were background in nature and not associated with precipitating electrons. This average counting rate of ~1000 counts/s yields an average flux of 324 el/cm$^2$ sr s in the interval $4 < L < 6$ (invariant latitudes 60°–65.9°). This region is where most of the precipitation of electrons above 1 MeV occurs. The area of this interval over 12 hours of local time is approximately $6 \times 10^{16}$ cm$^2$ in each of the northern and southern hemispheres. If the relativistic electron precipitation at all nighttime hours was the same as at ~2230 and

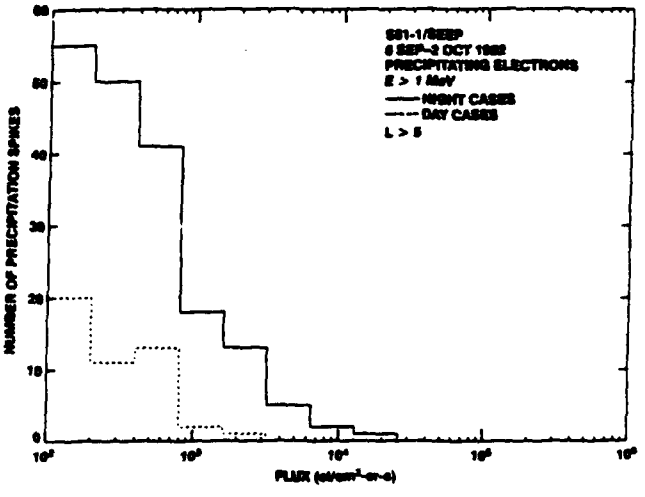


Fig. 14. Distribution in the peak flux of the spikes of precipitating electrons above 1 MeV, separately for day and night data. The time period covered is from September 6, 1982, through October 2, 1982. For $L > 5$ at nighttime there were 185 spikes, whereas in the daytime over this same time period there were 48 spikes.

was the same in both hemispheres, then the total rate of precipitation of electrons above 1 MeV was $\sim 1.2 \times 10^{20}$ el/s or $\sim 5 \times 10^{24}$ electrons in 12 hours. With an average energy per precipitated electron of 2 MeV [*Baker et al.*, 1987], the total nighttime energy input from electrons in the bounce loss cone during this 12-hour period on September 9, 1982, was $\sim 10^{19}$ ergs. We have shown that the frequency of occurrence of spikes of precipitating relativistic electrons is much smaller in the daytime than at night. We have also shown (Figure 11) that the precipitating flux is not strongly dependent upon longitude and therefore these same precipitating fluxes should apply on a global scale. After normalization for time duration differences this value is an order of magnitude less than the rough estimate of the total energy input for a 2.5-day period from >1-MeV electrons of $7 \times 10^{20}$ ergs reported by *Baker et al.* [1987] for a different electron event in June 1980. This finding may indicate that much of the precipitation is in the drift loss cone, a phenomenon not covered in the measurements reported here. A major cause of the difference between these two sets of values appears to be the large difference in invariant latitude width taken for the precipitation: 17° for Baker et al., compared to about 5.9° found in the present study.

The total loss rate into the atmosphere of electrons in the bounce loss cone above 1 MeV as measured at low satellite altitudes seems to be inconsistent with the loss rates inferred from synchronous high-altitude measurements. The difference between low-altitude and synchronous measurements is even greater when the low-altitude measurements are limited to $L$ shells near those at synchronous satellites, about 6.7. Precipitation spikes of electrons above 1 MeV were not often evident in the low-altitude satellite data acquired near $L = 6.7$. Suitable high-altitude measurements at other $L$ shells are not available in the published literature. Precipitating fluxes as high as 1400 el/cm$^2$ s were inferred from synchronous data by *Baker et al.* [1987], and such fluxes were observed in the bounce loss cone low-altitude measurements presented here only at very localized positions. It would appear that many of the relativistic electrons lost from the synchronous positions were not precipitated in the bounce loss cone directly into the atmosphere but were perhaps in the drift loss cone or were transported radially inward or outward.

A possible mechanism for the acceleration of electrons to relativistic energies has been postulated by *Baker et al.* [1989]. The mechanism involved inward radial diffusion of the electrons in which a large energy gain was followed by an energy-preserving outward transport, thus returning the accelerated population to the outer magnetosphere. Baker et al. suggested that in the inner magnetosphere the electrons are scattered in pitch angle with many not being scattered completely into the loss cone. In the present observations, significant fluxes of precipitating electrons were observed on September 6 prior to the time of an event, at $L = 2.5$–$3.5$, as shown in Figure 3. This finding is not presented as a validation of any mechanism, but it may be important to realize that enhanced fluxes of relativistic electrons were precipitating in the inner magnetosphere near the time of maximum flux of relativistic electrons at geostationary orbit.

*Acknowledgments.* The SEEP experiment on the S81-1 satellite was sponsored by the Office of Naval Research (contract N00014-79-C-0824). Much of the data analysis presented here was sponsored by the Air Force Office of Scientific Research (contract F-49620-88-C-0072) and by the Office of Naval Research (contract N00014-88-C-0033). The Lockheed Independent Research program provided partial support for the analysis. The dedicated efforts of J. P. McGlennon and D. P. Eaton in data reduction are gratefully acknowledged. We also thank D. N. Baker for making some synchronous altitude data available to us.

The Editor thanks P. R. Higbie and J. B. Blake for their assistance in evaluating this paper.

## REFERENCES

Baker, D. N., J. B. Blake, R. W. Klebesadel, and P. R. Higbie, Highly relativistic electrons in the Earth's outer magnetosphere, 1, Lifetimes and temporal history 1979–1984, *J. Geophys. Res.*, *91*, 4265, 1986.

Baker, D. N., J. B. Blake, D. J. Gorney, P. R. Higbie, R. W. Klebesadel, and J. H. King, Highly relativistic magnetospheric electrons: A role in coupling to the middle atmosphere?, *Geophys. Res. Lett.*, *14*, 1027, 1987.

Baker, D. N., J. B. Blake, L. B. Callis, R. D. Belian, and T. E. Cayton, Relativistic electrons near geostationary orbit: Evidence for internal magnetospheric acceleration, *Geophys. Res. Lett.*, *16*, 559, 1989.

Büchner, J., and L. M. Zelenyi, Regular and chaotic charged particle motion in magnetotaillike field reversals, 1, Basic theory of trapped motion, *J. Geophys. Res.*, *94*, 11,821, 1989.

Cain, J. C., S. J. Hendricks, R. A. Langel, and W. V. Hudson, A proposed model for the International Geomagnetic Reference Field, *J. Geomagn. Geoelectr.*, *19*, 335, 1967.

Fritz, T. A., High-latitude outer-zone boundary region for ≥40-keV electrons during geomagnetically quiet periods, *J. Geophys. Res.*, *73*, 7245, 1968.

Fritz, T. A., Study of the high-latitude, outer-zone boundary region for ≥40-keV electrons with satellite Injun 3, *J. Geophys. Res.*, *75*, 5387, 1970.

Imhof, W. L., Fine resolution measurements of the $L$-dependent energy threshold for isotropy at the trapping boundary, *J. Geophys. Res.*, *93*, 9743, 1988.

Imhof, W. L., J. B. Reagan, and E. E. Gaines, Fine-scale spatial structure in the pitch angle distributions of energetic particles near the midnight trapping boundary, *J. Geophys. Res.*, *82*, 5215, 1977.

Imhof, W. L., J. B. Reagan, and E. E. Gaines, Studies of the sharply defined $L$ dependent energy threshold for isotropy at the midnight trapping boundary, *J. Geophys. Res.*, *84*, 6371, 1979.

Koons, H. C., A. L. Vampola, and D. A. McPherson, Strong pitch angle scattering of energetic electrons in the presence of electrostatic waves above the ionospheric trough region, *J. Geophys. Res.*, *77*, 1771, 1972.

Nagai, T., "Space weather forecast": Prediction of relativistic electron intensity at synchronous orbit, *Geophys. Res. Lett.*, *15*, 425, 1988.

Popielawska, B., E. Szalinska-Piechota, and N. A. Tsyganenko, On the nonadiabatic particle scattering in the Earth's magnetotail current sheet, *Planet. Space Sci.*, *33*, 1433, 1985.

Thorne, R. M., and L. J. Andreoli, Mechanisms for intense relativistic electron precipitation, in *Exploration of the Polar Upper Atmosphere*, edited by C. S. Deehr and J. A. Holtet, p. 381, D. Reidel, Hingham, Mass., 1980.

Vampola, A. L., Electron pitch angle scattering in the outer zone during magnetically disturbed times, *J. Geophys. Res.*, *76*, 4685, 1971.

Vampola, A. L., The effect of strong pitch angle scattering on the location of the outer-zone electron boundary as observed by low-altitude satellites, *J. Geophys. Res.*, *82*, 2289, 1977.

Voss, H. D., J. B. Reagan, W. L. Imhof, D. O. Murray, D. A. Simpson, D. P. Cauffman, and J. C. Bakke, Low temperature characteristics of solid state detectors for energetic X-ray, ion and electron spectrometers, *IEEE Trans. Nucl. Sci.*, *NS-29*, 164, 1982.

D. W. Datlowe, E. E. Gaines, W. L. Imhof, J. Mobilia, and H. D. Voss, Lockheed Palo Alto Research Laboratory, 3251 Hanover Street, Palo Alto, CA 94304.

(Received July 9, 1990;
revised October 15, 1990;
accepted October 17, 1990.)

# APPENDIX B

## RELATIVISTIC ELECTRON ENHANCEMENTS; SIMULTANEOUS MEASUREMENTS FROM SYNCHRONOUS AND LOW ALTITUDE SATELLITES

GEOPHYSICAL RESEARCH LETTERS, VOL. 18, NO. 3, PAGES 397-400, MARCH 1991

# RELATIVISTIC ELECTRON ENHANCEMENTS: SIMULTANEOUS MEASUREMENTS FROM SYNCHRONOUS AND LOW ALTITUDE SATELLITES

W. L. Imhof, H. D. Voss, J. Mobilia, D. W. Datlowe, J. P. McGlennon

Lockheed Palo Alto Research Laboratory, Palo Alto, California

and D. N. Baker

Goddard Space Flight Center, Greenbelt, Maryland

*Abstract.* We present here for the first time simultaneous measurements of trapped relativistic electron enhancements at synchronous altitude and precipitating electrons in the bounce loss cone at low altitudes. The measurements show that the daily variations in the precipitation flux for L>5 correlated well with the daily variations in the total flux at high altitude, both with respect to sudden enhancements as well as flux depletions. The daily averaged precipitating flux (E > 1 MeV) at L = 6.1 to 7.1 was about 0.3 percent of the daily averaged directional flux (E $\geq$ 1.5 MeV) observed at synchronous altitude, whereas within narrow spikes the precipitating directional fluxes were often within a factor of 10 of the daily averaged trapped fluxes. Strong depletions in the synchronous altitude $\geq$ 1.5 MeV electron intensities are shown to be associated with low altitude measurements of the equatorward movement of precipitating spikes to lower L shells.

## Introduction

*Relativistic electron enhancements* have been studied extensively using measurements taken on synchronous-orbit satellites (e.g. Baker et al., 1986). Detailed information on the frequency of occurrence of these events and on the energy spectra was obtained. In the past, good correlations have been found between the relativistic electrons at synchronous altitude and the > 1 MeV electron fluxes at 840 km altitude (Baker et al., 1990), but the low altitude observations were not limited to directly precipitating electrons in the bounce loss cone. These measurements have not provided much knowledge of the extent in L-shell of the enhanced region or of the fluxes of relativistic electrons precipitating directly into the atmosphere. Vampola (1971) reported S3-3 measurements of precipitating relativistic electrons at altitudes from 362 to 4480 km. Some information on the L-shell extent and on the fluxes of relativistic electrons precipitating in the loss cone has currently become available for a few events (Imhof et al., 1991) from low altitude satellite measurements. However, many critical questions still remain unanswered. How well do electrons trapped at high altitude and those in the bounce loss cone track each other? In particular, when flux decreases are observed at synchronous altitude near the beginning of an event what are the corresponding changes at low altitude? How does the L-shell extent at low and high altitudes compare? Many of these questions can be answered with simultaneous relativistic electron measurements at high and low altitudes. Here such data are presented, and of particular interest are strong events with relatively steep onsets.

## Description of Instrumentation

We present here a comparison of the data from electron detectors on the low altitude S81-1 satellite with the electron data from the synchronous altitude 1982-019 satellite. The instrumentation for the S81-1 payload is described in Voss et al. (1982) and in Imhof et al. (1991) and the instrumentation for the 1982-019 payload is described in Baker et al. (1986).

The Stimulated Emission of Energetic Particles (SEEP) experiment on the S81-1 spacecraft contained an array of cooled silicon solid state detectors to measure electrons and ions. The data were acquired over the period from May 28, 1982 until December 5, 1982. The S81-1 three-axis stabilized satellite was in a sun synchronous 1030 and 2230 local time polar orbit (inclination = 96.3°) at altitudes from 170 to 280 km. The electron spectrometer ME1 at a zenith angle of 0° (less than 30° pitch angle for much of the data presented and therefore in the bounce loss cone) and ME2 at a zenith angle of 180° had acceptance angles of $\pm$30°. At these altitudes the field-of-view of the ME1 detector is entirely within the bounce loss cone. The silicon detectors in ME1 and ME2 were surrounded (except for the entrance aperture) by plastic scintillator anticoincidence shields. Counts were recorded in each corresponding anticoincidence counter, both singles and in coincidence with the silicon detector; only one threshold level was used and for electrons the threshold energy for detection was ~1 MeV. The geometric factor for the singles response was 3.09 cm$^2$ sr with an acceptance angle of $\pm$30°.

Electron flux measurements at high altitude were taken with the Spectrometer for Energetic Electrons (SEE) flown at geostationary orbit on board spacecraft 1982-019. The spectrometer is a two element telescope consisting of two silicon detectors (operated in parallel) and a bismuth germanate scintillation crystal. The SEE sensor makes integral electron measurements at energies $\geq$ 1.5 MeV and four differential measurements at higher energies.

## Presentation of Data

A survey for relativistic electron spikes well within the bounce loss cone was conducted with the SEEP data. To qualify as an event in this survey, it was required that the plastic scintillator singles counting rate in the ME1 spectrometer, which was viewing upward, increase above background by at least a factor of two and that the increase be significantly above that in the scintillator of the ME2 detector which was viewing downward.

Precipitating electrons above 1 MeV were measured with the anticoincidence detector in the ME1 spectrometer as noted above. When these fluxes were enhanced they were typically above background in the form of spikes near the trapping boundary with 10 second observation or less (equivalently a spatial width of less than 100 km (Imhof et al., 1991)). Precipitation spikes observed for less than one second were not included in the survey. For studying the time profiles one can use either the maximum flux or the time integrated flux (fluence) measured in each spike during a satellite pass. Both approaches have been used for comparisons of S81-1 data with measurements at synchronous altitude and give consistent results. Here we present analyses based on the maximum flux in each spike.



Paper number 91GL00132
0094-8534/91/90GL-00132$03.00

Averages of the peak fluxes have been obtained both for spikes at all L values and also restricting their inclusion only to spikes at L>5. In the latter case the enhancements were more pronounced; accordingly, all flux plots presented here are limited to L values above 5. Figure 1 shows these fluxes plotted as a function of time. The background rate which was typically about 60 counts per second has been subtracted from the peak counting rate in each spike. The spike fluxes vary considerably from one satellite pass to the next. Also shown are 24 hour averages of the average peak flux recorded on each pass; for these averages zero flux is assumed for a pass when no spikes were observed at L>5. On some days the averaged precipitating fluxes were below the threshold level for reporting a spike since no precipitation spikes were observed on many of the passes. Analyses of the low altitude data were performed for median flux values in addition to average values and gave nearly the same results.

For comparison, the two sets of data, S81-1 and S/C 1982-019, are plotted in Figure 2 as a function of day number in 1982. Daily averages of the precipitating electron flux above 1 MeV measured in the ME1 anticoincidence detector on the S81-1 spacecraft are shown. In converting from counting rate to flux we have used a geometric factor of 3.09 $cm^2$ sr which is rigorously applicable only to isotropic fluxes. Based on other measurements of electron precipitation near the trapping boundary (e.g. Imhof, 1988) we have assumed that many of the electron precipitation spikes considered here are isotropic. Also plotted are 24 hour averages (multiplied by a factor of 0.01) of the electron directional flux $\geq$ 1.5 MeV measured in the SEE detector on S/C 1982-019. It is clear that on a daily basis the > 1 MeV precipitating electrons in the bounce loss cone as observed at low altitudes track rather well the $\geq$ 1.5 MeV electrons trapped at synchronous altitude.

The daily averaged fluxes of electrons precipitating at L>5 were about an order of magnitude less than the fluxes of electrons trapped at high altitude on L = 6.6. The daily averaged fluxes of precipitating electrons at L = 6.1 to 7.1 were about 0.3 percent of the daily averaged fluxes observed at synchronous altitude. However, in the narrow spikes the precipitating fluxes were often within a factor of 10 of the daily averaged fluxes trapped at high altitude. Much of the reduction in the daily averaged precipitating fluxes relative to the trapped fluxes at high altitude can perhaps be attributed to irregular access of electrons to the bounce loss cone. Of course in many cases the precipitation may be only in the drift loss cone.

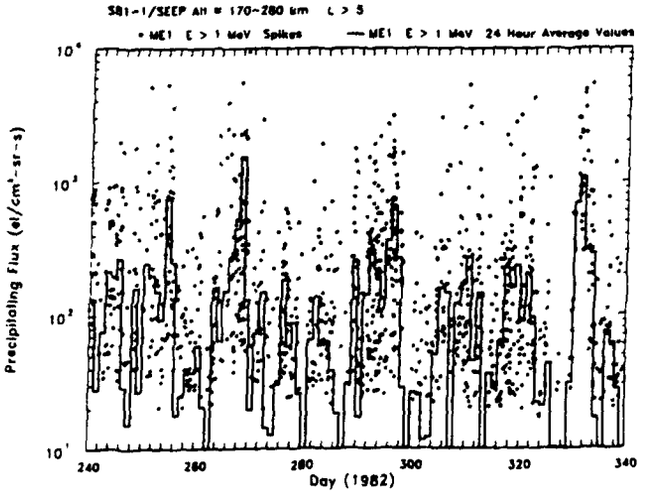


Fig. 1. The maximum fluxes in each spike of precipitating electrons >1 MeV at low altitudes from the S81-1 satellite plotted as a function of time. Also shown are 24 hour averages of the maximum fluxes.

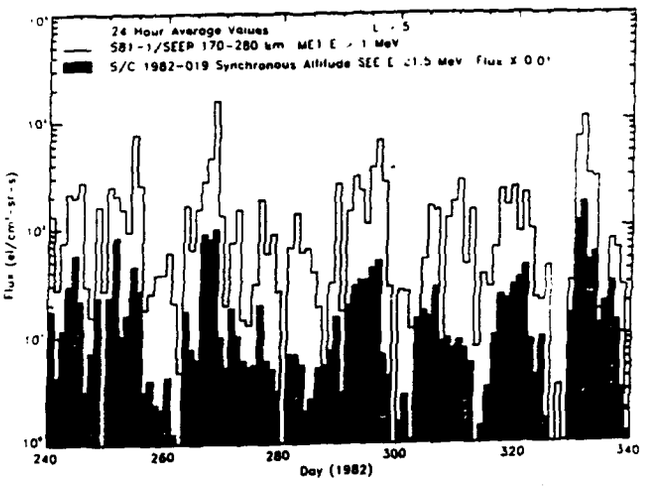


Fig. 2. Daily averaged fluxes of precipitating electrons >1 MeV measured at low altitudes on the S81-1 satellite and electrons recorded at synchronous altitude on S/C 1982-019. The latter electrons are at energies of $\geq$ 1.5 MeV and their corresponding fluxes are multiplied by 0.01 for clarity.

In prior studies of the high altitude data (e.g., Baker et al., 1986), there has been much attention paid to the 27-day recurrence tendency seen in the relativistic electron component. In the present study we have only 100 days of concurrent low-altitude and high-altitude data available and it is difficult to verify a true periodicity in such a limited interval. Moreover, the strong 27-day recurrences reported by Baker et al. for the SEE data become particularly prominent later (i.e., in 1984-85) than the present analysis interval. Nonetheless, Figure 2 does show some tendency for 27-day enhancements with, perhaps, an interleaving of two cycles to give evidence of 13-day recurrences.

In Figure 3 the daily averaged fluxes of precipitating electrons above 1 MeV as measured at L>5 in the anticoincidence scintillator of the ME1 spectrometer on the low altitude S81-1 satellite are plotted versus the daily averaged electron fluxes $\geq$ 1.5 MeV recorded at synchronous altitude in

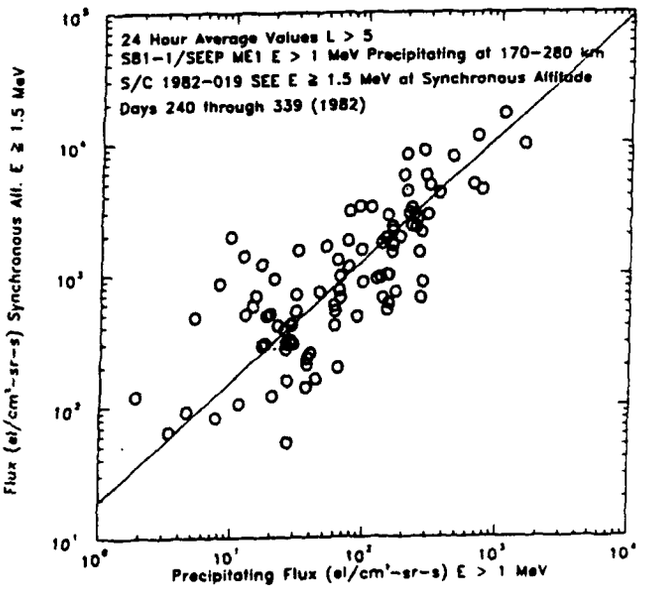


Fig. 3. Daily averaged electron fluxes $\geq$ 1.5 MeV obtained at synchronous altitude on S/C 1982-019 versus the daily averaged fluxes of precipitating electrons >1 MeV as measured on the satellite S81-1.

the SEE instrument. By inspection, one can see that the precipitating flux > 1 MeV correlates well with the high altitude flux ≥ 1.5 MeV. The correlation coefficient is 0.77, significant at the 11.8 sigma level for 96 points. For spikes at L≤5 no significant correlations were found. The low altitude observations occurred at exactly the same L value (6.6) as the synchronous measurements for only a small fraction of the time, but the low altitude coverage of the precipitation spikes is sufficient to make a comparison of the two sets.

We have investigated the correlation between the precipitation fluxes at low altitudes and the rates of decrease of electrons at high altitudes. The latter quantities were obtained by considering the correlations between the precipitation flux at low altitudes and the trapped flux at high altitudes on the previous day and on the previous two days as well as on the following day and the following two days. These results are summarized in Table 1. The correlations are clearly best when both sets of measurements are simultaneous within one day.

At times of pronounced decreases in the high altitude flux there is often a significant equatorward movement in the L-value of the precipitation spikes, suggesting that the drop outs in the high altitude flux, which often occurred at times of increased geomagnetic activity, may be due to an inward movement of the trapped electrons. In Figure 4 the daily averaged high altitude fluxes of electrons ≥1.5 MeV are plotted as a function of the daily averaged L values of the spikes of precipitating electrons above 1 MeV. The correlation coefficient is 0.62, significant at the 7.8 sigma level for 100 points. There is a reasonably clear relationship between the logarithm of the flux at 6.6 $R_E$ and the averaged L value: thus the decrease at synchronous altitudes is associated with an inward motion.

Table 1. Correlation Values Between the Precipitation Flux at Low Altitudes and the Trapped Flux at High Altitudes (for 96 Days)

| SEE Data | Correlation Coefficient | Statistical Significance (Sigma) |
|---|---|---|
| 2 Days Before | +0.13 | 1.2 |
| 1 Day Before | +0.36 | 3.7 |
| Same Day | +0.77 | 11.8 |
| 1 Day After | +0.50 | 5.5 |
| 2 Days After | +0.16 | 1.5 |

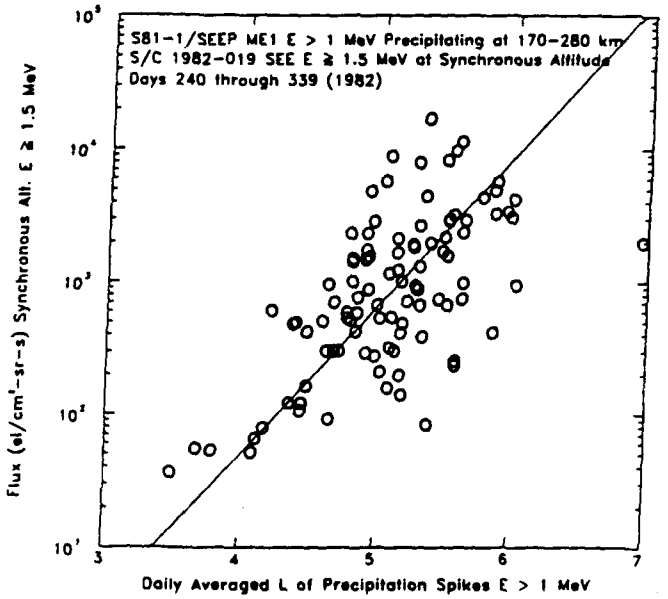


Fig. 4. Daily averaged fluxes of electrons ≥ 1.5 MeV at high altitude versus the daily averaged L values of electron > 1 MeV spikes measured in the bounce loss cone.

## Summary

We have found good correlations between the time dependence of the fluxes of relativistic electrons trapped at synchronous altitude and of relativistic electrons precipitating into the atmosphere. During narrow spikes well within the loss cone the precipitating directional intensities were often within a factor of 10 of the daily averaged trapped directional intensities at high altitudes, whereas the daily averaged precipitating fluxes were only about 0.3 percent of the trapped fluxes. A proper comparison of the high and low altitude electron populations would be to map adiabatically conserved quantities according to Liouville's theorem in a realistic magnetic field model. Such a comparison has not yet been performed in detail for each event. Additional precipitation may appear primarily only near the edge of the loss cone and not be within the field-of-view of the ME1 detector.

We have also investigated the L shell dependence of the precipitation of electrons above 1 MeV as a function of time. At the times of pronounced depletions in the high altitude fluxes the precipitation spikes observed at low altitudes appeared to move to lower L shells.

Ultimately, of course, it is likely that the transport of electrons into the equatorial loss cone is due to wave-particle interactions. The correlation between the fluxes of relativistic electrons measured at 6.6 $R_E$ and the precipitating electron fluxes measured by the SEEP ME1 instrument was highest when data from the same day for the respective instruments were used (see Table 1). Thus, in this sense it is the current near-equatorial flux level that determines the precipitating fluxes rather than the time rate of change of the fluxes (at least on day-long time scales). From this behavior one might conclude that the precipitation of relativistic electrons observed in spikes in the bounce loss cone is not the principal or dominant loss mechanism. From this point of view, the data are consistent with the precipitation flux resulting from interaction of the flux trapped at high altitudes with a strength of waves that is constant on a long-term basis. Then the precipitation flux would be proportional to the flux trapped at high altitude and not the rate of change of flux trapped at high altitude.

On the other hand, Baker et al. (1987) suggested that relativistic electrons may be precipitated quite rapidly. They suggested that the electrons are strongly dumped into the atmosphere when fluxes are high in the outer zone. When such flux levels are lower (as is true much of the time), they evidently are not precipitated significantly. Thus, Baker et al. envisioned the electron fluxes and the wave levels going up and down together ( on time scales < 1 day) primarily driven by variable source strength for the electrons. Hence the waves that ultimately precipitate the electrons could wax and wane along with the electron population rather than remaining constant over long periods. In this view, precipitation would be a much more significant loss process for the outer zone.

It is important to understand more globally what the outer zone electron flux variations are. It would be particularly valuable to measure relativistic electron flux variations at several different equatorial L values at the same time as we observe geosynchronous enhancements. This would more clearly delineate the global significance of this magnetospheric population and would shed light on its contribution to the global atmospheric ionization input (Baker et al., 1987; Imhof et al., 1991).

*Acknowledgments.* The SEEP experiment on the S81-1 satellite was sponsored by the Office of Naval Research (contract N00014-79-C-0824). Much of the data analysis presented here was sponsored by the Air Force Office of Scientific Research (contract F-49620-88-C-0072) and by the Office of Naval Research (contract N00014-88-C-0033). The Lockheed Independent Research program provided partial support for the analysis. The dedicated efforts of D.P. Eaton in data reduction are gratefully acknowledged. Portions of this work were also supported by the U. S. Department of Energy and by NASA.

## References

Baker, D.N., J.B. Blake, D.J. Gorney, P.R. Higbie, R.W. Klebesadel, and J.H. King, Highly relativistic magnetospheric electrons: a role in coupling to the middle atmosphere?, *Geophys. Res. Lett.*, 14, 1027, 1987.

Baker, D.N., J.B. Blake, R.W. Klebesadel, and P.R. Higbie, Highly relativistic electrons in the earth's outer magnetosphere, 1. Lifetimes and temporal history 1979-1984., *J. Geophys. Res.*, 91, 4265, 1986.

Baker, D.N., J.B. Blake, R.W. Klebesadel, D.D. Sentman, D.J. Gorney, P.R. Higbie, Highly relativistic magnetospheric electrons: lower ionospheric conductivity and long-term atmospheric variability, *Adv. Space Res.*, 10, 229-233, 1990.

Imhof, W.L., Fine resolution measurements of the L-dependent energy threshold for isotropy at the trapping boundary, *J. Geophys. Res.*, 93, 9743, 1988.

Imhof W.L., H.D. Voss, J. Mobilia, D.W. Datlowe, and E.E. Gaines, The precipitation of relativistic electrons near the trapping boundary, *J. Geophys. Res.*, *in press*, 1991.

Vampola, A. L., Electron pitch angle scattering in the outer zone during magnetically disturbed times, *J. Geophys. Res.*, 76, 4685, 1971.

Voss, H.D., J.B. Reagan, W.L. Imhof, D.O. Murray, D.A. Simpson, D.P. Cauffman, and J.C. Bakke, Low temperature characteristics of solid state detectors for energetic X-ray, ion and electron spectrometers, *IEEE Trans. Nucl. Sci.*, NS-29, 164, 1982.

D. W. Datlowe, W. L. Imhof, J. P. McGlennon, J. Mobilia, H. D. Voss, Lockheed Palo Alto Research Laboratory, Dept 91-20 Bldg. 255, 3251 Hanover Street, Palo Alto, CA 94304

D. N. Baker, NASA Goddard Space Flight Center, Code 690, Greenbelt, MD 20771

(Received: November 26, 1990;
Accepted: January 10, 1991)

# APPENDIX C

# LONGITUDE AND TEMPORAL VARIATIONS OF ENERGETIC ELECTRON PRECIPITATION NEAR THE TRAPPING BOUNDARY

JOURNAL OF GEOPHYSICAL RESEARCH, VOL. 95, NO. A4, PAGES 3829-3839, APRIL 1, 1990

# Longitude and Temporal Variations of Energetic Electron Precipitation Near the Trapping Boundary

W. L. IMHOF, J. MOBILIA, D. W. DATLOWE, H. D. VOSS, AND E. E. GAINES

*Lockheed Palo Alto Research Laboratory, Palo Alto, California*

Electron precipitation occurring at latitudes near the midnight trapping boundary was measured remotely with a satellite-borne x ray imager (>21 keV). This investigation has demonstrated for the first time the repetitive mapping of precipitation at the trapping boundary with x rays. The satellite spin motion (5.5 second period) provided repeated scans of each scene during a single pass of the satellite. When the in situ electron precipitation, measured directly with a spectrometer (>68 keV) on the same satellite, was limited to a narrow region at the trapping boundary the precipitation inferred from the x rays was generally fairly uniform over a median longitude interval of at least 45°. Significant decreases of x rays at longitudes away from the satellite crossing seldom occurred, but significant increases at certain longitudes were sometimes observed. The widespread arc patterns of the precipitation have important implications for both understanding the nature of the responsible loss mechanisms and for assessing the atmospheric effects.

## INTRODUCTION

Energetic electrons are known to precipitate into the atmosphere by a variety of mechanisms. Strong precipitation often occurs in conjunction with substorms. Short bursts of precipitation from the radiation belts can result from wave particle interactions with whistlers and chorus. Very energetic electrons are sometimes produced in discrete aurora as reported by *Swift and Gorney* [1989] and postulated by them to result from scattering by upper hybrid waves generated when the beam of electrons interacts with the ionospheric plasma. Another class of precipitation that often occurs is located near the outer edge of the radiation belt or the trapping boundary. The occurrence of an isotropic pitch angle distribution over the upper hemisphere or a filled loss cone at this location in space is quite common [e.g., *Fritz*, 1970]. Fritz measured the frequency of occurrence of isotropy as a function of magnetic local time.

The energy spectra of electrons precipitating near the trapping boundary have revealed a threshold energy for isotropy that is strongly dependent upon the $L$ value [*Imhof et al.*, 1977, 1979; *Imhof*, 1988]. The precipitation near the trapping boundary has been attributed to the radius of curvature of the magnetic field at the equator for that $L$ value [*Sergeev and Tsysganenko*, 1982; *Sergeev et al.*, 1983; *Popielawska et al.*, 1985; *Sergeev et al.*, 1987]. If the magnetic field line radius of curvature is not an order of magnitude greater than the gyroradius of the particles, the magnetic moment is not conserved [*Alfven and Fallhammer*, 1963] and consequently the particles may be precipitated. Related phenomena apply to both electrons and protons, but here we address only electron precipitation. To date evaluations of the importance of this precipitation mechanism for energetic electrons have been based primarily on measurements localized to the position of the satellite. Such observations at best do not provide a complete description of the phenomenon. To learn more about the precipitation near the trapping boundary, it is important to measure simultaneously both the longitude variations and the time dependence of the intensity of the precipitating electrons.

With remote imaging of electron precipitation, it is possible to measure both the time and spatial dependence of the precipitation near the outer edge of the radiation belt. The imaging can be accomplished with bremsstrahlung x ray mappings, a technique which has been used to investigate the profiles of energetic electron precipitation at high latitudes [e.g., *Imhof*, 1981; *Mizera et al.*, 1984; *Voss et al.*, 1983]. With this technique one can map values for the total deposition rates of energy into the atmosphere over a large area. From x ray imagery at 4 to 40 keV the precipitation patterns are frequently observed to be arc-shaped, and the observed x rays are often poleward of the radiation belt boundary [*Datlowe et al.*, 1988]. For cases when the energetic electron precipitation is limited to the immediate vicinity of the outer radiation belt boundary, the total precipitation rate is generally small compared to that in precipitation events that extend over a wider range in $L$ value. Accordingly, precipitation very close to the radiation belt boundary has not been previously mapped in detail with x rays. Measurements of x rays >50 keV obtained with a single wide-angle sensor on a spinning satellite [*Imhof et al.*, 1975] provided evidence that the x rays were generated by electrons precipitating near the trapping boundary and an indication of some temporal variations summed over a large area, but no longitude mappings were obtained. Now, from the low altitude satellite P78-1 sufficient sensitivity was achieved to map in longitude the precipitation near the trapping boundary in the stronger cases and to investigate the persistence of the precipitation for times up to a few minutes. Here we shall invoke such data to investigate electron precipitation near the trapping boundary and to compare it with cases when the dominant precipitation is below the trapping boundary.

## DESCRIPTION OF THE INSTRUMENTATION

The data presented here were acquired with two energetic electron spectrometers and an array of bremsstrahlung x ray sensors on the P78-1 spacecraft. The instrumentation is described elsewhere [*Imhof et al.*, 1980] so only a brief



Paper number 89JA03048.
0148-0227/90/89JA-03048$05.00

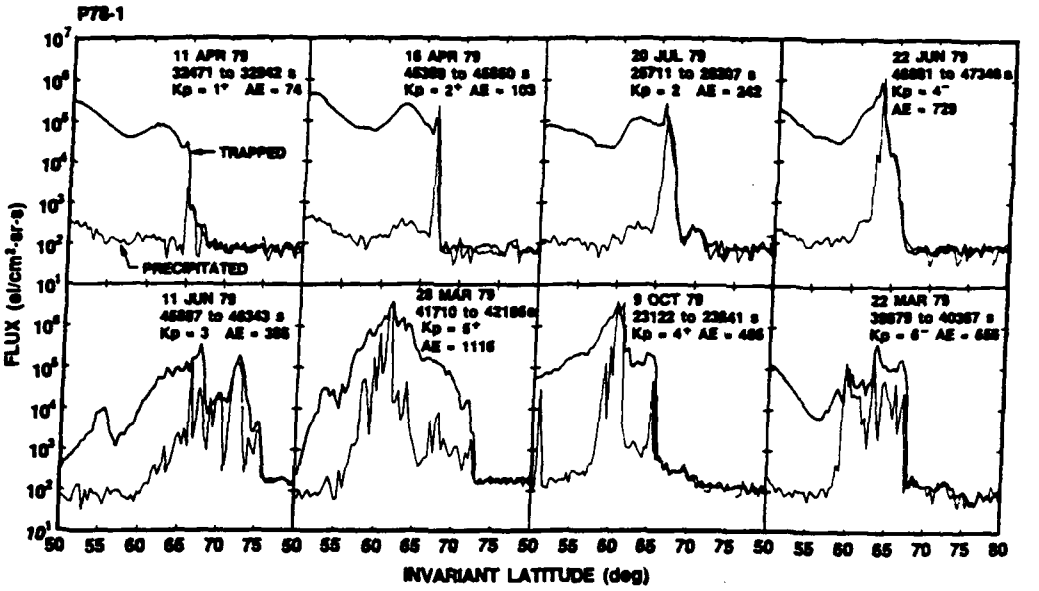


Fig. 1. Fluxes of trapped and precipitating electrons (>68 keV) measured with the EEM spectrometer as a function of the invariant latitude during each of 8 nighttime satellite passes across the trapping boundary.

presentation is given here. The P78-1 spacecraft was launched on February 24, 1979 into a sun-synchronous noon-midnight polar orbit with an apogee of about 610 km and a perigee of about 563 km. The satellite spun with a period of approximately 5.5 s about an axis perpendicular to the orbit plane. The array of x ray detectors oriented at selected view angles with respect to the spacecraft provided fine-scale mappings of the sources of x rays above 21 keV. Four CdTe sensors viewed to the right of the satellite path, and four to the left. The satellite spin motion provided repeated scans of each scene. All sensors had a viewing aperture of ±40° along the spin direction. Two of the sensors, Aa and Ab, were oriented at central view angles of 10° and 30° to the right of the plane normal to the spin axis and had a collimation of ±10° perpendicular to the spin direction. Two additional sensors viewing to the right, Ca and Cb, were oriented at 44° and 56° and had a collimation of ±6° and likewise for two sensors viewing to the left, Da and Db. A few days after launch the two sensors oriented at angles of 10° and 30° to the left failed; thus in all x ray images gaps occur at the regions viewed by these detectors.

The rectangular CdTe sensors were 2 mm thick and 7 × 22 mm in area. The threshold levels for signal analysis were set by command at 21 keV and the six energy channels spanned the following x ray energies: 21–30, 30–46, 46–68, 68–98, 98–139 and >139 keV. Counting rates were recorded with a time resolution of 0.032 second. The relative gains of the different spectrometers were monitored on-orbit through various intercomparisons, including observations of the diffuse cosmic x ray spectrum. From these in-flight measurements it was concluded that the gains of the CdTe spectrometers were stable throughout the mission and that the calibrations were almost identical in all six.

Energetic electron data were acquired with the EEM (Energetic Electron Monitor) spectrometer over the energy range 68 to 1120 keV. The detector consisted of 1000 $\mu$ of silicon of 4.5 cm$^2$ area, surrounded by a plastic scintillator-photomultiplier anticoincidence shield. Continuous multichannel spectra were obtained with a 256-channel pulse height analyzer. The inherent energy resolution of the spectrometer was 20 keV full width at half maximum (FWHM). The EEM spectrometer was designed with a collimation angle of ±15° FWHM and a relatively large geometric factor

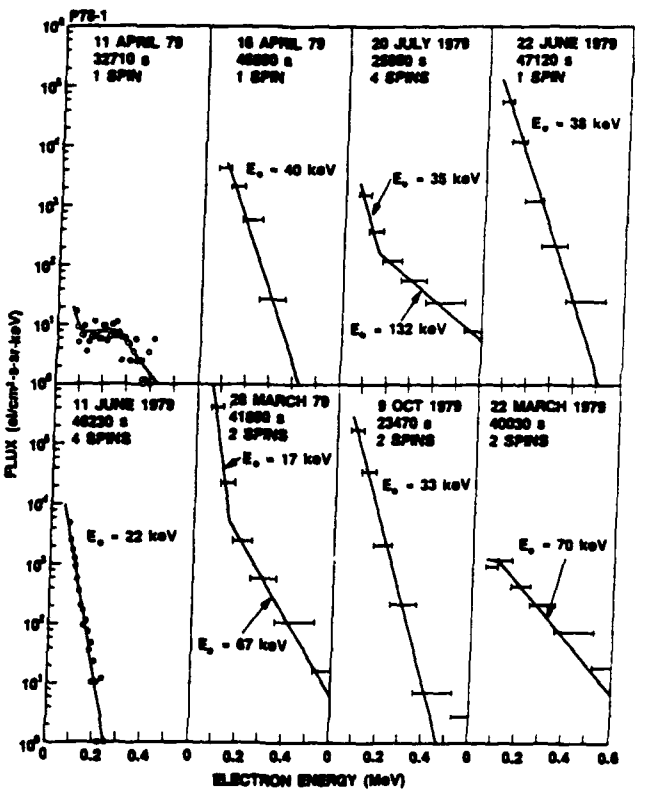


Fig. 2. The precipitating electron energy spectra measured with the EEM and the PRM spectrometers during each of the 8 nighttime satellite passes shown in Figure 1. Each of the channels are shown as open circles for the EEM data and as horizontal bars for the PRM measurements. The spectra were acquired at the time of maximum precipitation during each pass. Best-fit exponentials and the associated $E_0$ values are shown for each spectrum.

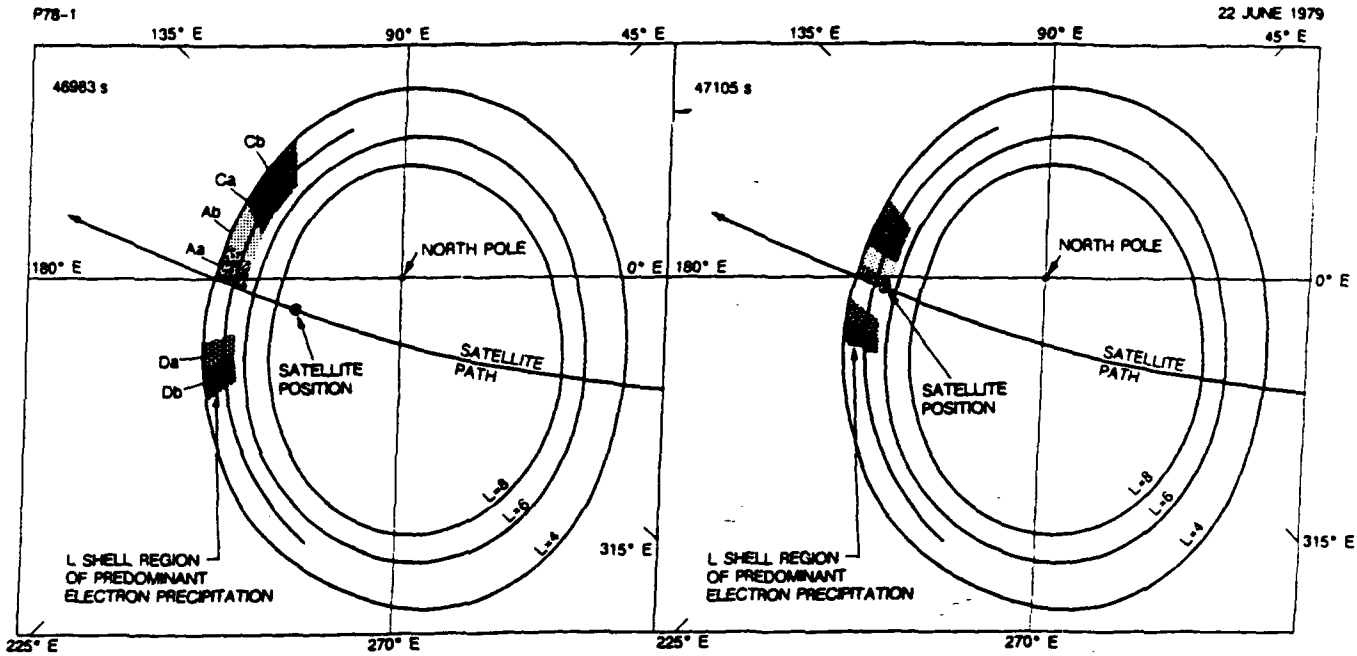


Fig. 3. The geometry for observations in x rays from the trapping boundary at two different times during a pass of the P78-1 satellite across the north polar cap.

of 0.69 $cm^2$ sr. The collimator axis was oriented at 90° to the satellite spin axis so that an electron pitch angle distribution was obtained on each spin. Counting rates were also recorded with a time resolution of 0.032 second.

Another spectrometer, designated PRM, was designed to cover approximately the same energy range, 59 keV to 1 MeV, but with a much smaller geometric factor ($10^{-3}$ $cm^2$ sr), a smaller collimation angle of ± 3.5°, and a six-channel pulse height analyzer.

In the data analysis, $L$ values were calculated using the Goddard Space Flight Center (GSFC 12/66) geomagnetic field model [*Cain et al.*, 1967] for the epoch 1980.

## PRESENTATION OF DATA

A wide variety of patterns for energetic electron precipitation from the outer radiation belt were commonly observed with the electron spectrometers. Examples of these patterns observed at night are shown in Figure 1 where the fluxes of trapped and precipitating electrons >68 keV measured with the EEM spectrometer are plotted as a function of satellite position in invariant latitude during various passes of the spacecraft. The invariant latitude is defined as $\cos^{-1}(1/(L)^{1/2})$. Both the trapped and precipitating electrons were measured with the same electron spectrometers, just at different portions of each 5.5-s satellite spin. The trapped electrons were those observed when the electron spectrometer had a central viewing angle of 65° to 115° to the magnetic field line, whereas the precipitating electrons were those traveling toward the atmosphere with the central detector angle within 25° of the field line. Both the trapped and precipitating fluxes drop sharply to the background level at invariant latitudes above ~65° on most of the satellite passes in Figure 1; this location where the trapped fluxes drop to zero is often called the trapping boundary or the outer edge of the radiation belt. On three passes, when $Kp$ was $2^+$ or less, significant electron precipitation occurred only in a very narrow region at the outer edge of the radiation belt. On another pass, with $Kp = 4^-$, the precipitation was also near the boundary, but it spanned a wider interval in $L$. Precipitation spikes sometimes occurred at a variety of $L$ values in the outer radiation belt, as illustrated in the lower four of the examples of Figure 1. As with most in situ measurements from a satellite, spatial and temporal variations are not separately identifiable in the data itself. In this sense the spacecraft motion was not deconvolved. In these particular cases the geomagnetic activity level was high. However, from analysis of the data on more satellite passes it was clear that the nature of the precipitation patterns was not well correlated with $Kp$ or $AE$.

The energy spectra of the precipitating electrons shown in Figure 1 at the positions of maximum intensity are plotted in Figure 2. Depending on the flux level the spectra shown were those acquired with either the EEM or the PRM spectrometer and accordingly have many channels shown as open circles or have a few much wider channels plotted as bars. At very large fluxes the counting rates were beyond an acceptable range for the EEM spectrometer and data from the PRM instrument were used. Best fit exponentials and the associated $E_0$ values are shown for each. These spectra are summed over one to four spins of the satellite, as indicated in the figure. The times listed are center times for accumulation of the spectra. In some cases the integration times encompass and therefore mask fine scale variations in the spectra such as the common appearance of an energy threshold for isotropy at the trapping boundary [*Imhof*, 1988]. Although a threshold for the onset of isotropy is not evident in any of the energy spectra shown in Figure 2, the spectra on July 20, 1979 displayed a pronounced threshold during one spin.

From the surveys undertaken for this investigation it was found that the fluxes of precipitating energetic electrons, with pitch angles within 40° of the field line were often

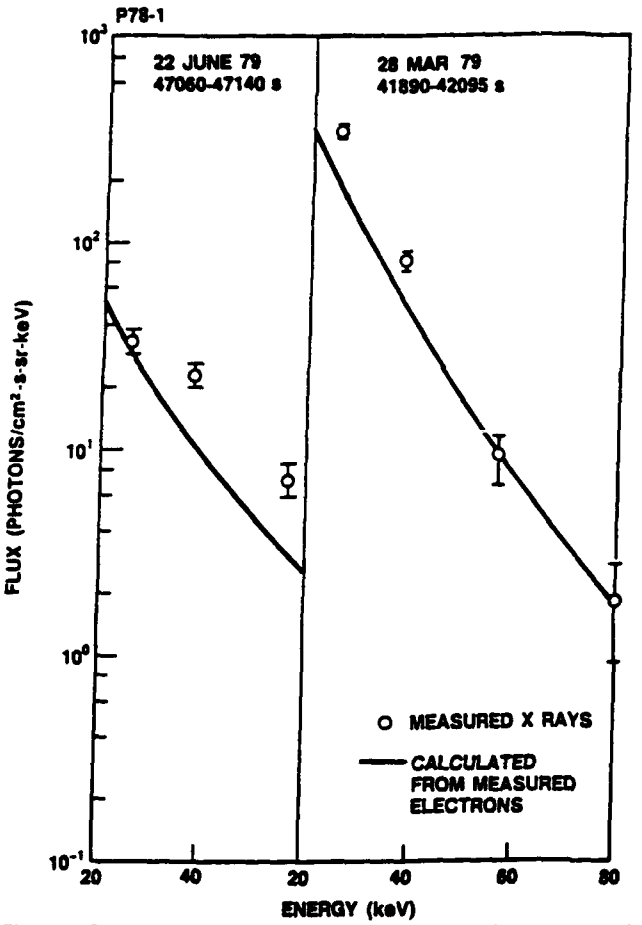


Fig. 4. Energy spectrum of x rays on two occasions measured directly and also calculated on the basis of the measured precipitating electrons.

comparable to the trapped fluxes over a narrow latitude range at the outer zone boundary on 69% of the midnight satellite passes. In these cases of isotropy the loss cone is filled and strong precipitation occurs. Due to the spinning motion of the satellite and therefore the lack of complete time coverage of the precipitating and trapped electrons, a very narrow isotropic distribution might be missed and therefore this percentage may be an underestimate. From the Injun 3 satellite *Fritz* [1970] found that an isotropic pitch angle distribution for electrons at 40 keV or higher occurred near the radiation belt boundary on 90% of the passes near local midnight. The difference from the results obtained here is perhaps statistical, but it may indicate that some instances of isotropy were missed in the present experiment because of the spinning motion of the satellite.

In this paper a distinction is made between electron precipitation localized to the trapping boundary and precipitation equatorward of this position. The exact location of the trapping boundary then becomes a critical matter. However, the precise specification of the boundary has been subjected to various definitions [e.g., *McDiarmid et al.*, 1976]. Here we shall consider the trapping boundary to be the position where the electron detector counting rate is essentially at the background rate. Slightly equatorward of this position the electron pitch angle distribution is often nearly isotropic, indicating a significant flux of precipitating electrons. The occurrence of isotropy has been used as a possible definition of the trapping boundary [*Fritz*, 1970], but here we shall locate the trapping boundary as being the position of the background boundary. However, the x ray detectors are clearly responding to the region of isotropy.

When the precipitation was confined to a region within one degree of the background boundary, i.e., the position where the electron detector counting rate was essentially at the background rate, the precipitating electron fluxes were sufficiently high on some passes to produce bremsstrahlung observable with the x ray spectrometers on the P78-1 spacecraft. The geometry for this type of measurement is illustrated in Figure 3. The figure shows the position of the satellite with respect to $L$ shell contours at two different times during a pass. Each sensor viewed the trapping boundary, the polar cap, and outer space sometime during each spin of the satellite. The angular distribution of the response thereby provides a measurement of the background. When the satellite was poleward of the trapping boundary the background in the x ray detectors was quite low. Each pixel of x ray data gives a measure of the electron precipitation summed over a wide magnetic latitude range; the six pixels give a distribution of the electron precipitation spanning 44° to 61° of longitude as illustrated in the figure. The sensors are labelled Aa, Ab, Ca, Cb, Da, and Db with the corresponding observed precipitation regions shaded. The fields of view extended over ranges of $L$ shells, but the $L$ shell values of the precipitation were obtained with broad resolution from the measured angular distributions of x rays. Because of the failure of the two sensors observing to the immediate left of the orbital plane, data are not available for these two pixels.

It is important to establish that the measured x rays truly represent the precipitating electrons. In Figure 4 are shown the x ray energy spectra obtained with spectrometer Aa which covered a region adjacent to the satellite path, during two different passes of the satellite. On one of these passes, June 22, the electron precipitation as measured with the EEM spectrometer occurred only near the trapping boundary taken to be the background boundary. On the other pass stronger precipitation occurred well within the outer radiation belt at latitudes more than one degree below the background boundary. Conversion of observed x ray flux to x ray emission was based on the positions of the satellite and the x ray production region, the known longitude width of the area viewed, and the width of the electron precipitation region measured along the satellite track by the electron spectrometer. The x ray emissions were also predicted on the basis of the spectrum and intensity of precipitating electrons measured with the EEM and PRM spectrometers. On June 22 the electron energy spectrum was taken from the single spin where the dominant precipitating flux occurred. The electron energy spectra measured during the events on March 28 were summed over the 2 spins of the satellite with the highest counting rate. Variations in spectra shape were within counting rate statistics for the two spins as well as the next most intense spin, about 30 s earlier. Fluxes at other times/latitudes are at least two orders of magnitude less than at the peak spins. Based on the measured electron spectra the x ray spectra were calculated using methods similar to those described by *Walt et al.* [1979] and recently used by *Gaines et al.* [1986]. In the two cases of Figure 4 the measured x ray values were found to be in reasonable agreement with the calculated fluxes, substantiating the assumption that x rays are produced by the precipitating electrons. However, when the precipitation spike was very

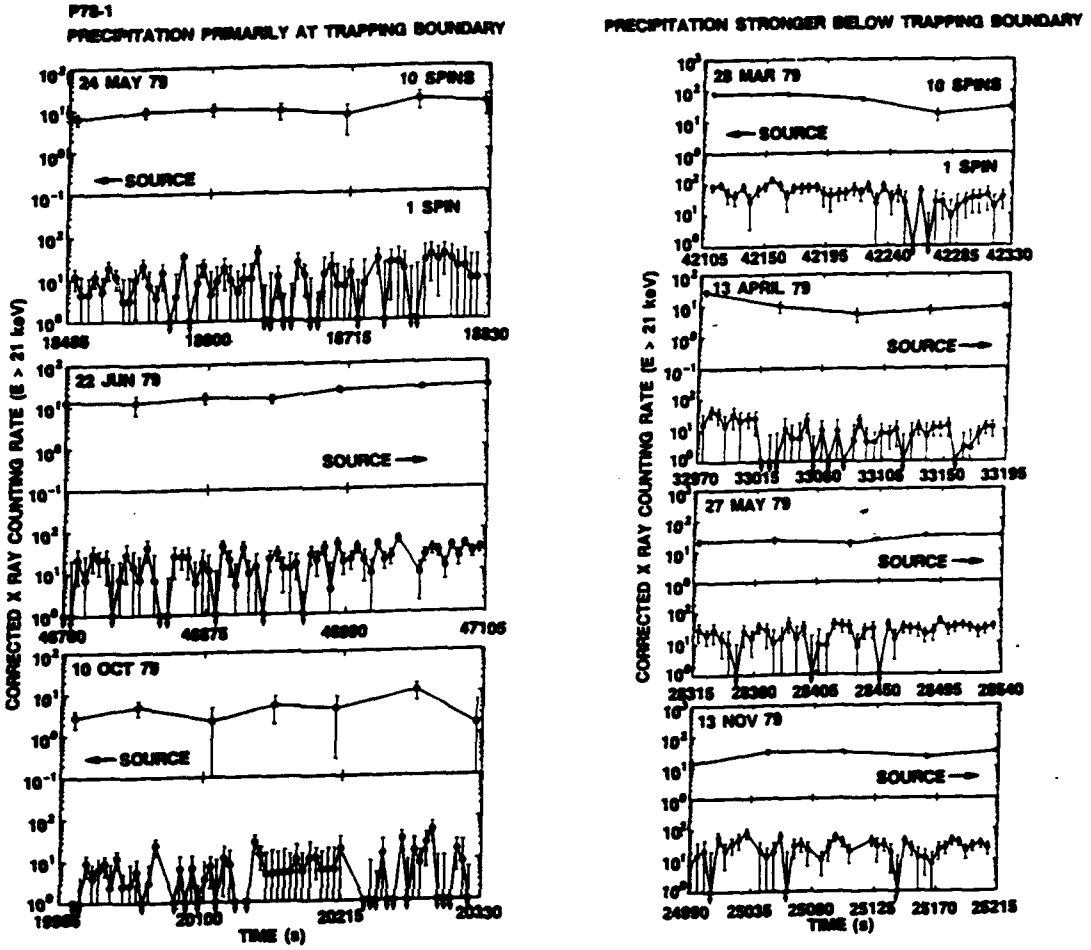


Fig. 5. The x ray counting rates in the Aa sensor multiplied by $r^2/1000d$ plotted as a function of time. In the left section the electron precipitation as measured with the EEM spectrometer was predominantly near the trapping boundary. In the right section the directly measured electron precipitation was predominantly at latitudes more than one degree below the trapping boundary. The direction of motion of the satellite, either toward or away from the trapping boundary, is indicated by an arrow marked "source".

narrow the measured x ray fluxes were sometimes considerably higher than those calculated from the measured precipitating electrons. Such discrepancies may be attributed to the fact that the precipitating electrons were measured with the EEM spectrometer during only approximately one sixth of a satellite spin period and hence the maximum intensity may be missed. However, from comparisons between the electron and x ray spectra in many cases it has been established that x rays can be used for mapping the electron precipitation.

We have considered some intense electron precipitation events with hard energy spectra that extend over wide longitude ranges. Many of these events occurred at latitudes equatorward of the trapping boundary. These may be identical to the "relativistic electron precipitation (REP)" events first identified by *Bailey* [1968] on the basis of anomalous decreases in the daytime strength of forward scatter radio signals at high frequencies.

An example of high x ray flux occurred on 28 March 1979 when the directly measured precipitating electron energy spectrum was quite hard as shown in Figure 4. Significant electron fluxes were measured at energies of ~600 keV, and the event would surely be considered relativistic electron precipitation even though it is not known whether there are any distinctive characteristics associated with REP's other than a high intensity [e.g., *Rosenberg and Lanzerotti*, 1979]. In order to have a significant effect on the transmission of radio signals during an REP event it is probably necessary for the electron precipitation to extend over a large area and to persist for at least many seconds. Here, imaging measurements have demonstrated that some such extend over hundreds of kilometers and last for at least several seconds.

Next, the temporal variations of the trapping boundary precipitation are considered. The x ray counting rate for detector Aa that views the region near the satellite path is plotted as a function of time in the left section of Figure 5 for three passes when the electron counting rate was fairly high and the precipitation was predominantly near the trapping boundary. Each point in the upper section for each satellite pass represents the x ray counts accumulated during appropriate portions of ten spins of the satellite. The counting rates have all been corrected for viewing geometry by multiplying by $r^2/1000d$ where $r$ is the distance in km from the satellite to the center of the region at the trapping boundary viewed by each of the x ray detectors and $d$ is the width in km of the area viewed perpendicular to the satellite path. This correction factor is approximately proportional to $r$, which is the geometric correction factor for a narrow arc.

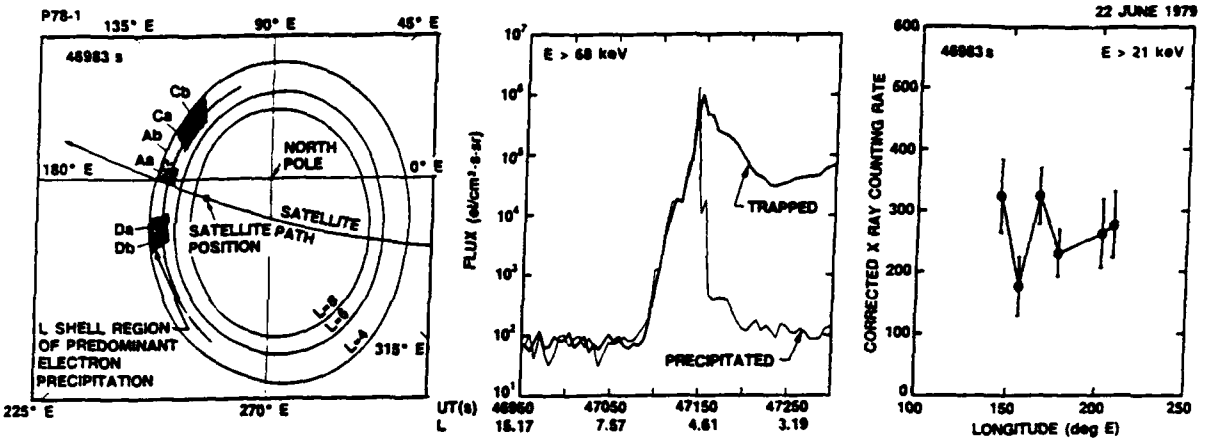


Fig. 6. The geometry for observation of x rays from the trapping boundary at the specified date and time (left section). The precipitating and trapped electrons measured with the EEM spectrometer (center section). The x ray counting rates in the various sensors multiplied by $r^2/1000d$ (right section).

except that the actual field-of-view has been taken into account. The x ray sources were assumed to occur at an altitude of 100 km and to be narrow and constant in $L$ width. This normalization procedure has been used previously [*Imhof et al.*, 1982]. In this and other figures the error bars represent statistical uncertainties only. The lower sections show the same data plotted as single spin counts. The x ray flux persisted over time scales as long as several minutes. In these cases, the x ray emission or electron precipitation rate, when corrected for the geometry of viewing the electron precipitation region, did not undergo large changes during that time. Temporal periodicities associated with precipitation near the boundary are not evident on scales of about 10 s to 5 min.

To study the time dependence of precipitation equatorward of the trapping boundary consider the x ray flux in detector Aa when the directly measured precipitation is at latitudes more than one degree below the background boundary as illustrated in the right section of Figure 5. The format of the figure is similar to that on the left-hand side except the corrected counting rates are plotted for four passes of the satellite instead of three. As with the three passes when the precipitation was predominantly near the trapping boundary, temporal periodicities are not evident in the top three panels on a time scale between about 10 s and 5 min. However, in the bottom panel there may be some evidence for a pseudo periodicity.

Let us next consider the longitude variations in x ray intensity based on all 6 operating detectors for satellite passes in which the precipitation measured with the electron spectrometer was predominantly near the trapping boundary. An example of the longitude dependence of the x ray measurements is shown in Figure 6. As a selection criterion for this and all of the other examples shown it was required that detectors Aa and Ab have a positive net counting rate above background. In the left hand section of the figure the geometry for viewing the trapping boundary and nearby $L$ shells is shown for 22 June 1979 at 46,983 s. In the center section the fluxes of trapped and precipitating electrons >68 keV are plotted as a function of time. In the right hand section the counting rates in the downward direction minus those in the upward direction are plotted as a function of the central viewing longitude of each of the 6 sensors at a time when the satellite was poleward of the trapping boundary. The counting rates have all been corrected for the viewing geometry, as described for Figure 5.

The longitude variations in x ray intensity derived from the observations can be expressed in terms of dependence upon magnetic local time (MLT). For three passes of the satellite, the MLT distributions in corrected x ray counting rate are shown in Figure 7 at six successive times during each crossing. The distributions are for passes when the precipitation measured with the electron spectrometer was entirely or at least predominantly near the trapping boundary. The selected passes occurred at times when the trapped

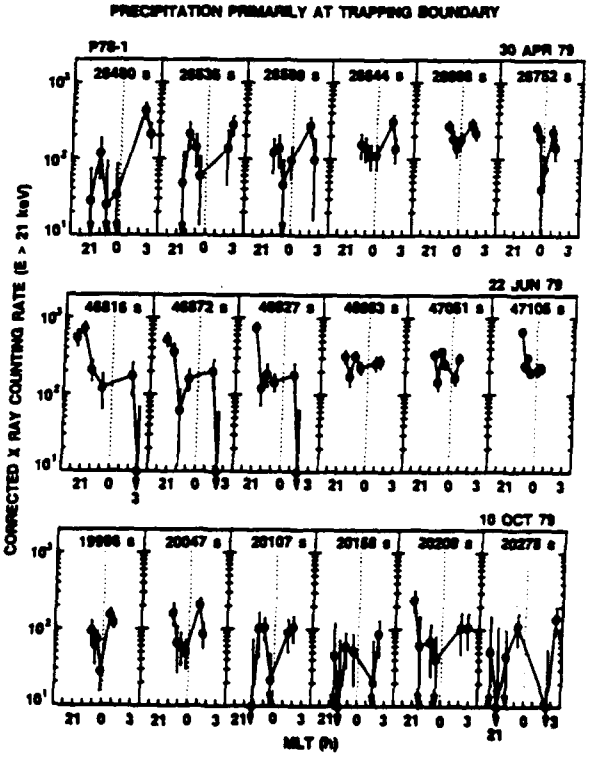


Fig. 7. The x ray counting rates in the various sensors multiplied by $r^2/1000d$ plotted as a function of MLT when the electron precipitation as measured with the EEM spectrometer was predominantly at $L$ values near the trapping boundary.

electron fluxes were quite high and hence the precipitating electron and the bremsstrahlung x ray fluxes tended to be large. In each of these cases the electron precipitation near midnight extended ~2.5 to ~7 hr in MLT. Some of the observed variations with MLT may have been due to the occurrence of additional precipitation at lower $L$ values, but the precipitation along the path of the satellite was predominantly confined to a region near the trapping boundary.

For each of 18 passes the counting rate for appropriate portions of a single 10 spin interval is plotted in Figure 8 as a function of MLT. Three of the passes are also shown in Figure 7. In Figure 8 a vertical dashed line is shown at MLT = 0. For comparison, horizontal dashed lines are drawn through the corrected counting rate of detector Aa, which viewed a region adjacent to the satellite path. Within the statistical uncertainties the x ray flux emitted at MLT values or longitudes different from the satellite crossing of the boundary showed no significant decreases. Any corrected flux increase on 8 of the 18 passes was no more than a factor of three at all observed longitudes. These findings are consistent with precipitation at the midnight trapping boundary on approximately half of the occasions being equally intense over a longitude range of 28° to 79° with a median value of 45°.

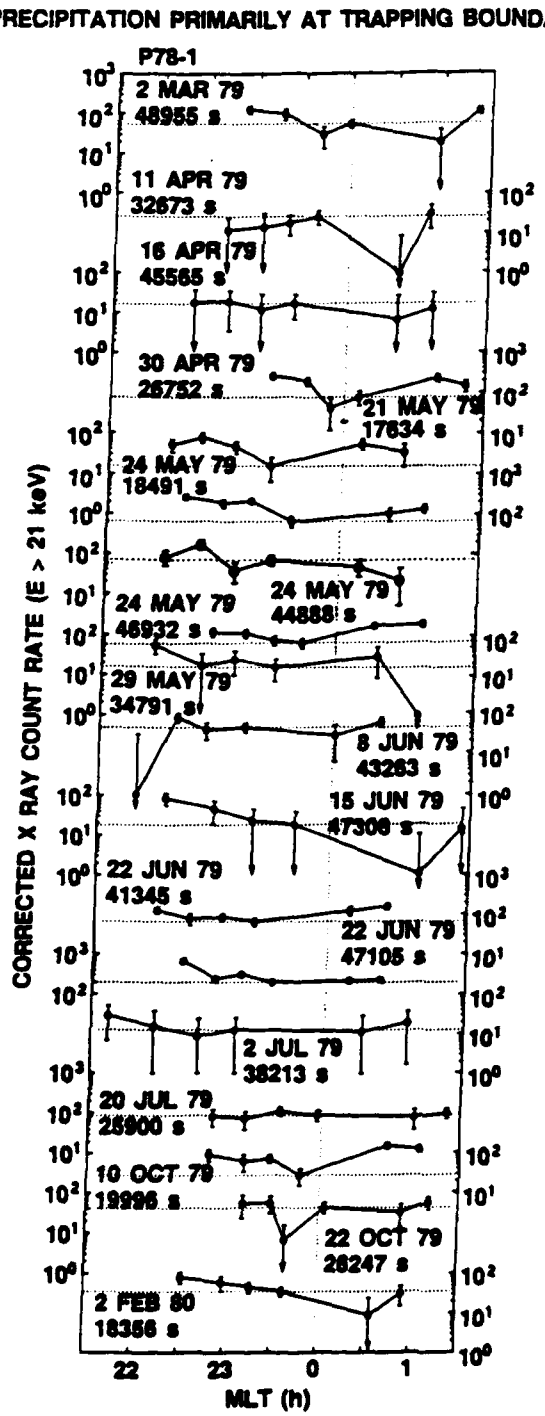


Fig. 8. The x ray counting rates in the various sensors multiplied by $r^2/1000d$ plotted as a function of MLT. In all cases the electron precipitation as measured with the EEM spectrometer was predominantly at latitudes near the trapping boundary.

For many of the nighttime passes in which a high flux of x rays was observed, the dominant precipitation as measured with the electron spectrometer occurred in narrow latitude regions, but at latitudes more than one degree below the position where the measured electron flux was not above the background. A good example of the x ray counting rates in this situation is shown in Figure 9 where the dependence on MLT is plotted for six successive times during a single satellite crossing. In this case large deviations from uniformity in the x ray flux with respect to MLT are evident.

For thirteen passes in which the electron spectrometer measured a much higher precipitation rate over narrow $L$-shell intervals but at latitudes more than one degree below the background boundary, the corrected counting rates are plotted versus MLT in Figure 10 for single 10 spin intervals. Strong variations with magnetic local time in the x ray flux were more often observed in contrast with many of the passes in which the directly measured precipitation was solely at the trapping boundary. Significant electron precipitation extended over a longitude interval of 30° to 90° with a median value of 44°.

The data included in Figures 8 and 10 were selected on the basis of the directly measured electron profiles and the requirement that a significant x ray counting rate above background be measured in detectors Aa and Ab. For each of the two conditions in these figures, electron precipitation predominantly near the background boundary and stronger at lower latitudes, respectively, the distribution in the $AE$ index is shown in Figure 11. The $AE$ index tends to be larger when the electron precipitation is stronger at latitudes below the trapping boundary, but there is clearly much overlap and the electron precipitation pattern is not determined solely by the $AE$ index. A similar result was found for the $Kp$ index.

In the bottom sections of Figure 12 the average corrected counting rates in detectors Da and Db are plotted versus the average corrected counting rates in detectors Ca and Cb for the following two situations with the direct electron measurements; in the left section the electron precipitation measured at the satellite was predominantly near the trapping boundary and in the right sections the precipitation was greater at lower latitudes. A line in each panel is drawn for equal corrected counting rates in the corresponding sets of detectors. For precipitation well within the outer radiation belt the total flux of x rays >21 keV and hence the precipitating electron fluxes summed over a broad $L$ shell range often tend to be an order of magnitude greater than when the precipitation is limited to the immediate vicinity of the background boundary. Also, when the directly measured

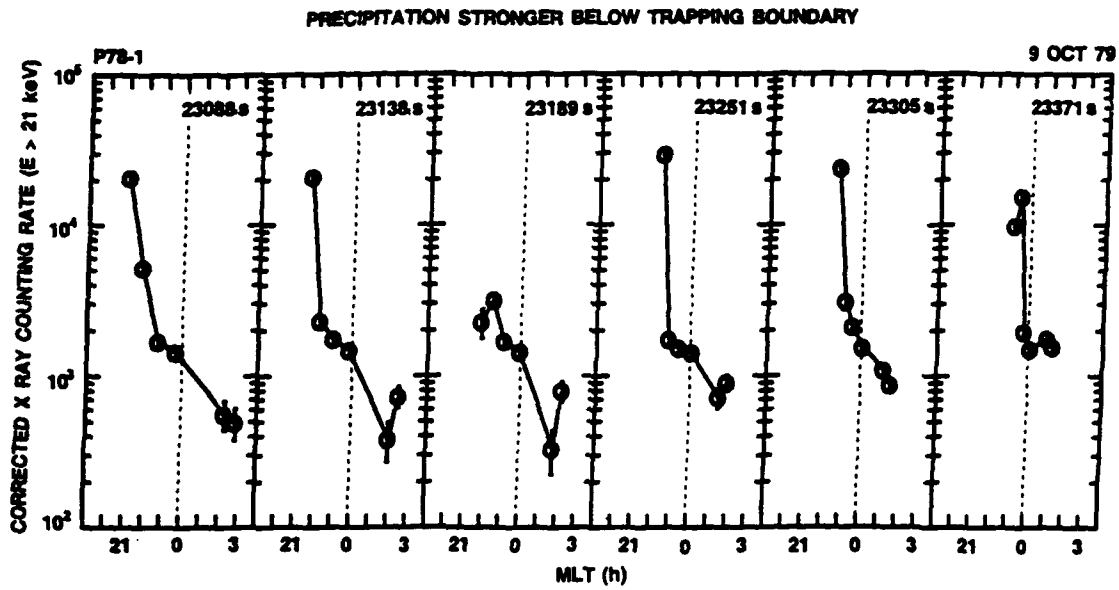


Fig. 9. The x ray counting rates in the various sensors multiplied by $r^2/1000d$ plotted as a function of MLT. In this case the electron precipitation as measured with the EEM spectrometer was predominantly at latitudes below the trapping boundary.

precipitation was primarily at the trapping boundary the plot shows less scatter or equivalently there is less variation with longitude.

In the top sections of Figure 12 the average corrected counting rates in detectors Ca and Cb and in Da and Db are plotted versus the average corrected counting rates in the detectors viewing to the immediate right of the orbit plane. This part of the figure shows that when the precipitation on the satellite path was primarily at the trapping boundary the precipitation at other longitudes was generally the same or greater. On the other hand, when the directly measured precipitation was greater at latitudes below the trapping boundary the precipitation at other longitudes was often quite different.

## DISCUSSION

From the direct electron measurements just presented we have seen that near local midnight the precipitation of electrons in the tens of kilovolt range is typically confined to narrow latitude regions. The locations are often near the immediate vicinity of the trapping boundary, but frequently they occupy one or more narrow $L$ shell regions within the outer radiation belt. This spatial distribution contrasts with the more widespread extent that often occurs in low energy electron precipitation.

When pitch angle isotropy along the satellite path was limited to the immediate vicinity of the trapping boundary the precipitation was often great enough that it could be mapped in x rays with the detectors on the P78-1 satellite. Previous investigations [*Imhof*, 1988] have addressed precipitation near the trapping boundary at midnight based solely on direct measurements of the electrons. Now, for the first time, with x ray imaging it has been found that such precipitation frequently may extend in an arc pattern over a median longitude interval of 45° and the intensity is almost constant with longitude. From the x ray measurements, temporal periodicities in the flux of electrons precipitating near the background boundary were generally not observed on a time scale of about ten seconds to five minutes. These findings are consistent with electron precipitation at this location being caused by characteristics of the magnetic field which are not strongly dependent upon longitude.

From direct measurements of the energetic electron precipitation fluxes, it was found that the precipitation may be much more intense at latitudes below the trapping boundary and may extend over a much broader $L$ shell range than the precipitation that often occurs within one degree of the background boundary. Whereas precipitation at the trapping boundary was observed on 69% of the satellite passes across that region, precipitating fluxes at more than one degree lower latitude were higher on about 38% of the passes. Although strong precipitation events at invariant latitudes as low as about 60° occurred less often than the weaker ones near the trapping boundary, their intensity was frequently great enough and they extended over such a wide longitude interval as to lead to a greater input to the atmosphere.

Information on the mechanisms responsible for the precipitation might be obtained from examination of the energy spectra. Wide variations occur in the energy spectra of the precipitation spikes both at the trapping boundary and within the outer radiation belt. Near the trapping boundary the energy spectra often show a prominent $L$-dependent threshold for isotropy that has been interpreted as evidence that the electrons are precipitated as a result of the radius of curvature being less than an order of magnitude greater than the gyroradius of the particles [e.g., *Imhof*, 1988]. Within the outer radiation belt the spectral shape of the precipitating electrons was often the same as for the trapped electrons just above and below the latitude of the event. This behavior suggests that the precipitation mechanism(s) acts with the same strength on electrons of any energy.

The widespread spatial character of either class of precipitation has important implications for the responsible mechanisms. If the electron precipitation at the trapping boundary is associated with characteristics of the magnetic field,

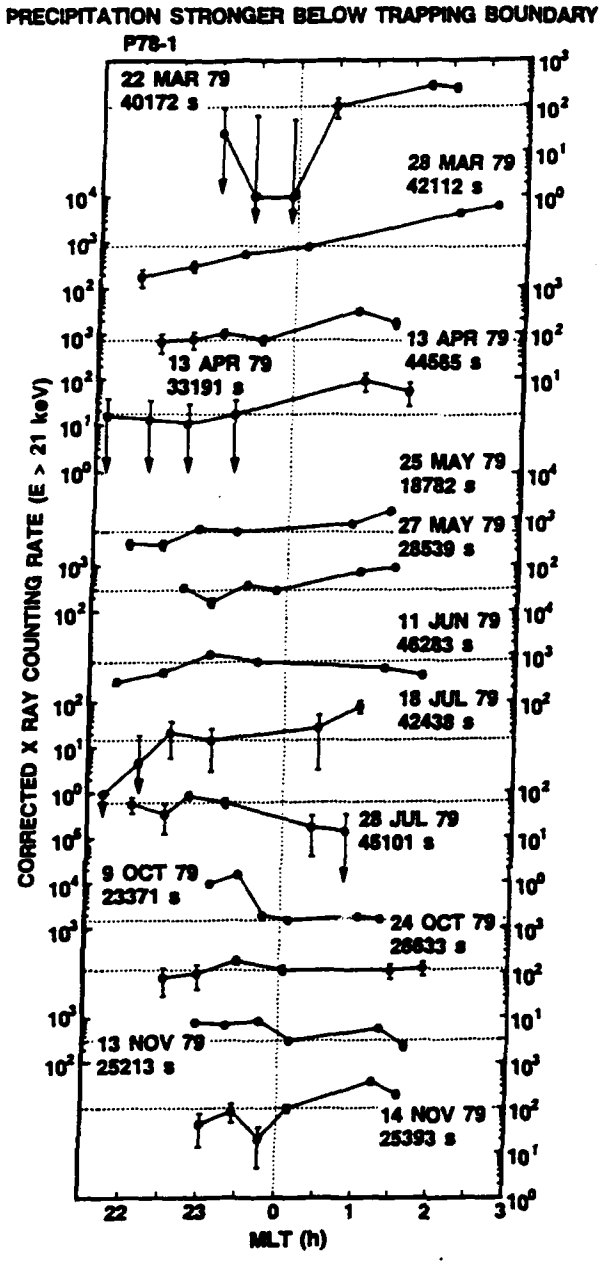


Fig. 10. The x ray counting rates in the various sensors multiplied by $r^2/1000d$ plotted as a function of MLT. In all cases the electron precipitation as measured with the EEM spectrometer was predominantly at latitudes below the trapping boundary.

instantaneous mappings in longitude can provide information on the magnetic field topology over a range of local times. For precipitation at latitudes below the trapping boundary the mappings may shed light on the responsible mechanisms.

A greater understanding of the mechanisms responsible for the arc-shaped precipitation patterns might be achieved by comparing these patterns with arcs observed at visible wavelengths. In this regard, we have compared the present observations with the occurrence characteristics of detached arcs observed at visible wavelengths by *Moshupi et al.* [1979] and *Wallis et al.* [1979]. The detached arcs show a much higher frequency of occurrence between 17 and 19 MLT, whereas all of the phenomena reported here occurred between 21 and 03 MLT. On the other hand, the published energy spectra of the electrons associated with detached arcs generally fall within the wide range of spectral shapes and intensities reported here in Figure 2. The detached arcs were found by *Moshupi et al.* [1979] to occur about 10 to 12 hours after a peak in the *AE* index and at a time when the interplanetary field component Bz is positive following an extended period when it was negative. However, no such pattern was evident in the present data. The lack of any distinctive behavior is perhaps to be expected since each precipitation pattern, spikes predominantly near the trapping boundary or stronger below it, occurred during more than a third of the satellite crossings.

For a detailed study of the precipitation mechanism(s) one needs finer scale mappings over a broader range in MLT than acquired in this experiment, but here we have used the x ray technique for a preliminary study of the longitude distributions in conjunction with direct measurements of the precipitating electrons. In the future, a higher sensitivity can be achieved with a larger area detector, and with more counts smaller fractional variations in total intensity and in energy spectrum can be mapped. Also, from mappings with finer resolution in both $L$ shell and longitude, the precipitation at the trapping boundary and at lower latitudes can be intercompared and followed in time. For these future measurements, it is important to have the sensitivity to map the precipitation also at quiet times when the trapped and precipitating electron fluxes are relatively low.

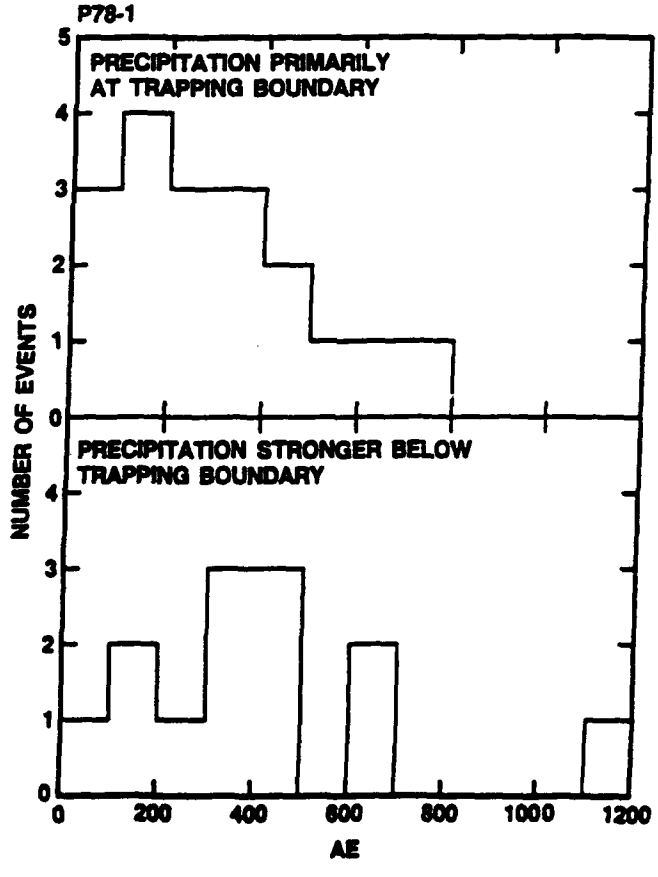


Fig. 11. The distributions in the AE index for the two classes of electron precipitation: predominantly near the trapping boundary and stronger at lower latitudes.

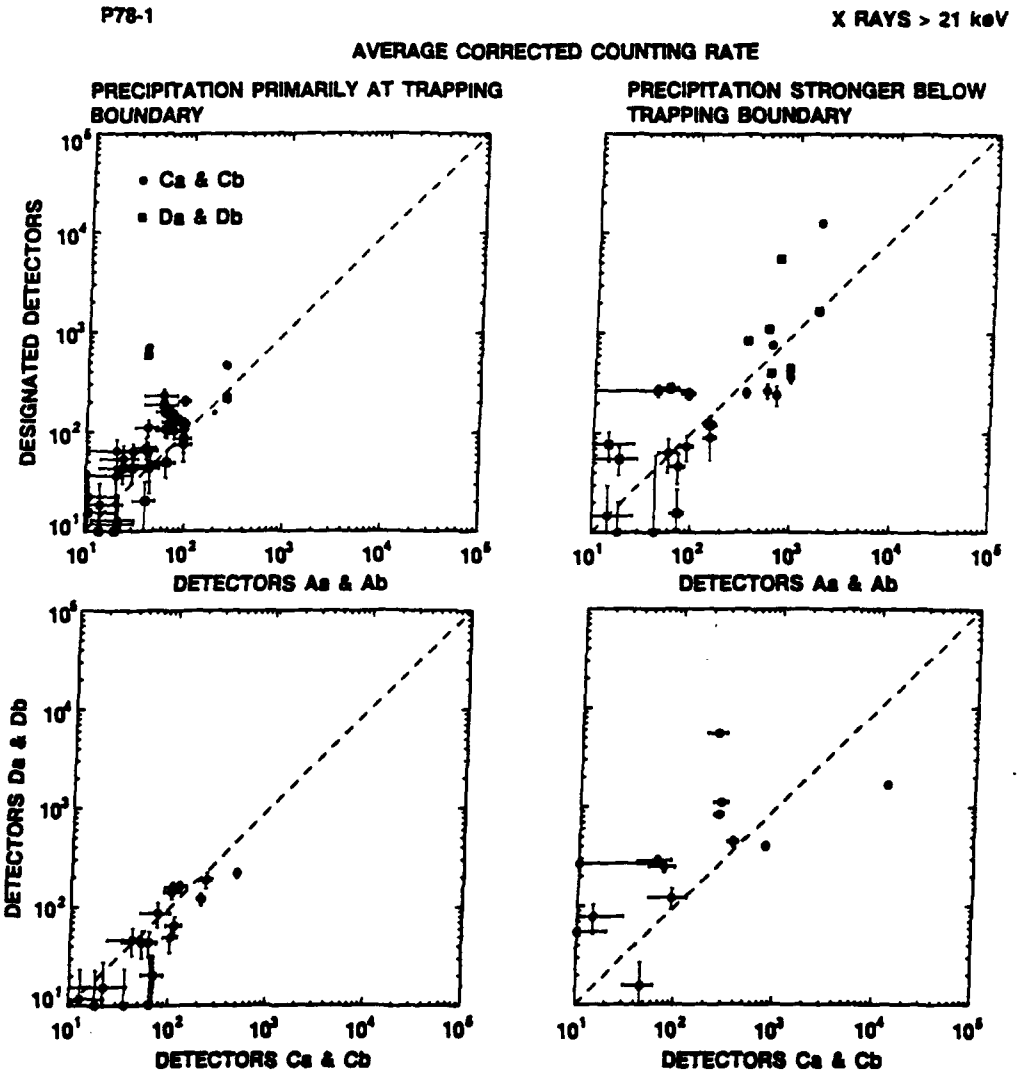


Fig. 12. In the top sections the corrected average counting rates in the various detectors versus the corrected average counting rate in detectors Aa and Ab. All counting rates have been multiplied by $r^2/1000d$. The directly measured precipitating flux was predominantly at the trapping boundary (in the left section) and at latitudes below the boundary (in the right section). In the bottom sections are plotted the average counting rates in detectors Da and Db versus those in detectors Ca and Cb.

*Acknowledgments.* The development of the satellite instrumentation was sponsored by the Defense Advanced Research Projects Agency through the Office of Naval Research (contract N00014-78-C-0070). Much of the data analysis presented here was sponsored by the Air Force Office of Scientific Research (contract F49620-88-C-0072). The Lockheed Independent Research Program provided partial support for the analysis. The consultation and advice of R. R. Vondrak are greatly appreciated as are the comments from M. Walt. The efforts of J. P. McGlennon and S. J. Siegal in data reduction are gratefully acknowledged. We also thank W. E. Francis for his contribution in obtaining the calculated x ray fluxes.

The Editor thanks S. H. Werden and another referee for their assistance in evaluating this paper.

## REFERENCES

Alfven, H., and C. G. Fallhammar, *Cosmical Electrodynamics, Fundamental Principles*, 2nd ed., Clarendon, Oxford, 1963.

Bailey, D. K., Some quantitative aspects of electron precipitation in and near the auroral zone, *Rev. Geophys. Space Phys.*, *6*, 289, 1968.

Cain, J. C., S. J. Hendricks, R. A. Langel, and W. V. Hudson, A proposed model for the international geomagnetic reference field, *J. Geomagn. Geoelectr.*, *19*, 335, 1967.

Datlowe, D. W., W. L. Imhof, and H. D. Voss, X ray spectral images of energetic electrons precipitating in the auroral zone, *J. Geophys. Res.*, *93*, 8662, 1988.

Fritz, T. A., Study of the high-latitude outer zone boundary region for ≥40-keV electrons with satellite Injun 3, *J. Geophys. Res.*, *75*, 5387, 1970.

Gaines, E. E., W. L. Imhof, W. E. Francis, M. Walt, and T. J. Rosenberg, Correlated electron and x ray measurements of quiet time electron precipitation: A comparative study of bremsstrahlung production and transport in the atmosphere, *J. Geophys. Res.*, *91*, 13455, 1986.

Imhof, W. L., Review of energetic (>20 keV) bremsstrahlung x-ray measurements from satellites, *Space Sci. Rev.*, *29*, 201, 1981.

Imhof, W. L., Fine resolution measurements of the *L*-dependent energy threshold for isotropy at the trapping boundary, *J. Geophys. Res.*, *93*, 9743, 1988.

Imhof, W. L., G. H. Nakano, and J. B. Reagan, Satellite observations of x rays associated with energetic electron precipitation near the trapping boundary, *J. Geophys. Res.*, *80*, 3629, 1975.

Imhof, W. L., J. B. Reagan, and E. E. Gaines, Fine scale spatial structure in the pitch angle distributions of energetic particles near the midnight trapping boundary, *J. Geophys. Res.*, *82*, 5215, 1977.

Imhof, W. L., J. B. Reagan, and E. E. Gaines, Studies of the sharply defined *L* dependent energy threshold for isotropy at the midnight trapping boundary, *J. Geophys. Res.*, *84*, 6371, 1979.

Imhof, W. L., J. R. Kilner, G. H. Nakano, and J. B. Reagan,

Satellite x ray mappings of sporadic auroral zone electron precipitation events in the local dusk sector, *J. Geophys. Res.*, *85*, 3347, 1980.

Imhof, W. L., J. Stadsnes, J. B. Reagan, J. R. Kilner, E. E. Gaines, D. W. Datlowe, J. Mobilia, and G. H. Nakano, Satellite Bremsstrahlung x ray measurements of the onset of a magnetospheric substorm, *J. Geophys. Res.*, *87*, 8149, 1982.

McDiarmid, I. B., E. E. Budzinski, and J. R. Burrows, Comparison of the Mead-Fairfield magnetic field model with particle measurements, *J. Geophys. Res.*, *81*, 3459, 1976.

Mizera, P. F., D. J. Gorney, and J. L. Roeder, Auroral x-ray images from DMSP-F6, *Geophys. Rev. Lett.*, *11*, 255, 1984.

Moshupi, M. C., C. D. Anger, J. S. Murphree, D. D. Wallis, J. H. Whitteker, and L. H. Brace, Characteristics of trough region auroral patches and detached arcs observed by ISIS 2, *J. Geophys. Res.*, *84*, 1333, 1979.

Popielawska, B., E. Szalinska-Piechota, and N. A. Tsyganenko, On the non-adiabatic particle scattering in the earth's magnetotail current sheet, *Planet. Space Sci.*, *33*, 1433, 1985.

Rosenberg, T. J., and L. J. Lanzerotti, Direct energy inputs to the middle atmosphere, Middle Atmosphere Electrodynamics, report of the workshop on the role of electrodynamics of middle atmosphere on solar-terrestrial coupling, *NASA Conf. Publ.*, *CP-2090*, 43, 1979.

Sergeev, V. A., and N. A. Tsyganenko, Energetic particle losses and trapping boundaries as deducted from calculations with a realistic magnetic field model, *Planet. Space Sci.*, *30*, 999, 1982.

Sergeev, V. A., E. M. Sazhina, N. A. Tsyganenko, J. A. Lundblad, and F. Sorass, Pitch-angle scattering of energetic protons in the magnetotail current sheet as the dominant source of their isotropic precipitation into the nightside ionosphere, *Planet. Space Sci.*, *31*, 1147, 1983.

Sergeev, V. A., S. N. Kuznetsov, and Yu. V. Gotselyuk, The dynamics of the structure of the high-latitude magnetosphere according to data on solar electrons, *Geomag. Aeron.*, *27*, 380, 1987.

Swift, D. W., and D. J. Gorney, Production of very energetic electrons in discrete aurora, *J. Geophys. Res.*, *94*, 2696, 1989.

Voss, H. D., W. L. Imhof, J. B. Reagan, R. R. Vondrak, M. Walt, J. Mobilia, D. W. Datlowe, D. P. Cauffman, W. Calvert, and R. G. Joiner, SEEP x ray imaging of the Earth's aurora (abstract), *Eos Trans. AGU*, *64*, 292, 1983.

Wallis, D. D., J. R. Burrows, M. C. Moshupi, C. D. Anger, and J. S. Murphree, Observations of particles precipitating into detached arcs and patches equatorward of the auroral oval, *J. Geophys. Res.*, *84*, 1347, 1979.

Walt, M., L. L. Newkirk, and W. E. Francis, Bremsstrahlung produced by precipitating electrons, *J. Geophys. Res.*, *84*, 965, 1979.

D. W. Datlowe, E. E. Gaines, W. L. Imhof, J. Mobilia, and H. D. Voss, Lockheed Missiles and Space, Department 91-20, Building 255, 3251 Hanover Street, Palo Alto, CA 94304.

(Received June 27, 1989;
revised September 1, 1989;
accepted September 22, 1989.)

# APENDIX D

## RELATIVISTIC ELECTRON ENHANCEMENTS OBSERVED OVER A RANGE OF L SHELLS TRAPPED AT HIGH ALTITUDES AND PRECIPITATING AT LOW ALTITUDES INTO THE ATMOSPHERE

JOURNAL OF GEOPHYSICAL RESEARCH, VOL. 97, NO. A5, PAGES 6397–6403, MAY 1, 1992

# Relativistic Electron Enhancements Observed Over a Range of $L$ Shells Trapped at High Altitudes and Precipitating at Low Altitudes Into the Atmosphere

W. L. IMHOF AND R. W. NIGHTINGALE

*Lockheed Palo Alto Research Laboratory, Palo Alto, California*

The fluxes of relativistic electrons at high altitudes were measured at the SCATHA satellite over the $L$ shell range of 5.3–8.7 during both enhancements and depletions. Simultaneous observations of the precipitating fluxes of electrons (>1 MeV) were performed at low altitudes from the P78-1 satellite. On a given pass of this satellite the fluxes of directly precipitating electrons in the bounce loss cone displayed bursts of enhancement, generally with observing times of less than 10 s. On the average these fluxes had a maximum value at $L$ = 4.5–5.0. In the drift loss cone the quasi-trapped electrons, all of which were about to precipitate into the atmosphere within a few minutes, were less intermittent and generally more intense, thereby providing a greater sensitivity for detecting precipitation. The ratio of the average fluxes of the directly precipitating electrons to the quasi-trapped electrons increased with increasing $L$ value. The coordinated data presented here have permitted for the first time a comparison to be made as a function of $L$ shell between the precipitating and the high-altitude trapped electron fluxes during relativistic electron enhancement events, some of which included electrons with energies extending to at least 5 MeV. The low- and high-altitude fluxes of >1-MeV electrons were found to track each other during the period studied (April–June 1979), with respect to both time and $L$ shell variations. The average precipitating electron fluxes measured at low altitudes in the drift loss cone were lower than those at high altitude by a factor of about $3 \times 10^2$. For $L$ = 5.3–7 the average fluxes in the bounce loss cone at low altitudes were estimated to be lower than the trapped fluxes at high altitude by a factor of about $3 \times 10^4$.

## INTRODUCTION

In the outer magnetosphere the fluxes of electrons with an energy greater than 1 MeV are well known to undergo pronounced increases and decreases [e.g., *Baker et al.*, 1986; *Nagai*, 1988]. However, little is known about the correlated precipitation into the atmosphere of these energetic electrons undergoing bounce motion over a broad $L$ shell region, at times of relativistic electron enhancements. Previous simultaneous low-altitude precipitation and high-altitude studies have involved only synchronous-orbit satellites. The data leave in doubt the full distribution in $L$ shell of relativistic electrons at high altitudes, and the eventual destination of these electrons. A question to be addressed is what is the fractional rate of loss of the high-altitude electron population into the atmosphere due to scattering interactions. This matter is more fully answered by obtaining simultaneous measurements over a range of $L$ shells of trapped electrons at high altitudes and precipitating electrons observed at low altitudes.

Measurements of trapped >1-MeV and >280-keV electrons were reported for low and for high altitudes by *Williams et al.* [1968]. However, precipitating electron fluxes were not available from this presentation, nor were any high-altitude measurements at $L$ values greater than 5.5. Only limited comparisons have been made between relativistic electron enhancements observed simultaneously at synchronous satellite altitude and electron precipitation into the atmosphere as observed at low altitudes [*Baker et al.*, 1990; *Imhof et al.*, 1991*a*]. A small fraction of the electrons present at near-synchronous orbit reach low altitudes in their bounce motion. Those electrons within the "loss cone" can be detected by a low-altitude satellite. Baker et al. used electron data taken on the DMSP spacecraft at 840 km altitude. The measured >1-MeV electrons were those near the edge of the equatorial loss cone. No detailed $L$ shell analyses were presented, nor was any distinction made between those trapped electrons about to precipitate into the atmosphere and those that are more stably trapped. The measurements of Imhof et al. were of electrons which precipitate into the atmosphere within one bounce, and these electrons were therefore considered to be in the bounce loss cone. However, the precipitating electrons were observed primarily in bursts for typical times of less than 10 s, and therefore the duty cycle for measuring the electrons on a given $L$ shell from a polar-orbiting satellite was quite low.

Here we present concurrent >1-MeV electron data from the SCATHA satellite, which was in near-synchronous orbit and covered $L$ = 5.3–8.7 at near-equatorial positions, and the P78-1 satellite at 600 km altitude in a polar orbit, which covered the full range of $L$. From the latter satellite, two classes of precipitating electrons were observed: those in the bounce loss cone are in contrast to those in the drift loss cone, which precipitate into the atmosphere sometime during their longitudinal drift around the world. Depending on their energy and the longitude of injection they may remain in the drift loss cone for times up to many minutes. Since the fluxes of electrons in the drift loss cone were steadier in time and generally much larger, a higher detection efficiency was achieved with an increased duty cycle for detecting electron precipitation. Observations of directly precipitating electrons in the bounce loss cone achieve a more direct measure of the inputs to the atmosphere, but the probability of observing short-duration or spatially narrow bursts is quite low. Comparisons between these two classes of precipitation



Paper number 92JA00229.
0148-0227/92/92JA-00229$05.00

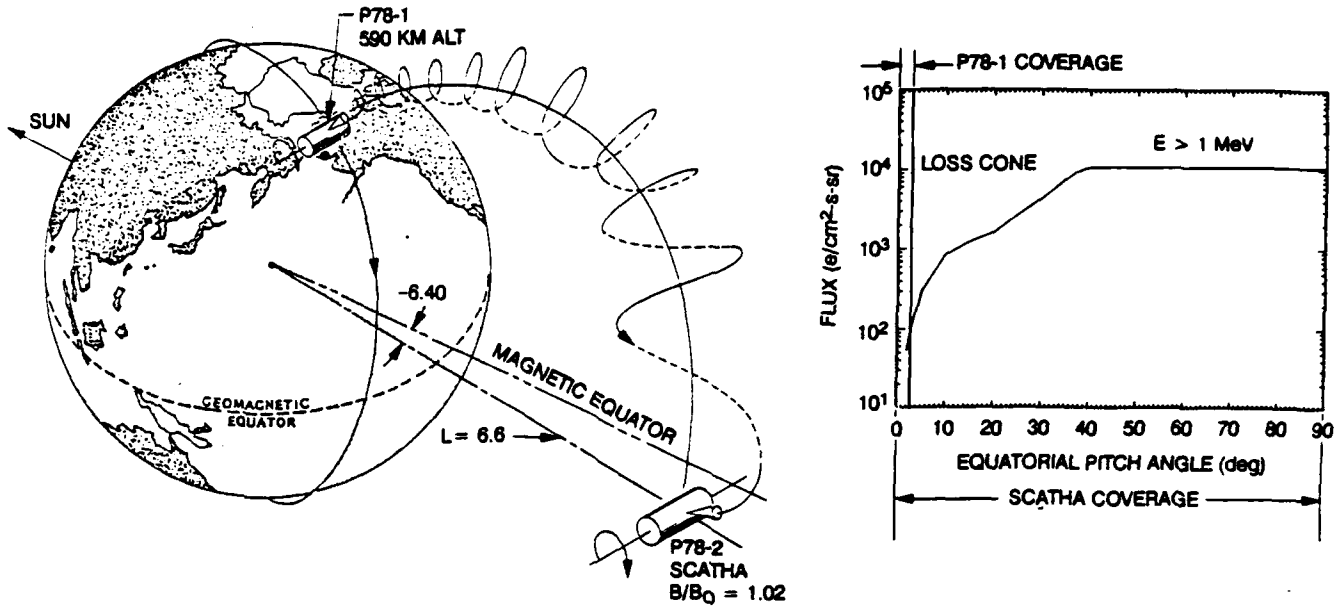


Fig. 1. Schematic illustration of the geometry for measuring electrons simultaneously from low- and high-altitude satellites. A representative pitch angle distribution from SCATHA is also shown.

should be made from the same satellite. Here data from the P78-1 spinning satellite are presented which satisfy this need.

## Description of Instrumentation

The P78-1 satellite was launched on February 24, 1979, into a Sun-synchronous, noon-midnight, near-circular polar orbit at ~600 km altitude with an inclination of 96.7°. The section of the satellite containing the electron spectrometer EEM 002 (which provided the data used here) spun about an axis perpendicular to the orbit plane with a period of about 5.5 s. Worldwide coverage of the measurements was achieved through use of tape recorders on board the satellite. The EEM 002 electron sensor, covering a range of energies from 68 keV to 1050 keV, was surrounded by a plastic scintillator anticoincidence shield for background reduction [*Imhof et al.*, 1981]. In the present study, the counts recorded in the anticoincidence counter were used, as this integral counter had the desired threshold energy of 1 MeV for electrons. The geometric factor was 0.77 $cm^2$ sr with an acceptance angle of ±15°. Electrons above ~15 MeV could be detected with a nearly omnidirectional response, but any such counts would show little variation with orientation within a spin and were subtracted as background in the analysis performed here. The background was based on the counts accumulated when the spectrometer was pointed along the magnetic field lines and toward the atmosphere.

The SCATHA satellite was launched on January 30, 1979. In its final orbit the satellite nominally spins at ~1 rpm and traverses an altitude range between ~27,500 km at perigee and ~45,200 km at apogee twice a day within a latitude range of ±15°. This coverage corresponds to an $L$ shell range of about 5.3–8.7 in the near-geosynchronous region. The Lockheed high-energy particle spectrometer, SC3, is a solid-state particle telescope employing a series of surface barrier silicon detectors. It primarily measures energetic electron fluxes as a function of energy and pitch angle. The instrument normally operates in two energy modes with the lower mode covering the electron energy range between 47 and 299 keV in 12 channels, each about 21 keV wide. The higher-energy mode extends over the electron energy range from 256 to 4970 keV in 12 channels each 393 keV wide. For the present study the differential number flux was multiplied by the channel energy width and summed over the electron energy range of 1026–4970 keV. The field of view of the detector is 3°. In addition, there is a 3° sweep of the detector for each 0.5-s accumulation period. This detector response should be compared with the expected loss cone full width of ~6° to ~10° in the near-synchronous region. The spectrometer is aligned perpendicular to the spin axis of the satellite, sweeping most pitch angles (from 0° to 90°) four times per minute. However, pitch angles near 0° were often not covered. A more complete description of the instrument can be found in the work by *Reagan et al.* [1981].

## Presentation of Data

The pertinent geometry for performing correlated measurements of trapped electrons at high altitudes and precipitating electrons at low satellite altitudes is illustrated schematically in Figure 1, which contains a representative pitch angle distribution as measured on the SCATHA satellite. The low-altitude polar-orbiting satellite P78-1 detected electrons within the bounce loss cone and, separately, electrons that mirror at altitudes of ~100 km to ~600 km and that may be in the drift loss cone, depending upon the longitude. However, the orientation of the SCATHA spin axis was such that electrons in the bounce loss cone were often not sampled during many of the correlated cases considered here.

A SCATHA/P78-1 conjugacy case when the two spacecraft were in the same magnetic flux tube is illustrated in Figure 2. The low-altitude energy spectra include two classes of precipitating electrons: those in the drift loss cone, labeled quasi-trapped electrons, and those in the bounce loss cone, labeled precipitating electrons. The angular resolution of the high-altitude measurements in the loss cone included

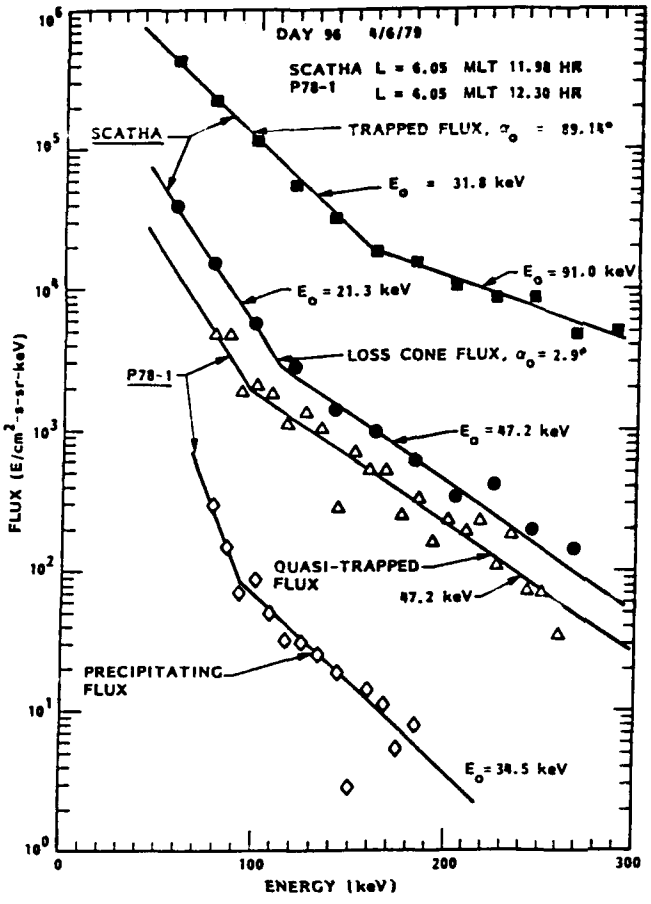


Fig. 2. Nearly simultaneous measurements of the energy spectra on the SCATHA and P78-1 satellites at various pitch angles.

both of these classes of precipitating electrons. Up to 300 keV the high-altitude loss cone measurements agree well with the dominating quasi-trapped component of the precipitating fluxes observed at low altitudes. The relativistic electron flux statistics above 300 keV were too low for individual case comparisons. The following study uses the SCATHA fluxes of trapped >1026-keV electrons.

Previously, from the low-altitude S81-1 satellite, electrons above 1 MeV were found to precipitate into the atmosphere in bursts with observation times typically of 1–10 s [*Imhof et al.*, 1991*b*]. In these bursts the fluxes of precipitating electrons in the bounce loss cone were often equal to the fluxes of trapped electrons at 600 km altitude. In Figure 3 the fluxes of trapped and precipitating >1-MeV electrons are plotted versus invariant latitude for four passes of the low-altitude satellite P78-1. Also shown for comparison are plots of the trapped >1-MeV electrons measured during the 12-hour half orbit of SCATHA which encompassed the low-altitude data. The low-altitude passes shown here occurred near local midnight, whereas the SCATHA data spanned a wide range of local times. From the entire data set for this time period (not shown) one concludes that during the 12-hour interval required for SCATHA to scan the full $L$ shell range, the low-altitude profiles typically displayed a wide variety of patterns. Often, however, the flux cutoffs were similar at low and high altitudes.

During each 5.5-s spin of the low-altitude P78-1 satellite, measurements were provided of both the trapped and precipitating electrons. The locally trapped electron fluxes were obtained during the two portions of each spin when the electron spectrometer was pointed within 25° of the normal to the geomagnetic field line. At certain longitude intervals

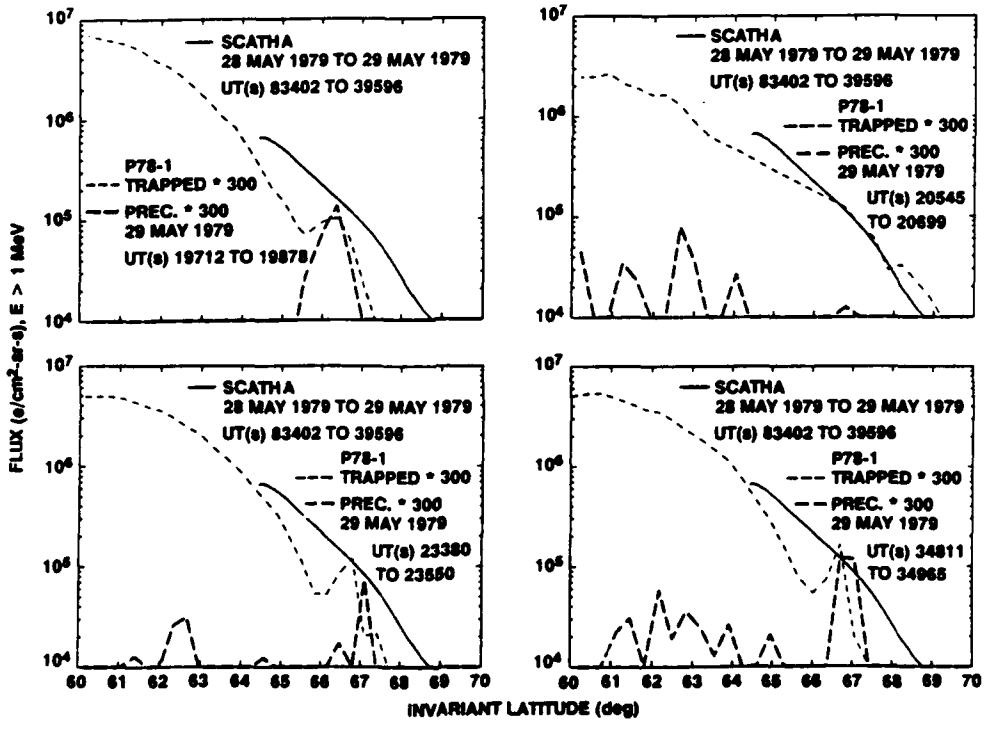


Fig. 3. The fluxes of trapped and precipitating >1-MeV electrons versus invariant latitude for four passes of the satellite P78-1 on May 29 (day 1979). Also plotted are >1-MeV fluxes from SCATHA.

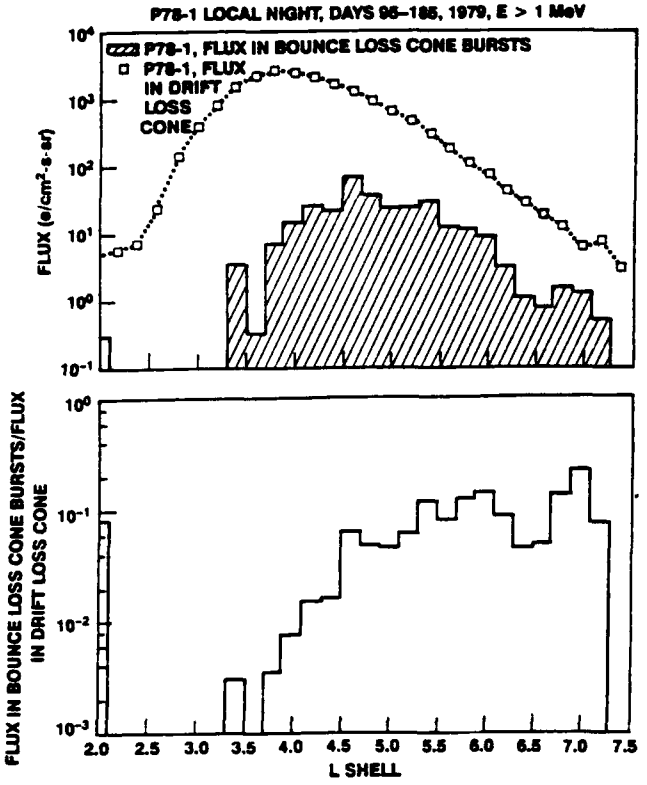


Fig. 4. (Top) The daily averaged electron fluxes in the bounce loss cone during precipitation bursts and the averaged electron fluxes in the drift loss cone plotted versus $L$ shell. (Bottom) The ratios of fluxes in the bounce loss cone during precipitation bursts to those in the drift loss cone.

these electrons were about to precipitate into the atmosphere within a few minutes after drifting eastward to the South Atlantic anomaly and are therefore considered to be in the drift loss cone. The precipitating electrons in the bounce loss cone were taken from data acquired when the collimator view direction was within 25° of the field line in the upward direction. From the low-altitude P78-1 satellite data, let us compare as a function of $L$ in Figure 4 the average fluxes of electrons in the bounce loss cone during bursts with those in the drift loss cone. Both are shown in the top panel. For the former quantity we consider averages of the nighttime maximum flux recorded in the bounce loss cone on each pass of the satellite, including zero flux for passes when no bursts were observed. To qualify as a burst, the counting rate in the upward direction must increase to a net counting rate (with background subtracted) of at least 100 counts per second, which is equivalent to a threshold of 130 electrons $(cm^2\ sr\ s)^{-1}$. When averaged, the bounce loss cone fluxes are less than the threshold level due to the frequent occurrence of no measurable precipitating flux in the bounce loss cone. From an extrapolation of the intensity distribution of bursts above 130 electrons $(cm^2\ sr\ s)^{-1}$ to lower flux values it was concluded that the error in the average fluxes caused by neglect of fluxes below this value is probably no more than about 3%. These fluxes reached a maximum value at an $L$ shell of about 4.5. The data presented were taken on days 95–185 in the year 1979.

In the bottom panel of Figure 4 the ratios of the average fluxes in the bounce loss cone bursts to those in the drift loss cone are plotted as a function of $L$. The ratio shows considerable scatter, but there is a trend for the ratio to become progressively larger with increasing $L$. This trend may be due at least partly to the decreasing size of the loss cone at higher $L$ values. For $L$ = 5–7 the average drift loss cone fluxes are about an order of magnitude larger than the average fluxes in the bounce loss cone precipitation bursts. To compare the rates of loss of electrons in the two loss cones, one should consider fluxes in the bounce loss cone averaged over all times rather than only during precipitation bursts. On the basis of the data presented here and the data obtained from the S81-1 low-altitude satellite [*Imhof et al.*, 1991*b*], it is estimated that the average bounce loss cone fluxes in bursts during a pass are ~10 times as large as the average fluxes in the bounce loss cone. It then follows that the average fluxes in the drift loss cone are about 2 orders of magnitude larger than the average fluxes in the bounce loss cone for $L$ = 5.3–7.

In an earlier study, the fluxes of precipitating relativistic electrons in the bounce loss cone were found to track rather well the trapped fluxes of electrons measured at synchronous satellite altitude [*Imhof et al.*, 1991*a*]. Now we make such a comparison for low-altitude quasi-trapped electrons. In Figure 5 the daily averaged fluxes of precipitating electrons in the drift loss cone are plotted versus day number for $L$ = 5.5. The trapped fluxes observed at high altitude have been overlaid on this figure. The high- and low-altitude electron fluxes are seen to track each other. For comparison, the *Kp* and *Dst* values are also shown.

Expanding in $L$ shell from 3 to 6.5 for electrons above 1 MeV, we plot both the high-altitude fluxes and the 24-hour-averaged precipitating fluxes measured in the drift loss cone as a function of day number in Figures 6*a* and 6*b*. At $L$ > 5.3 the fluxes of relativistic electrons at both high and low

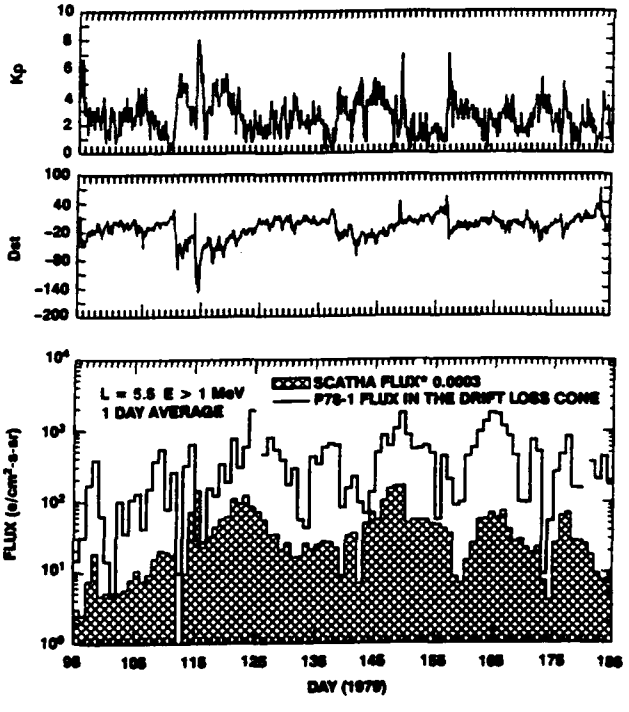


Fig. 5. For $L$ = 5.5 the 24-hour-averaged precipitating electron fluxes in the drift loss cone and high-altitude electron fluxes plotted as a function of day number in 1979. Also plotted are the *Kp* and *Dst* indices.

altitudes show pronounced enhancements and depletions beginning around day 115 of 1979 (April 25). For $L$ values near 3.0, based on the precipitation rates, the relativistic electrons were slowly decaying. At these lower $L$ values the temporal variations were distinctly different.

Although in the correlations presented here, only electrons above 1 MeV were considered, the major enhancements, which included days 115, 123, and 149, involved highly relativistic electrons extending to energies of at least 5 MeV, as illustrated in Figure 7 for SCATHA observations near $L = 5.5$. Other spectra included in the figure for comparison are the spectrum for the most geomagnetically quiet day, 332, in 1979 and the average for March–December 1979.

The promptness of the correlation between the primarily trapped fluxes measured on the SCATHA satellite and the precipitating fluxes observed on the P78-1 satellite is investigated by considering the correlation coefficients between the two classes of fluxes. These are plotted in Figure 8 as a function of $L$ shell for various time delays between the two sets of fluxes. The best correlation coefficients generally occur for no time delay up to a 1-day delay between the two sets of data, but for delays of about 2 days in the precipitation fluxes as compared to the trapped fluxes the correlation coefficients are still high. For the correlation coefficients marked by solid squares, which are the larger coefficients, the probability that the coefficients could have resulted from an uncorrelated population is <0.003. Thus there is a high probability that the two sets of data are correlated with a degree of correlation of 0.6–0.7 for time delays of zero to 1 day for $L = 5.5$–6.0. At $L = 6.5$ the degree of correlation drops to ~0.45. These correlations indicate that trapped relativistic particle enhancements can take up to 1 day to scatter into the loss cone and that they primarily occur for $L < 6.5$.

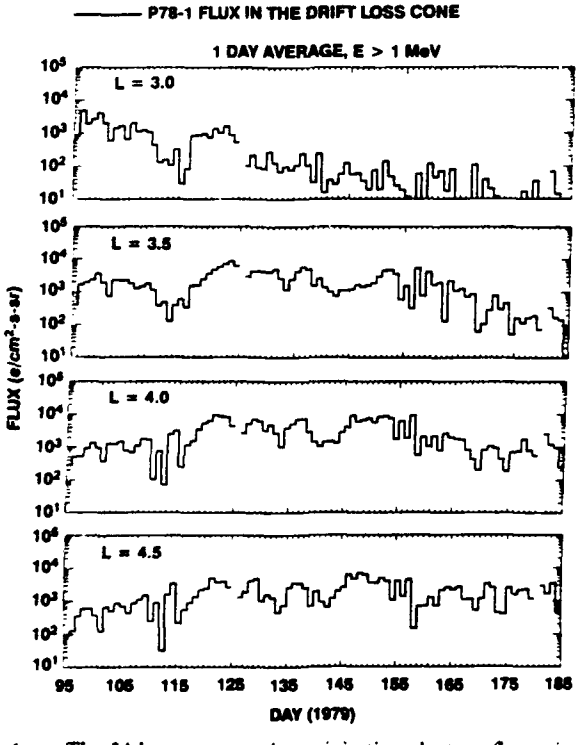


Fig. 6*a*. The 24-hour-averaged precipitating electron fluxes in the drift loss cone plotted versus day number for $L = 3$–4.5.

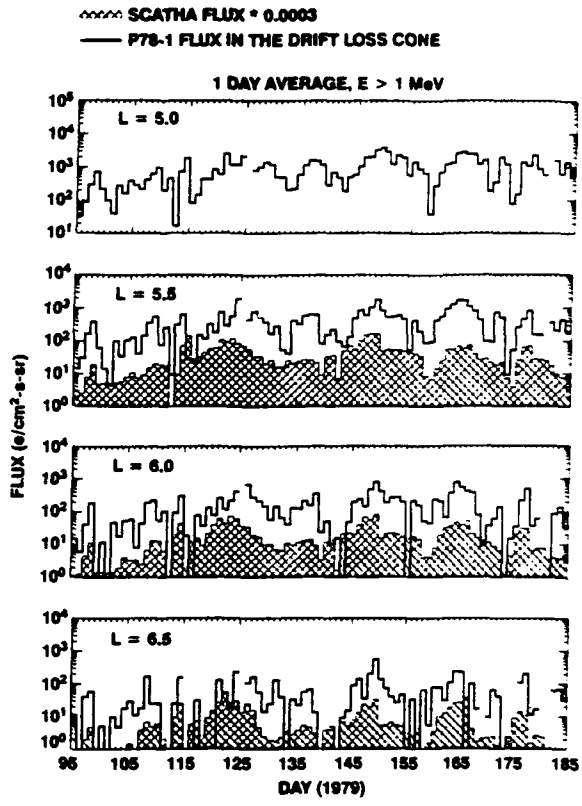


Fig. 6*b*. The 24-hour-averaged precipitating electron fluxes in the drift loss cone and the high-altitude electron fluxes plotted as a function of day number in 1979 for $L = 5$–6.5.

The correlation between the geomagnetic activity as specified by the $Kp$ index and the SCATHA and P78-1 electron fluxes has been investigated by calculating the correlation coefficients as a function of the time delay between the flux and $Kp$. The degree of correlation (0.4) weakly indicates that at $L = 5.5$ and 7.0 there is a delay of about 2–4 days in the rise of the electron fluxes above 1 MeV at high altitudes as observed by SCATHA as compared to $Kp$. For other $L$ values at high altitudes, similar delays are indicated, but the correlations are very weak and could possibly have resulted from uncorrelated populations. At low altitudes from the P78-1 data, significant correlations are not found with respect to $Kp$ at these $L$ values. However, in this paper the high- and low-altitude fluxes have been found to be well correlated with each other with delays of zero to 1 day from $L = 5.5$ to 6.0.

For selected time intervals we compare in Figure 9 the $L$ dependences of the fluxes of precipitating electrons in the drift loss cone with those trapped at high altitudes. A dotted line indicates the center location of a synchronous orbit ($L = 6.6 \pm 0.2$) from which previous high-altitude comparisons with low-altitude fluxes have been made. The flux versus $L$ shell patterns vary strongly with time, but in each time interval both classes of electrons show a similar $L$ dependence. The fluxes in the drift loss cone have been multiplied by 300, and therefore one concludes from the plot that the average fluxes in the drift loss cone were lower than those at high altitude by this factor. Note that the flux observed at

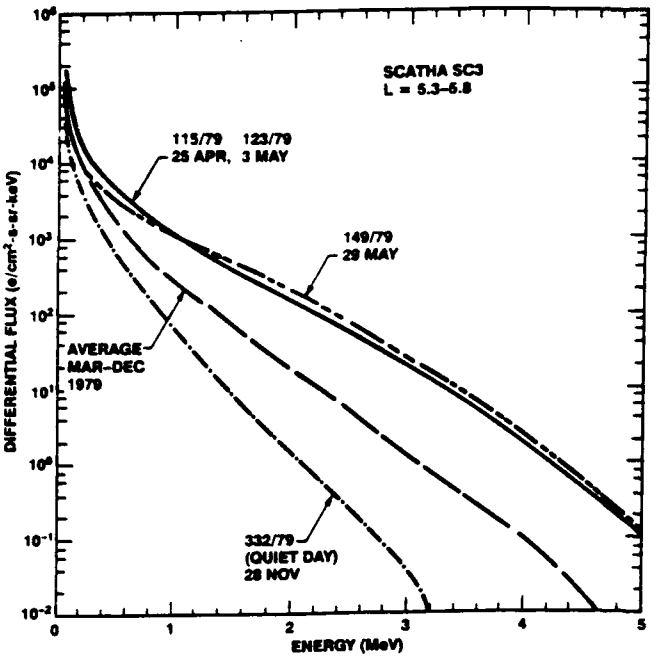


Fig. 7. Energy spectra from the SCATHA measurements averaged over 10 min in the $L$ shell interval 5.3–5.8 for selected days as well as the average for March–December 1979.

low altitudes peaks at a lower $L$ value (top panel) before the high-energy enhancements occur (next three panels).

Upon entering the atmosphere, the electrons above 1 MeV energy penetrate down to altitudes as low as 50 km, and the bremsstrahlung X rays produced by these electrons penetrate down to altitudes of about 20 km. During the more intense bounce loss cone bursts in the data reported here the ion pair production rates can reach values as high as $\sim 10^2$ $(cm^3\ s)^{-1}$ near 50 km altitude. A more detailed consideration of the energy deposition rates into the atmosphere is beyond the scope of this paper.

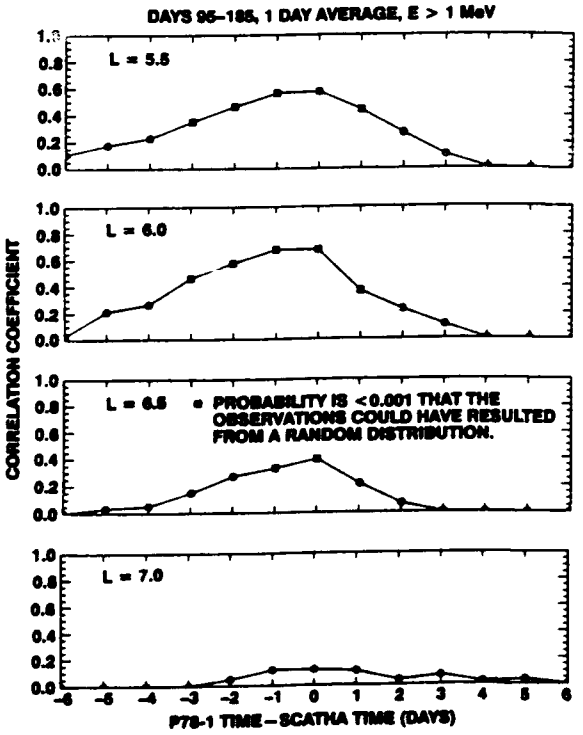


Fig. 8. The correlation coefficients between the fluxes of >1-MeV electrons measured on the SCATHA and the P78-1 satellites plotted as a function of the time delay between the two sets of data.

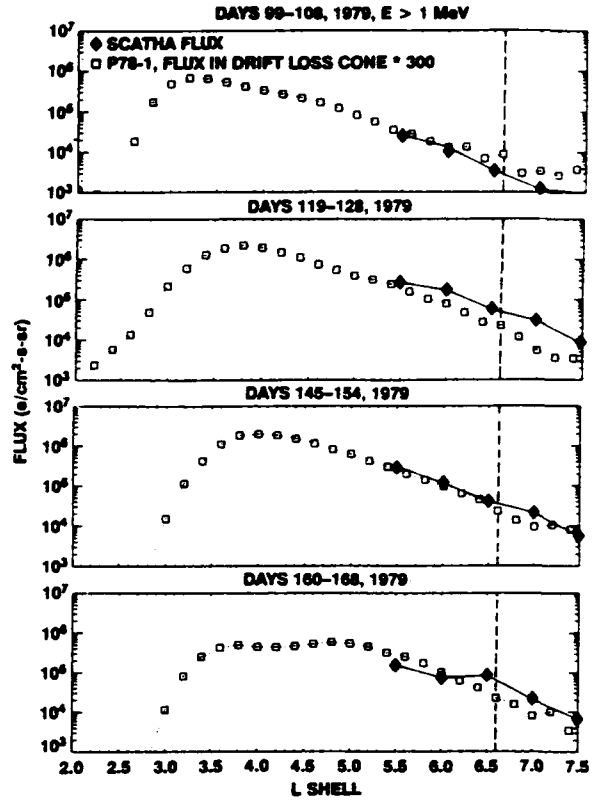


Fig. 9. The fluxes of precipitating >1-MeV electrons in the drift loss cone and the high-altitude fluxes of >1-MeV electrons versus $L$ shell.

## SUMMARY AND DISCUSSION

There has been much speculation on the source of the electrons observed during relativistic enhancement events [*Chenette et al.*, 1988; *Baker et al.*, 1989; *Fujimoto and Nishida*, 1990]. One class of models involves the recirculation of electrons in which energy is gained during inward radial diffusion followed by an energy-preserving outward transport. A key element of the recirculation model as originally proposed by *Nishida* [1976] for Jupiter is that after the acceleration by inward radial diffusion, outward trans-$L$ diffusion occurs in the low-altitude region where the cross-field diffusion results in little energy loss. However, there is an inconsistency with the radial diffusion time scale; it takes much too long for electrons to diffuse to low $L$ shells [*Baker et al.*, 1989]. Measurements over a wide range of altitudes and $L$ shells of the flux increase and decrease rates associated with relativistic electron enhancement events, such as those presented here, should be useful for further investigation of this mechanism.

In previous investigations it was found that enhancements and depletions in the fluxes of electrons above 1.5 MeV observed at synchronous satellite altitude were well correlated with those of precipitating electrons above 1 MeV at low altitudes. Here for the first time a comparison between

the fluxes of relativistic electrons trapped at high altitudes and those precipitating into the atmosphere has been extended to the $L$ shell range of 5.3–8.7. The low-altitude fluxes in the bounce and drift loss cones tracked each other rather well, suggesting that the electron precipitation associated with relativistic electron enhancement events may be investigated on the basis of either category of electrons. A much higher sensitivity and more continuous coverage can be achieved with measurements of electrons in the drift loss cone. Relativistic electrons are present in the drift loss cone during a large fraction of the time, but sometimes the magnitudes of the average maximum fluxes in the bounce loss cone are close to those of the locally trapped fluxes in the drift loss cone, indicating isotropy in the pitch angle distributions. The averaged fluxes in the drift loss cone were lower than the high-altitude fluxes by a factor of approximately $3 \times 10^2$. At $L = 5.3$–7 the average fluxes in the bounce loss cone precipitation bursts were lower than those at high altitude by a factor of about $3 \times 10^3$, and when averaged over all times the average fluxes in the bounce loss cone are estimated to be down from the high-altitude fluxes by a factor of about $3 \times 10^4$.

This investigation has provided information relating to the loss mechanisms for relativistic electrons. Although each precipitation burst is narrowly located in $L$ shell or time, over an extended period of time the precipitation in both the bounce loss cone and the drift loss cone covers a broad region in $L$. The direct precipitation does not extend to as low an $L$ shell as does the drift loss cone precipitation, but that difference may be attributed to the large pitch angle extent of the loss cone at lower $L$ values. This finding does not necessarily preclude much of the precipitation occurring near the trapping boundary, since that location frequently undergoes large variations. Precipitation near the trapping boundary may be caused by the magnetic field line irregularities that occur in that location [e.g., *Imhof et al.*, 1991*b*]. On the other hand, the principal precipitation mechanism operating over a wide $L$ shell interval is apt to involve wave-particle interactions. The bounce loss cone and drift loss cone electron precipitation may well result from the same loss mechanism, the former just requiring a larger scattering in pitch angle. The smaller required scattering angle and the much longer accumulation times for quasi-trapped electrons may account for their fluxes typically being larger and steadier.

*Acknowledgments.* The P78-1 satellite payload was sponsored by the Defense Advanced Research Project Agency through the Office of Naval Research (contract N00014-78-C-0070). Much of the data analysis presented here was sponsored by the Air Force Office of Scientific Research (contract F49620-88-C-0072) and by the Office of Naval Research (contract N00014-88-C-0033). The SCATHA SC-3 payload and initial data analysis were sponsored by the Office of Naval Research under contract N00014-76-C-0444. The P78-2 SCATHA spacecraft was sponsored and operated by the USAF Space Test Program. The Lockheed Independent Research Program provided partial support for this analysis. Special thanks are extended to D. P. Eaton for his dedicated data analysis contributions. We also appreciate the contributions of J. Mobilia and J. P. McGlennon in the analysis of the data. E. E. Gaines was responsible for much of the design and calibration of the EEM 002 spectrometer. Thanks go to R. R. Vondrak, R. M. Robinson, D. W. Datlowe, and H. D. Voss for various contributions. J. B. Reagan played a major role in both the SCATHA and P78-1 experiments.

The Editor thanks D. J. Gorney and another referee for their assistance in evaluating this paper.

## REFERENCES

Baker, D. N., J. B. Blake, R. W. Klebesadel, and P. R. Higbie, Highly relativistic electrons in the Earth's outer magnetosphere, 1, Lifetimes and temporal history 1979–1984, *J. Geophys. Res.*, *91*, 4265, 1986.

Baker, D. N., J. B. Blake, L. B. Callis, R. D. Belian, and T. E. Cayton, Relativistic electrons near geostationary orbit: Evidence for internal magnetospheric acceleration, *Geophys. Res. Lett.*, *16*, 559, 1989.

Baker, D. N., J. B. Blake, R. W. Klebesadel, D. D. Sentman, D. J. Gorney, and P. R. Higbie, Relativistic magnetospheric electrons: Lower ionospheric conductivity and long-term atmospheric variability, *Adv. Space Res.*, *10*(10), 229, 1990.

Chenette, D. L., R. W. Nightingale, and W. L. Imhof, How are geosynchronous electrons related to the Jovian component?, paper presented at 27th COSPAR Meeting, Espoo, Finland, July 1988.

Fujimoto, M., and A. Nishida, Energization and anisotropization of energetic electrons in the Earth's radiation belt by the recirculation process, *J. Geophys. Res.*, *95*, 4265, 1990.

Imhof, W. L., E. E. Gaines, and J. B. Reagan, Observations of multiple, narrow energy peaks in electrons precipitating from the inner radiation belt and their implications for wave-particle interaction, *J. Geophys. Res.*, *86*, 1591, 1981.

Imhof, W. L., H. D. Voss, J. Mobilia, D. W. Datlowe, J. P. McGlennon, and D. N. Baker, Relativistic electron enhancements; simultaneous measurements from synchronous and low altitude satellites, *Geophys. Res. Lett.*, *18*, 397, 1991*a*.

Imhof, W. L., H. D. Voss, J. Mobilia, D. W. Datlowe, and E. E. Gaines, The precipitation of relativistic electrons near the trapping boundary, *J. Geophys. Res.*, *96*, 5619, 1991*b*.

Nagai, T., "Space weather forecast": Prediction of relativistic electron intensity at synchronous orbit, *Geophys. Res. Lett.*, *15*, 425, 1988.

Nishida, A., Outward diffusion of energetic particles from the Jovian radiation belt, *J. Geophys. Res.*, *81*, 1771, 1976.

Reagan, J. B., R. W. Nightingale, E. E. Gaines, W. L. Imhof, and E. G. Stassinopolous, Outer-zone energetic electron spectral measurements, *J. Spacecr. Rockets*, *18*, 83, 1981.

Williams, D. J., J. F. Arens, and L. J. Lanzerotti, Observations of trapped electrons at low and high altitudes, *J. Geophys. Res.*, *73*, 5673, 1968.

W. L. Imhof and R. W. Nightingale, Lockheed Missiles and Space Co., Department 91-20, Building 255, 3251 Hanover Street, Palo Alto, CA 94304.

(Received September 23, 1991;
revised December 16, 1991;
accepted January 24, 1992.)